Reference copy

REPORT NO. DOT-TSC-CG-71-3

TWO CANDIDATE SYSTEMS FOR UNMANNED FOG DETECTION

JACK R. LIFSITZ
HECTOR C.INGRAO
TRANSPORTATION SYSTEMS CENTER
55 BROADWAY
CAMBRIDGE, MA. 02142

JUNE 1971
TECHNICAL REPORT

Prepared for
UNITED STATES COAST GUARD
WASHINGTON, D.C. 20591

TECHNICAL REPORT STANDARD TITLE PAGE

1. Report No.	2. Government Accession No.	3. Recipient's Catalog No.
DOT-TSC-CG-71-3		

4. Title and Subtitle	5. Report Date
Two Candidate Systems for Unmanned Fog Bank Detection	June 1971
	6. Performing Organization Code
7. Author(s)	8. Performing Organization Report No.
Jack R. Lifsitz and Hector C. Ingrao	
9. Performing Organization Name and Address	10. Work Unit No.
Transportation Systems Center 55 Broadway Cambridge, Ma. 02142	CG-02/99-712104
	11. Contract or Grant No.
	13. Type of Report and Period Covered
12. Sponsoring Agency Name and Address	Technical Report
U.S. Coast Guard, DAT Washington, D.C. 20591	14. Sponsoring Agency Code

15. Supplementary Notes

16. Abstract

The detection of coastal fog banks by remote sensing methods is discussed. The feasibility of laser backscattering (LIDAR) and infrared radiometry is explored in detail. These techniques are analyzed theoretically and experimental data are presented supporting the analysis. A design study is carried out for several laser systems, considering safety, reliability, cost, convenience, efficiency and maximum range. A fog bank detector utilizing a GaAs laser array is described which best satisfies these criteria. Before the prototype design is selected, a brief *in situ* test program is recommended, using apparatus designed at the Transportation Systems Center under Contract No. CG-02/99-712104, with the U.S. Coast Guard. In addition to clarifying several critical questions underlying the LIDAR design, the proposed test program would allow further evaluation of the infrared radiometric method. The latter technique, if its reliability can be verified, offers the advantages of being simpler and less expensive for fog bank detection than the LIDAR method.

17. Key Words	18. Distribution Statement
• Fog Bank Detection • LIDAR • Aid-to-Navigation • Radiometer	Unlimited

19. Security Classif. (of this report)	20. Security Classif. (of this page)	21. No. of Pages	22. Price
Unclassified	Unclassified		

Form DOT F 1700.7 (8-69)

ACKNOWLEDGEMENTS

We wish to acknowledge the contributions of William Wade to the signal processing design and Melvin Yaffee to the experimental program. Both are members of the Optical Devices Group of the Electromagnetics Division at TSC.

TABLE OF CONTENTS

LIST OF ILLUSTRATIONS

LIST OF ILLUSTRATIONS (Cont.)

LIST OF ILLUSTRATIONS (Cont.)

LIST OF TABLES

1.0 OBJECTIVES OF THE FOG BANK PROGRAM

1.1 INTRODUCTION

In July of 1970, the Optical Devices Group of the Radar and Navigation Branch at TSC undertook the task of recommending to the U.S. Coast Guard a system which automatically and remotely detects the presence of coastal fog banks.

This effort is part of a planned transition to fully automatic operation of lighthouse aids-to-navigation. A visibility meter (the Videograph B backscatter meter) has been tested and selected by the Coast Guard, for use as an unmanned fog detector[1]. The Videograph has been found to operate satisfactorily under uniform visibility conditions. However, this detector becomes unreliable in inhomogeneous atmospheric conditions. An example of such an inhomogeneity is a fog bank, which may linger several thousand feet or more off shore, effectively obscuring the view of mariners even when the on-shore detector reads "good visibility". These inhomogeneities are particularly characteristic of the West Coast where, during the Videograph evaluation trials, they accounted for almost 30% of the total number of low visibility occurrences[1].

The immediate goal of the present project is to recommend a method, complementary to the Videograph, for detecting the presence of non-uniform seeing conditions. The device, to be effective over ranges as large as 2-3 miles, must be considered from the point of reliability, simplicity, safety, cost and d.c.

power consumption. Furthermore, it must be rugged enough to withstand expected environmental extremes, have a fail-safe design and be easily maintained. The material in this report deals with all these concerns.

Many schemes for remote-sensing of fog banks were studied and our work rapidly narrowed to two main approaches. One, an optical backscatter method, is a logical extension of the principle underlying the Videograph. The other employs an infrared radiometer, and preliminary experiments reported herein have demonstrated its potential.

The report first considers the present techniques used to remotely detect poor visibility, including some discussion of the Videograph (Section 2.0). This chapter also introduces certain elementary concepts of optical scattering used throughout the remainder of the report.

Section 3.0 deals with *fog bank* detection. Section 3.2 relates the results of feasibility experiments on both the laser backscattering and the IR radiometry methods. The emphasis however, in both Sections 3.0 and 4.0, is on optical backscattering, since it is this method about which most data is available and for which a quantitative systems analysis was possible. Of the optical sources available, lasers appear to have many advantages and these are discussed in Section 3.3.

Starting with the demand criterion of an eye-safe source, the analysis presented in Section 4.0 proceeds to estimate backscatter signal strengths to be expected from fog banks and the

factors which will limit detectability. The problem of signal processing is treated and a comparison of several transmitter-detector combinations is made in terms of the maximum detectable range for each.

Section 5.0 and 6.0 deal with candidate systems and recommendations. The present study, although providing real encouragement for solving the fog bank detection problem, has shown up some areas of uncertainty. These include unmeasured scattering properties of real fog banks and environmental conditions attending fog banks, such as their physical extent and the background radiation scattered from them. Furthermore, the practicality of the IR technique has not yet been established and depends on effective temperature differences between fog, water and sky (or clouds). Since the infrared method, if practical, appears to be considerably less costly than the laser method, it is essential that these factors be tested *in situ*.

Appendices A and B provide experimental details for the material in Section 3.2. It is recommended that these experiments be extended and performed in the West Coast locale during the fog bank "season", where the data obtained will be relevant.

2.0 EXISTING AIDS TO FOG DETECTION

2.1 INTRODUCTION

The concept of visibility is familiar to everyone, though generally in a vague and intuitive form. The limit of seeing on a given day is a highly personal matter; but, nevertheless, estimates by one observer serve as useful guides for many others in operational situations such as airport landings or ship navigation.

It is possible to discuss "visibility" more quantitatively[2]. There are two common forms for the definition of visibility, one based on the apparent contrast of an object (its ability to be identified against a background) and the other on the apparent brightness of a light source (particularly useful at night).

In a generally illuminated scene, one of the most important means we have for identifying an object is its contrast. This is a measure of the difference between its luminance and that of the surrounding background. The contrast between an object and the background decreases exponentially with the observer's distance from the object. The variation is due to the scattering of light by the intervening atmosphere, which causes light from the object to be lost from the field of view and, also, extraneous light to be scattered into the field of view. If the inherent contrast (when seen up close) is C_o, then the apparent contrast C_R may be written

$$C_R = C_o e^{-\gamma R}$$

where γ= the *extinction coefficient* of the atmosphere, presumed here to be constant in the line of sight.

The *meteorological range V* is defined such that the object can just be distinguished at this distance. Koschmeider, whose theory forms the basis for the above equation, chose for liminal contrast the value $\frac{C_R}{C_o} = .02 = e^{-\gamma V}$ and thus, taking natural logarithms, $V = \frac{3.9}{\gamma}$. This widely used relationship will be used in this report to relate visibility to the extinction coefficient γ.

The extinction coefficient (which is related to the transmission of the atmosphere) consists of two parts, one of which leads to scattering and the second, to absorption. While there may be cases below where absorption plays a role, in general we will only consider scattering phenomena.

Scattering by the atmosphere can of course be due to many kinds of particles. In addition to water droplets, and suspended particles of soot, salt, etc, there are the molecular gases that constitute the atmosphere itself.

The nature of the scattering depends on many factors, such as the refractive index, size and shape of the particles, and on the distribution of the particles in space, as well as the wavelength and polarization of the radiation.

For particles with radii much smaller than the wavelength, the scattering is described by the Rayleigh theory[3] and the ex-

tinction coefficient is proportional to λ^{-4}. This theory is applicable to the dry permanent gases of the atmosphere but the visual range (or visibility) due just to those gases is several hundred kilometers and so we will not be concerned with Rayleigh scattering here.

Scattering by particles with radius a, comparable to the wavelength must be treated by the Mie theory [3] and in general is quite complex; tabulated values of the scattering amplitudes exist for various refractive indices and for a wide range of size parameters $\alpha \equiv \frac{2\pi a}{\lambda}$.

Since virtually all "measurements" of visibility are really determinations of the extinction coefficient γ, the relationship between γ and the magnitude of scattering observed under various conditions must be understood.

A quantity which denotes the strength of a particle's interaction with radiation is its "scattering cross-section." This is an effective area representing the likelihood that, for a given amount of flux falling on the particle, a fraction K of it will be scattered into some direction. Thus the cross-section can be written as $\sigma=K\pi a^2$ where πa^2 is the geometric cross-sectional area of the particle. As the size parameter α grows, K increases from very small values (in the Rayleigh region) to values greater than unity, approaching K=2 for very large $\alpha(\alpha \geq 40)$ (see reference 2, p.29, fig. 3.3, eg.)

The extinction coefficient γ is then a consequence of the

number density N of these particles. Thus, if we had a single wavelength and only one "kind" (size, refractive index, etc.) of particle, then $\gamma = NK\pi a^2 = N\sigma$. If the particles are of various kinds, then $\gamma = \pi \sum_i N_i K_i a_i^2$.

Most scattering experiments are designed to measure scattering into a certain region of space; namely, into the direction and area of the receiving device. Thus, an essential parameter characterizing any scattering interaction is its "differential cross-section" which specifies how much of the total scattered light goes into a given direction and solid angle. This quantity we call $\beta'(\vartheta)$ where ϑ is the angle between the directions of the incident beam and the scattered beam. The fraction of an incident beam which is scattered into a given solid angle by a length of scattering material ℓ is $N\beta'(\vartheta)\ell \equiv \beta(\vartheta)\ell$ where $\beta(\vartheta)$ is the angular scattering cross-section per unit volume and has dimensions of $(\text{distance})^{-1}$.

2.2 SOME PROBLEMS IN REMOTE SENSING OF VISIBILITY

One would like to deduce the visibility by measuring the strength of scattering of a light beam into a certain angle. To do so, a useful relation between γ and $\beta(\vartheta)$ must exist. However, the two quantities have very different dependencies on wavelength and droplet size spectrum and it is not in general true that a unique relation holds between them.[4]

For naturally-occurring droplet size distributions, and if *white* light is used for the measurements, Twomey and Howell[4], and Fenn[5] show that a useful relationship does exist between β and γ. This will be particularly true for sea and coastal fogs, where droplet sizes can be expected to range from about 1μ to 40μ and variations in the scattering coefficient should average out. Curcio and Knestrick[6] have shown that an empirical relationship holds of the form $V = CS^{-1.5}$, where V = visual range, C = constant and S = backscatter signal. Devices based on this relationship are capable of determining visibility with about a 20% accuracy[7].

Two additional factors can complicate the measurement of visibility by optical scattering. Multiple scattering effects are usually ignored in an analysis of backscatter (or at other angles). For large fields of view, and optically thick atmospheres, there can be significant contributions from this phenomenon.

Also, the most successful present methods of visibility measurement sample a restricted volume of space, and crucial atmospheric conditions which frequently arise outside of this region. Unless conditions are uniform everywhere throughout the area of interest (e.g., a harbor) misleading and perhaps dangerous conclusions result from the restricted data. Thus complementary methods are required to indicate when non-uniform conditions exist.

2.3 SURVEY OF PRESENT SYSTEMS

Instrumental methods for measuring visibility have been discussed in many publications. Two which are closely related to the present work are Hockreiter[8] and Lomer[2]. Here we present a brief summary of such methods, especially as they apply to coastal situations.

Virtually all devices for measuring visibility work at - or near-visible wavelengths and depend on either scattering or extinction.

In the most common technique, using a transmissometer, the extinction of light is measured over a fixed base line. The base line must be chosen appropriately for the desired application since, with good visibility, the base line must be large to give accuracy whereas, when the visibility is poor, the base line must be reduced. Furthermore, in order for the reading to be useful, the extinction over the base line must be representative of the entire space of interest; that is, the conditions determining visibility must be uniform.

The importance of uniform conditions applies to other techniques as well. However, those methods which depend on *scattering* can usually be made more flexible and allow, in principle, the probing of various directions in space without severe alignment problems. Also, by its nature, the transmissometer is not suited to measurements of off-shore fogs and other conditions which arise over water.

The most successful of the scattering techniques measures the light reflected essentially backwards by the particulate matter in the atmosphere. One distinct advantage of this method is that it is *single-ended* (i.e., the source and the receiver are mounted very close to one another). In addition, if the source had a sufficiently intense collimated output, then the effective "baseline", in analogy with the transmissometer, would be variable, being long in good visibility and short under the strong scattering conditions attending poor visibility[9].

Though the ideal source for the backscatter technique would be a laser, no such system has yet been demonstrated to be acceptable. The main problems with laser backscatter methods have been the delicate alignment requirements, potential eye safety hazards and, perhaps most important, the difficult task of interpreting the backscatter data in terms of visibility. No doubt, in the near future, these difficulties will be overcome and line-of-sight laser backscatter systems will become practical[9,10].

In lieu of a laser solution, backscatter equipment presently available uses high intensity light sources and limits the scattering region to a well-defined volume, relatively close to the instrument. For many applications in which visibility conditions are homogeneous, these devices serve well, with accuracies on the order of 20% attainable.[7]

Several backscatter visibility devices are described in references 2 and 8. The U.S. Coast Guard has chosen the Video-

graph B (Impulsphysics) as the visibility meter for its Lighthouse Automation program. Since the fog bank detector with which the main body of this report is concerned must interface with the Videograph, essential details of the latter are summarized in Section 2.4 below.

2.4 THE VIDEOGRAPH FOG DETECTOR

The Videograph B fog detector is a backscatter device manufactured by Impulsphysik GmbH of Hamburg, Germany. It has been described by Frungel[11] and field-evaluated by Lomer[2]. Visibility is deduced from the amount of light scattered by the aerosols present in the atmosphere. The nominal range of visibilities is 0.1 to 10 nautical miles.

The source of light is a Xenon flash tube which emits blue-white pulses of about 10^9 cd. peak intensity. The receiver field-of-view intercepts the transmitted cone of light in a volume extending from 10 meters to 30 meters in front of the instrument. Light scattered into the receiver is detected photoelectrically and amplified by electronics selective to the pulse shape. This electronic filtering, along with a honeycomb screen between the lens and its glass coverplate, reduces the effects of stray light and background daylight.

The received signal, having been amplified, passes to a pulse-height discriminator and then energizes a feed-back circuit which causes a current to pass through a pair of thermistors which control the amplifier gain. By maintaining the gain such

that the signal pulses just pass the discriminator, the feed-back current serves as a direct measure of the visibility.

The instrument operates on 12 volts and consumes 45 watts, 90% of which goes to heat the windows. A newer version employs special non-frosting coatings on the glass surfaces, supposedly eliminating the need for window heaters.

The Videograph is provided with self-checking, delay and fail-safe circuitry. The light source and the receiver are checked automatically every 18 minutes and the fog alarm is initiated if detection sensitivity is found to be deficient.

If the detector indicates the visibility has fallen below the prescribed limit, there is a 2-minute delay before the alarm is triggered. Likewise there is a 15 minute delay on turn-off.

The fog bank detector described below will interface with the Videograph by means of the analog visibility output. As discussed in this report, only when the visibility is moderately good (>8-10 miles) will the search for fog banks be initiated.

3.0 THE DETECTION OF FOG BANKS

3.1 INTRODUCTION

Existing methods for detecting fog and measuring visibility are restricted to situations where atmospheric conditions are more or less homogeneous. Thus the Videograph detector samples a very restricted volume of space, about 20 meters in front of the detector, and interprets the backscattered light from this region to be indicative of conditions everywhere. As has been mentioned, the assumption of homogeneity is often an unsatisfactory one, especially on the West Coast. In particular, thick banks of sea fog often roll into shore and can, on an otherwise clear day, obscure the features of the shore line from a navigator's view. Unless the fog bank has reached the restricted volume seen by the Videograph, a reading of "clear" prevails. An effective fog detection system must be made sensitive to such situations as well.

The physical properties of the fog bank are of interest to us. These include both bulk size and particle size and density, speed and direction of motion and conditions of formation. In addition we need to know the steepness of the "front" of the bank; i.e., how well-defined it is.

Methods which have been proposed for remote detection of these large masses of water droplets include radar, passive infrared radiometry and optical backscattering. Radars can be used to sense the presence of fog and a radar system which would give

a usable return from a fog bank might be competitive in price with optical backscattering. However, there are circumstances when radar returns are received from the atmosphere even though no *visible* obstruction exists, and other cases where radar is hardly scattered by clouds which *do* obstruct visible radiation. It is this lack of correlation with visibility which led us to exclude radar techniques.

Because optical backscattering correlates well with the extinction coefficient of a distribution of particles[6,7], it is reasonable to consider this technique for sensing phenomena which diminish visibility. It is well known that pulses of light scattered from clouds give strong returns, a principle used in optical ceilometers. Although fog banks and clouds vary widely in their characteristics, the visual similarity of the former to certain kinds of clouds leads us to expect similar backscattering features.

Passive IR radiometers have been used to determine the presence of clouds (e.g. from the satellite Nimbus II MRIR flights). In general, one expects that the brightness temperature of fog would be sensibly different from that of clear sky (as well as sea water). Thus an infrared radiometer sensitive somewhere in the 8-13 μ atmospheric window might sense the presence of fog banks, particularly if scanned in a vertical plane. While the concept is simple, the prediction of the success of such a scheme is complicated and a theoretical analysis of the system,

such as we have made for backscattering systems, has not been attempted. However, we have adapted an infrared spectrometer to a vertical-scanning radiometer and experiments along these lines will be described in Section 3.2.2.

3.2 SOME FEASIBILITY EXPERIMENTS AND RESULTS

3.2.1 Laser Backscattering

Preliminary to a serious analysis of an optical backscatter (LIDAR) system, a brief series of experiments was performed using an available ruby laser. The purpose of these experiments was to test the validity of concepts underlying simple signal and noise estimates. In addition, experience was obtained relative to such experimental techniques as alignment and transmitter-receiver isolation.

Since fog formations with well-defined boundaries were not available, cumulus clouds were used as targets. Though adequate for many of our purposes, the clouds probably do not represent valid substitutes for fog banks. In particular, the optical thickness, particle size, density and uniformity may be significantly different for the two.

The experiments were carried out with a Holobeam 3 inch ruby laser. The Q-switched output (1-2 Mwatt) was directed toward the cloud and the backscattered light was received by a 12 cm diameter lens after passing through a "spike" filter, detected by a photomultiplier or a PIN diode. Details of the system are given in Appendix B. The entire LIDAR was mounted on a heavy-duty rolling tripod; a photograph is shown in Figure 3-1.

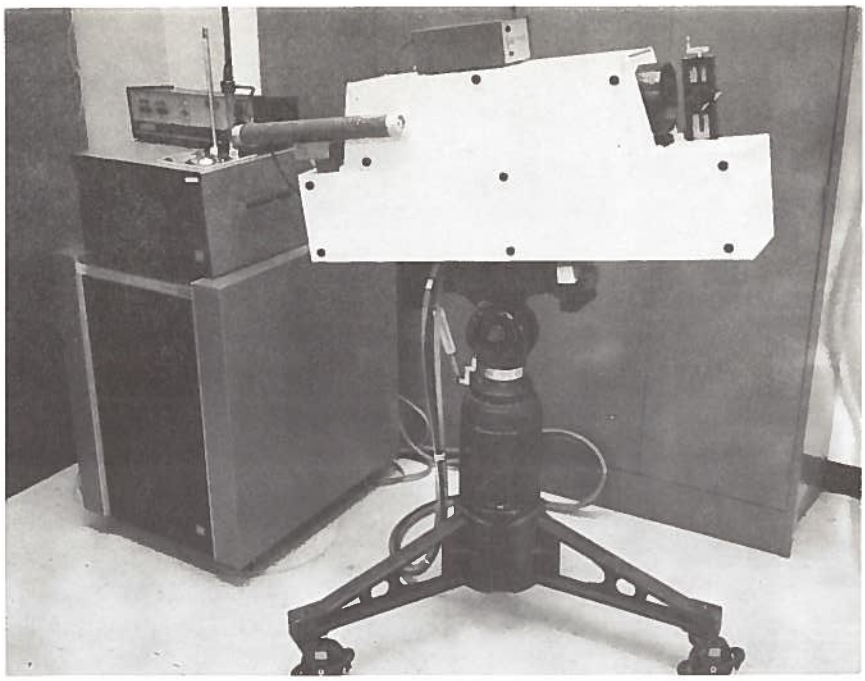

Figure 3-1.- Ruby laser backscatter system ("LIDAR")

Part of the output pulse ($\sim$ 50 n sec wide) was used to trigger an oscilloscope time base and thus the round-trip time could be measured.

Some results of the LIDAR experiments are shown in Figure 3.2. The visibility was measured with a Videograph B Fog Detector.

Figure 3-2(b) shows the return from the concrete wall of a building nearby. (The large initial signal is due to the atmospheric backscatter and is prominant because of the coaxial geometry of the LIDAR.) The reflected pulse from the building should be narrower than shown here but is distorted by the limited detection bandwidth (1 mc).

Figure 3-2(c) and (d) are examples of returns from clouds. These results are analyzed in Appendix B. They corroborate

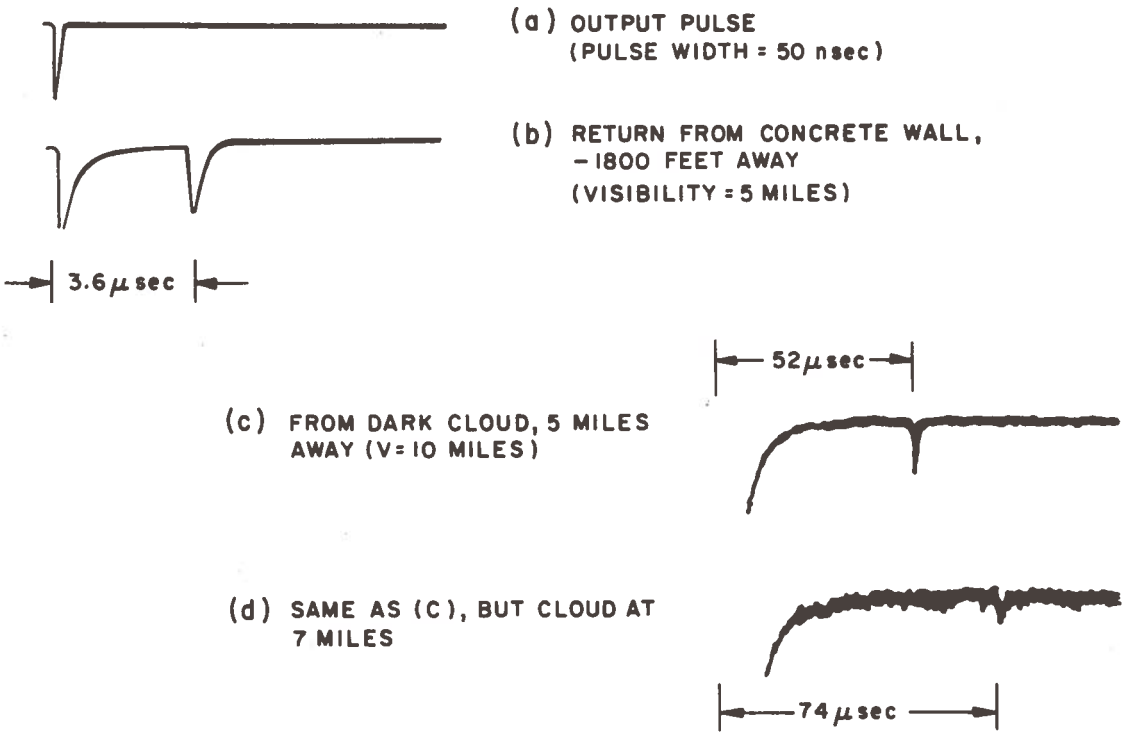

Figure 3.2- Oscillograms of LIDAR returns

(a) transmitted pulse
(b) return from nearby building
(c) return from cloud
(d) return from cloud

a priori expectations suggested by the theoretical treatment presented in Section 3.3.1 and clearly indicate the potential of optical backscattering for fog bank detection.

3.2.2 Infrared Passive Spectral Radiometry

A promising technique for sensing the presence of marine fog conditions is infrared radiometry. By observing the brightness temperature of segments of the seascape it is apparently possible to distinguish the case when the horizon is "visible" from the case when it is blocked from view by obstacles such as fog banks.

The spectral radiance of a body with a uniform temperature T is the product of the spectral radiance of a blackbody at this temperature and the spectral emissivity of the body in question. Planck's formula gives the blackbody radiation as a function of wavelength and temperature. Figure 3-3 shows the spectral radiance of a blackbody with temperatures in the range of ambient air temperature[12].

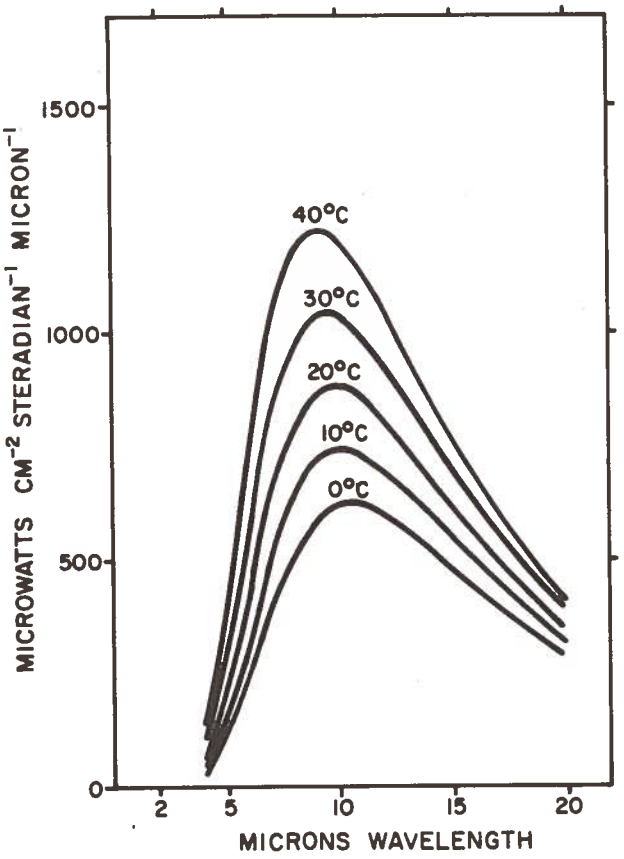

Figure 3-3.- Spectral radiance of blackbody with temperatures in the range of the ambient air temperature. (From reference 12)

The amount of infrared energy reaching the aperture of a radiometer from a distant target depends on the temperature of the target, its emissivity and the absorption properties and temperature of the intervening atmosphere. By operating in a so-called atmospheric window, the influence of the latter is largely removed. In the 8-13μ window, scattering of sunlight is also negligible.

One possible method of utilizing the radiometric concept is suggested in Figure 3-4. A vertical scan is made with a small field-of-view spectral radiometer located at position A, a height h above sea level. The scan, measured by the angle α from the horizontal, encompasses points from X = 100 meters (say) through the horizon (X=B) and into the sky. (See Appendix A)

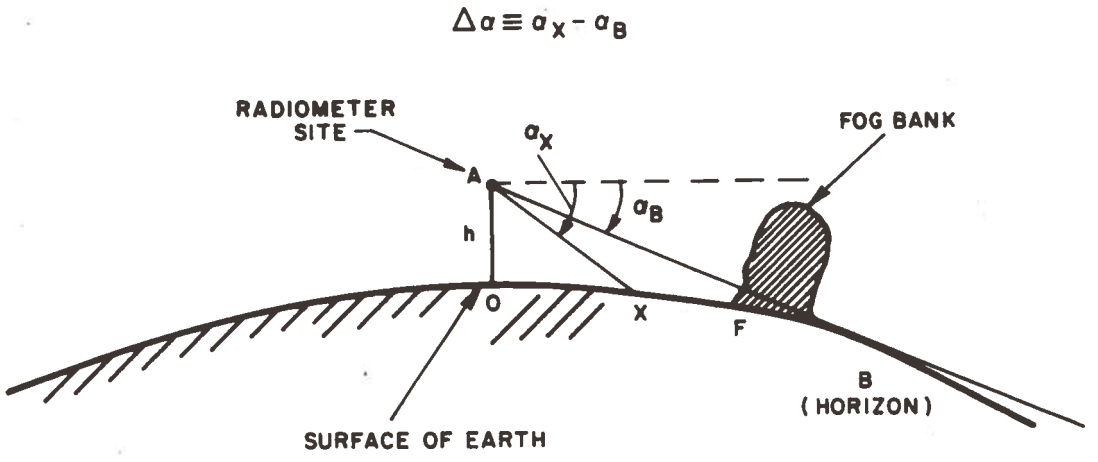

Figure 3.4.- The geometry for the vertical scanning infrared radiometric detection of fog banks

On a clear cloudless day, one would expect the radiance measured as a function of angle to resemble Figure 3-5(a).

If a body of fog is now assumed to appear at position F, between X and B, the radiance vs angle might look like Figure 3-5(b). The temperature of the fog has been taken to be uniform and greater than the water temperature. If such an effect does exist, then the fog bank presents a characteristic signature which can be used to turn on an alarm.

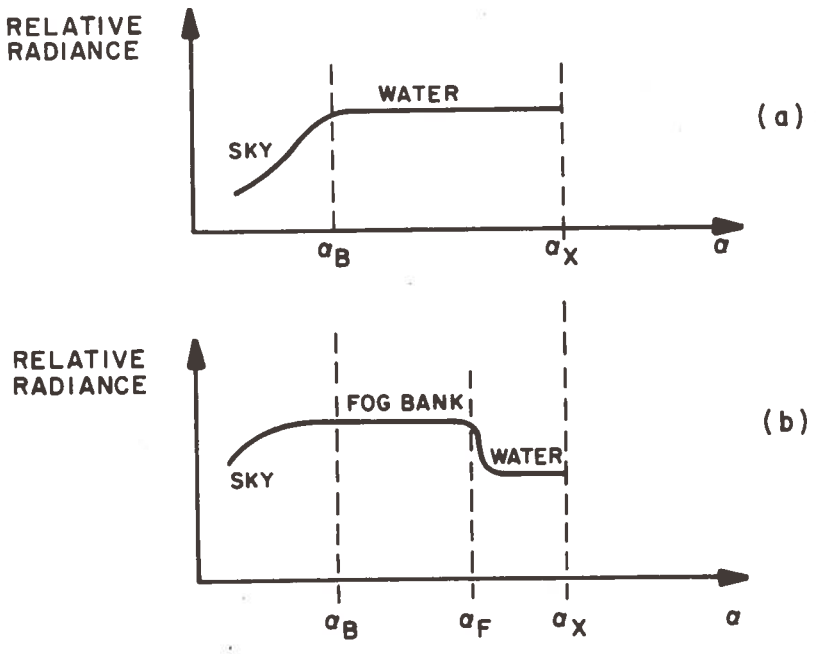

Figure 3.5.- Expected infrared radiometer output vs. "elevation angle", α.

(a) Clear cloudless day
(b) With fog bank at F (see Figure 3-4)

In order to understand such factors as a sea-state dependence of sea emittance, the effect of clouds on the horizon, and temperature differences between water, fog and sky, an experimental apparatus was assembled. This consisted of a motor-driven telescope which imaged a narrow field-of-view onto the slits of a Perkin-Elmer Model 99 IR spectrometer. Details of the system are given in Appendix A.

Preliminary experiments were carried out at the Coast Guard Station at Scituate, Massachusetts. The instrument was mounted in a small watch-tower at a height of 80 feet above sea-level. The vertical scan was begun with the roof of a nearby house in the field-of-view (See Figure A-5). This served as a reproducible angular index. The scan then continued upward and the recorder output of the spectrometer produced a trace of radiance versus angle.

Three examples of the results obtained are shown in Figure 3-6. These were obtained at $\lambda = 9\mu$.

Figure 3-6(a) shows the typical results on a clear day. The general features are similar to Figure 3-5(a). At the horizon ($\alpha=\alpha_B$) the sky appears to be warmer than the water. This surprising result, present on virtually all runs on clear days, has several possible explanations. Eisner et al.[13] points out that due to the multi-faceted nature of the sea-surface at the horizon, the radiation which appears to originate there is actually an average of reflected radiation emitted from a relatively large arc of sky. Thus, the sea surface, at small angles below the horizon.

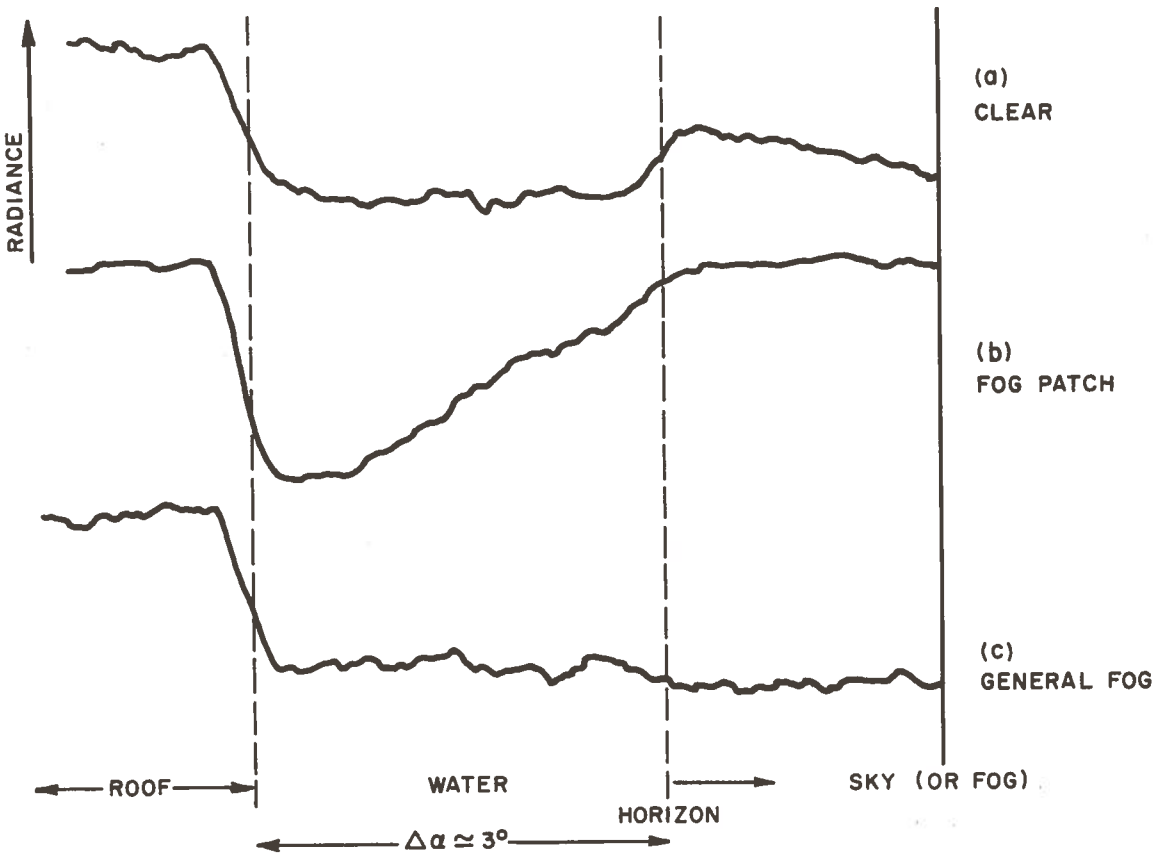

Figure 3-6.- Radiometer vertical scans (Scituate, Mass., March 1971)

(a) clear day
(b) fog patch, about 500 yds. off shore
(c) general fog

can look colder than the sky at correspondingly small angles above the horizon. Although this might explain the relative direction of the effect on the recorder trace, it is difficult to explain the qualitative shape of the bump.

A second phenomenon involves the refraction of rays in the atmosphere. For small angles above the horizon, the radiometer receives some radiation which arises from bodies of air and/or water beyond the horizon. This may increase the effective

emissivity of the "sky" for these angles, causing it to appear warmer. The "bump" at the horizon may be due to a combination of these two phenomena.

Figure 3-6(b) shows a result which is, at this writing, the only incidence of patchy fog we observed. There is a clear qualitative difference between this trace and the one above. A wispy cloud-like patch blew across the field of view during this scan and apparently was warmer than the water. This result gives us reason to hope that, for fog banks, similar tell-tale shapes will occur.

It is important to recognize the non-linear relationship between scan angle and off-shore distance. This is discussed in detail in Appendix A and causes a compression of large distances into a small range of angles. Thus the region between 3000 meters and the horizon is covered within the last 5% of the entire scan.

Finally, Figure 3-6(c) occurred when a general fog had settled over the entire area. Visibility was about 1 mile and the fog appears to dominate the view of the radiometer. Alternatively, there is no difference between the effective "temperature" of the water and the fog. However, we are not concerned with this situation, since the Videograph would sense the poor visibility and sound the alarm.

These preliminary results indicate that this technique may be able to sense fog banks. We plan to extend the measurements on the northern California coast late this summer, when the incidence of fog banks is highest.

There are several reasons why IR radiometers look attractive. Being passive devices, the cost and complexity of a source is eliminated. In addition, large-area scanning is more easily accomplished. The long wavelength region of operation removes the problem of scattered radiation background. Finally, instruments with the high sensitivity and narrow field of view required are available commercially (e.g., Barnes Engineering Infrared Research Radiometer Model 12-511).

Considerably more experimentation, especially in the presence of fog banks, is needed to assess the usefulness of this technique.

3.3 FOG BANK DETECTION USING OPTICAL BACKSCATTER METHODS

3.3.1 Backscatter Signals from Fog Banks

In this section we present a brief development of the theory of optical backscattering, with particular reference to return signals from a fog bank.

A beam of optical radiation is directed towards a bank of fog at some distance off shore. Part of the incident energy will be reflected from the fog and some fraction of this reflected radiation is incident on a receiver telescope adjacent to the transmitter. Passing through an appropriate spectral filter which discriminates against undesirable solar background radiation, the returning light strikes the surface of a photodetector, generating a characteristic electrical signal.

In our analysis we will assume that the source emits light in a short pulse of duration τ, since this allows us to determine the range of the fog bank if desired and also simplifies the detection process itself. The optimum pulse length is approximately determined by the time over which the light interacts with the fog. For "thick" fog (visibility $\lesssim$ 1/8 mile) this time is about 100 nanoseconds, corresponding to an optical depth Δr of roughly 100 ft. ($e^{-\gamma \Delta r} \simeq 1/e$). The details of the pulse shape on return are not easy to predict. The leading edge will be determined by the leading edge of the emitted pulse and the optical depth Δr. However, the remainder of the pulse energy is subject to spreading due to multiple scattering.

It should be made clear that the signal predictions which follow are based on a simplified model, and that uncertainties due, for example, to multiple scattering, pulse distortion and fog structure can only be clarified by direct experiment.

Figure 3-7 shows the angular fields-of-view for a bistatic transmitter-receiver combination. The transmitter beam intercepts the diffusely reflecting "surface" of the fog bank at a distance r_f. Ideally the receiver field-of-view (f.o.v.) would include the entire illuminated area on the fog surface. Because of the separation between transmitter and receiver, the degree of overlap can be made effectively complete within the first 50 meters or so, particularly if θ_R is made slightly larger than θ_T. Alternatively, a monostatic (or coaxial) system can be employed. There are practical considerations which enter into

the choice of one or the other of these configurations; for the moment, it is not necessary to distinguish.

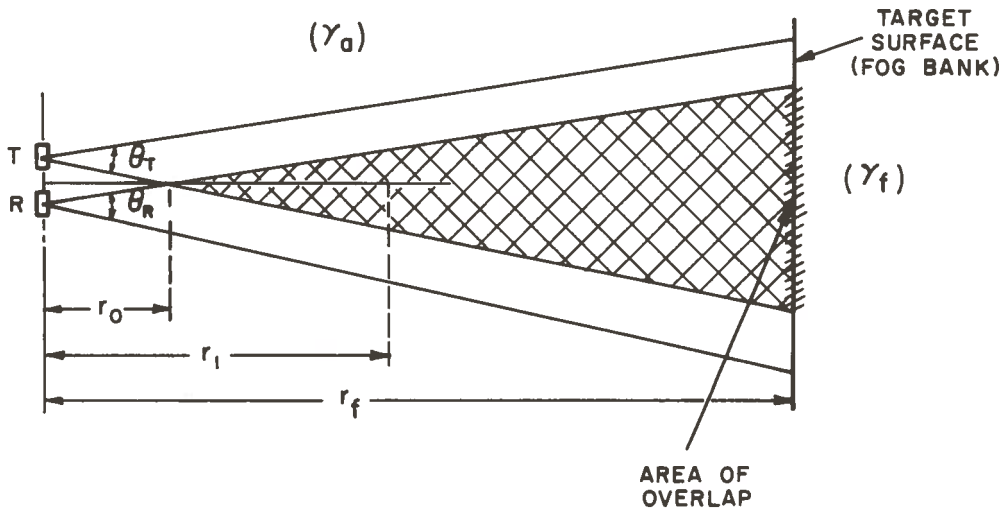

Figure 3-7.- Geometry of bistatic LIDAR configuration showing overlapping fields-of-view. γ_a, γ_f are the extinction coefficients of the atmosphere and the fog bank.

In what follows we analyze the light backscattered from the atmosphere and from the fog bank (target) separately. It will be seen that atmospheric backscattering can, under certain circumstances, interfere with the detection of a fog bank.

If the initial power emitted by the source is $P_o(\lambda,t)$ then the intensity at a surface which is a distance r away is:

$$I(r,t+r/c,\lambda) = \frac{P_o(t,\lambda)}{A_T(r)} e^{-\int_o^r \gamma(r')dr'} \qquad (3\text{-}1)$$

In this equation, r/c is the transit time of the light. The cross sectional area of the beam is $A_T(r)$. The exponential fac-

tor represents the attenuation by the atmosphere and the quantity γ is the extinction coefficient of the atmosphere. (We neglect absorption throughout our discussion.) By writing the extinction term in this form, we have included a possible r-dependence. This will be convenient for the following derivation. There is, of course, a wavelength dependence to γ which, for spectrally-broad sources, may be important. However, we will not include this dependence here.

The light power scattered backwards (per unit solid angle) from a region dr thick at r is (suppressing γ-dependence),

$$dP_{(\pi)}(t+r/c) = P_o(t)\ \beta'_\pi(r)\ e^{-\int_o^r \gamma dr}\ dr \qquad (3\text{-}2)$$

where $\beta'_\pi(r)$ is the volume backscatter coefficient = $N(r) \cdot \left(\frac{d\sigma}{d\Omega}\right)_\pi$ [$N(r)$ = number density of particles at r, $\left(\frac{d\sigma}{d\Omega}\right)_\pi$ = differential backscattering cross-section.]

In Eq. (3-2), $\frac{dr}{2}$ is assumed to be smaller than the pulse length $c\tau$. Also implicit in this development is the assumption that the receiver f.o.v. encompasses the entire illuminated area of a surface at r. We can use a factor f(r) to represent the actual fraction of overlap (for bistatic configurations). Then f(r) varies from 0 to 1. For coaxial systems f(r) = 1. The amount of light backscattered into the receiver (aperture R) from $\frac{(dr)}{2}$ is given by:

$$dP_R\left(r, t+\frac{2r}{c}\right) = f(r)P_o(t)\beta'(\pi)\frac{A_r}{r^2}\, e^{-2\int_o^r \gamma(r')dr'}\, dr$$

and

$$P_R(t) = A_R \int_o^\infty f(r)P_o\left(t-\frac{2r}{c}\right)\beta'(\pi)\frac{e}{r^2}\, e^{-2\int_o^r \gamma(r')dr'}\, dr \tag{3-3}$$

Here a simple time-shift has been used for convenience.

We can use Eq. (3-3) to describe both the atmospheric backscatter and the return from a fog bank. Referring to Figure 3-7, the fog front is at $r=r_f$ and we will assume the front is well-defined. The subscripts "a" and "f" stand for *atmosphere* and *fog*, respectively. Both the clear atmosphere and the fog, taken separately, are assumed *homogeneous*. Thus, the return at the receiver is given by (from Eq. 3-3)

$$P_R(t) = A_R\left[\int_o^{r_f} f(r)P_o\left(t-\frac{2r}{c}\right)\beta_a'(\pi)\frac{e}{r^2}\, e^{-2\gamma_a r}\, dr\right. \tag{3-4}$$

$$\left. + e^{-2\gamma_a r_f}\int_{r_f}^\infty P_o\left(t-\frac{2r}{c}\right)\beta_f'(\pi)\frac{e}{r^2}\, e^{-2\gamma_f\left[r-r_2\right]}dr\right]$$

Note that $f(r)\to 1$ in the second integral, since the fog bank is considered to be well beyond the place where the overlap is essentially complete.

We can make some simplifying assumptions regarding Eq. (3-4):

(i) It is well-known that the dominant scattering in the lower atmosphere (and in fog), for the wavelengths we are considering, is *Mie* scattering, from particulate matter whose size is comparable to or larger than the (visible or near-visible) wavelength. An empirical relationship exists between the volume backscatter coefficient and the extinction coefficient γ: $\beta'_\pi = (0.6)\frac{\gamma}{4\pi}$ (See Carrier et al, reference 14). This expression reflects the enhancement of forward scattering at the expense of backscatter; isotropic scattering would be represented by an absence of the factor 0.6.

(ii) We will be interested in situations for which atmospheric visibility is good $\left(V_a \simeq \frac{3.9}{\gamma_a} \geq 10\text{km}\right)$ and fog visibility is poor $\left(V_f \simeq \frac{3.9}{\gamma_f} \leq 200\text{m}\right)$. Therefore $\gamma_a << \gamma_f$.

Then Eq. (3-4) can be rewritten:

$$P_R(t) = \frac{0.6}{4\pi} A_R \left[\gamma_a \int_o^{r_f} f(r) P_o\left(t-\frac{2r}{c}\right)\frac{e}{r^2}^{-2\gamma_a r} dr \right.$$

$$\left. + \gamma_f e^{-2\gamma_a r_f} \int_{r_f}^{\infty} P_o\left(t-\frac{2r}{c}\right)\frac{e}{r^2}^{-2\gamma_f\left(r-r_f\right)} dr \right] \qquad (3\text{-}5)$$

(iii) Finally, we assume that the fog return arises mainly from a region of depth $\Delta r \simeq \frac{1}{\gamma_f} << r_f$, concentrated near the front. This allows us to simplify Eq. (3-5), since the second integral becomes:

$$\text{(fog)}\quad P_R(t) = \frac{0.6}{4\pi}\,\gamma_f e^{-2\gamma_a r_f} A_R \int_{r_f}^{r_f+\Delta r} P_o\left(t-\frac{2r_f}{c}\right)\frac{e}{r^2}^{-2\gamma_f\left(r-r_f\right)}\,dr$$

$$\simeq \frac{0.6}{4\pi}\,A_R e^{-2\gamma_a r_f}\,\gamma_f\,\frac{P_o\left(t-\frac{2r_f}{c}\right)}{r_f^2}\int_{r_f}^{r_f+\Delta r} e^{-2\gamma_f\left(r-r_f\right)}\,dr$$

$$\simeq \frac{0.6}{8\pi}\,A_R e^{-2\gamma_a r_f}\,\frac{P_o\left(t-\frac{2r_f}{c}\right)}{r_f^2}$$

If we now drop subscripts, so that $\gamma_a \to \gamma$ and $r_f \to r$, we have the fog return given by:

$$\frac{P_R(t)}{P_o} \simeq 0.026\,T_o\,\frac{A_R}{r^2}\,e^{-2\gamma r} \equiv G_R(r) \qquad (3\text{-}6)$$

(T_o = product of transmissions for receiver optics, narrow band filter, etc.). It is likely that this expression for G_R gives a pessimistic value for the return, since we have only included a simple model of single-scattering events. On the other hand, multiple scattering will have the effect of broadening the return pulse, and the width of a range gate will limit the amount of multiple scattering seen. Any more exact theoretical treatment seems unnecessary at this point but experimental data would be useful.

It is possible to write Eq. 3-6 in a slightly different form:

$$\frac{P_R}{P_o} = T_o \frac{\rho}{2\pi} \frac{A_R}{r^2} e^{-2\gamma r} \qquad (3\text{-}7)$$

where ρ = reflection coefficient of fog bank and we assume Lambertian scattering. Identifying Eq. (3-7) with (3-6), we have $\rho \simeq .15$. This agrees roughly with usual values of cloud reflectivity quoted in the literature. Eq. (3-5) now becomes

$$P_R(t) = \frac{0.6}{4\pi} \gamma A_R T_o \int_o^r f(r') P_o \left(t - \frac{2r'}{c}\right) \frac{e^{-2\gamma r'}}{r'^2} dr'$$

$$+ To \frac{\rho}{2\pi} \frac{A_R}{r^2} e^{-2\gamma r} P_o \left(t - \frac{2r}{c}\right) \qquad (3\text{-}8)$$

The LIDAR signal P_R has been plotted in Figure 3-8 for several values of γ_a, γ_f and fog bank ranges. Under certain conditions the atmospheric contribution can be considerable and may interfere with fog bank detection unless appropriate steps are taken to discriminate against it.

3.3.2 Laser vs. White Light Sources

The qualities of a laser which make it attractive for a fog bank detection system are its monochromaticity, highly collimated output and the short duration in which its energy can be emitted.

A major source of interference (or noise) in making decisive detection of a fog bank is the background originating from solar radiation. A monochromatic transmitter allows this noise to be considerably reduced in the receiver by use of a narrow-band optical filter. Thus instead of being sensitive to several

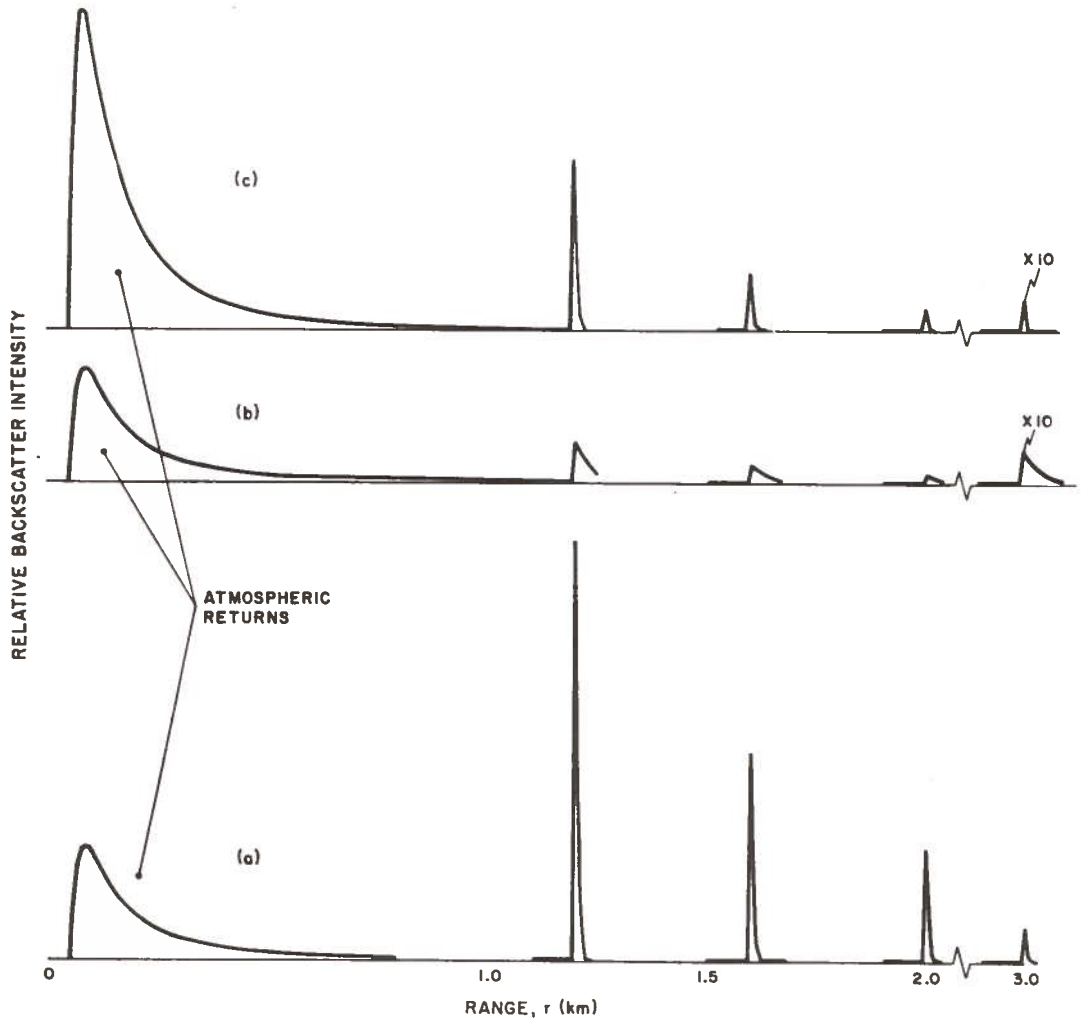

Figure 3-8.- LIDAR signals from atmosphere and fog banks. Solutions to Eq. 3-8 computed for the following parameters:

Curve (a): V_a = 15 km
V_f = 25 meters
x_f = 1.2,1.6,2.0,3.0 km
Curve (b): V_a = 15 km; V_f = 250 meters
Curve (c): V_a = 5 km; V_f = 25 meters

"X10" indicates scale magnification on peaks specified.

thousand angstroms in the visible, the system can be narrowed to at most 100A, with a considerable reduction in background sensitivity.

The collimated output of a laser ensures that all the energy can be used in a beam where divergence is low. Conventional sources, such as Xenon flash lamps, emit in all directions. It is generally difficult to collect 10 or 20% of this energy into a directed beam. Furthermore, if in addition one wishes to limit the divergence of the beam (to allow small receiver f.o.v. and thus keep down noise), even more energy must be sacrificed.

The laser energy can be bunched into packets of 20-100 nanoseconds duration. This represents a resolution, in ranging measurements, of meters. Although the immediate aim of the fog bank detector is simply to alert to the presence of fog, it is conceivable that eventually range information (and also direction and rate of motion) will be desired. Most conventional sources are limited to pulse widths of tens of microseconds and range resolutions at least 10 times worse than for the lasers.

There are several related advantages to using lasers. The atmospheric backscatter return can, under relatively poor visibility conditions, cause difficulty in "seeing" the fog bank signal. (See Section 3.3.1). A short transmitted pulse allows discrimination, in terms of rise times or power spectrum components, between scattering from a long-path backscatter source (the atmosphere, effectively thousand of meters long) and a dis-

tant but short-path source (the fog bank, with a reflecting volume only tens of meters long). In addition a short transmitter pulse allows "near-field blanking", in which the receiver is turned off while the pulse is emitted, and time-programmed gain (See Section 4.5).

For limited peak power sources, a moderate repetition rate (perhaps 100 pps) allows use of integration techniques to enhance signal-to-noise ratios and reduce false alarm probability. A number of laser systems are easily amenable to such pulsing rates. High intensity flash lamps, when pulsed at these rates, have very poor life expectancy.

There are other aspects of laser systems which must be considered. For one thing, a great deal of attention is directed to the question of eye-safety. Because of a laser's inherent collimation in a small, intense beam, the possibility exists for large amounts of optical energy to be brought to a small focus on the retina. Thus any practical system must have an output beam whose intensity has been reduced (by suitable optics) to a safe value. This increases the bulk and cost of the system in many cases. However, the optics required to collimate a flash lamp output are of the same size or larger.

The cost of the laser itself is in general higher than the cost of a high intensity flash lamp system, though when the power supply for a high rep. rate lamp is included, the differential is not too significant.

Flash lamp systems are less complex than laser systems and reliability of the latter might be a concern. However, laser systems are currently being used in applications, such as military-range finders and target designators, where their reliability, ruggedness and alignment-stability have been proven.

It should be pointed out that, in principle, there is no safety advantage of a high intensity flash lamp over a laser. Assuming each has the same intensity and divergence in the beam, the effect on the eye will be similar, as long as the radiation penetrates the ocular elements. Indeed, it is possible to select a laser wavelength which is strongly absorbed by the eye and might be far safer than a "white" source of comparable intensity.

Finally, lasers as a group are quite flexible in output wavelength. In particular, it is possible to find several types which emit in the infrared. Their invisibility means they cannot be confused with existing aids-to-navigation, a desirable feature for the LAMP program. Of the infrared lasers, the two most promising are GaAs ($\lambda \approx 9000\text{Å}$) and Nd: YAG ($\lambda = 1.06\mu$). Erbium ($\lambda = 1.54\mu$) is attractive from the safety aspect, as the eye does not transmit this wavelength (See Figure 3-9). However, we feel erbium systems are not yet suitably developed; perhaps more importantly, detection with high efficiency at 1.54μ is not yet convenient (See Section 4.4).

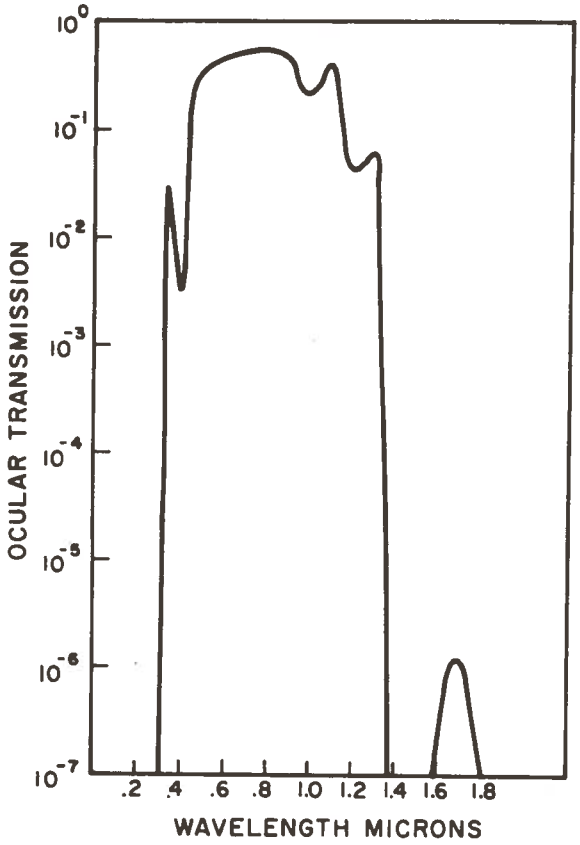

Figure 3-9.- Ocular transmission of the human eye

3.4 COMPARISON OF LASER SYSTEMS

3.4.1 General Features

All lasers have as a common physical basis the amplification of light by stimulated emission of radiation. A large fraction of the molecules in the active laser material are raised to excited energy states by some "pumping" scheme and these then emit under the influence of the coherent electromagnetic waves that grow as lasing action occurs. The build-up of coherent radiation is enhanced by end-mirrors which form the laser cavity. Generally one mirror (the "output" mirror) is only partially reflecting, and as the excited atoms radiate into the

cavity and increase the radiation density, some of the energy propagates through the mirror and forms a highly collimated, monochromatic and coherent optical beam.

The pumping of the laser medium can be accomplished in many ways, including optical excitation, chemical reactions, collisional exchanges in an electrical discharge and, in the case of semiconductor lasers, production of excess carriers at the junction by electric current. The conversion from (incoherent) pump energy to coherent optical radiation is done with a wide range of efficiencies, depending on laser medium, the efficiency of the primary pumping process, the relative lifetimes of the atomic processes, and optical losses characteristic of the entire cavity.

As discussed above, the lasing process is essentially in equilibrium with the pumping cycle and the emission occurs in the continuous-wave (CW) mode. With many systems, it is possible to hold off lasing action while pumping the material (by spoiling the Q of the cavity or reflectivity of the end-mirrors and preventing optical oscillation). Then, by switching to a high-Q value rapidly, the energy is emitted in a short burst of optical radiation. Also, some laser systems (e.g., nitrogen) can only work if they are pumped in very short times and thus their emission occurs in short pulses. Lasers, either Q-switched or pulse-pumped, have output peak powers ranging from kilowatts to hundreds of megawatts, and pulse widths of the order of 10 to hundreds of nanoseconds.

Furthermore the output wavelengths "available" at present range from 2358Å to 774μ.

Of the numerous classes and types of laser systems which have evolved in the last 10 years, only a few are potentially useful in detecting fog banks by backscattering.

Clearly, one essential criterion any practical system must satisfy is availability in a form engineered for reliable performance in severe environmental conditions. This criterion eliminates systems which employ bulky vacuum pumping equipment or have inconvenient cooling requirements. To be avoided also are lasers whose active (or passive) elements require frequent attention or replenishment, or which are excessively complex.

Although efficiency is not a major factor in the present evaluation, the power requirements must be considered in selecting any system. This is particularly true if the fog bank detector is to run from emergency battery packs in event of power failure.

Because a pulse output with significant peak power is required, gas lasers are excluded, in general, with the exception of the pulsed nitrogen and possibly Q-switched CO_2 lasers.

Finally, lasers whose wavelength is not transmitted by the atmosphere or for which there are no convenient detectors, are necessarily eliminated from fog detection applications.

Laser systems which appear to have potential application to fog bank detection are discussed in the remainder of this section.

3.4.2 Gallium Arsenide

A so-called semi-conductor injection laser, the gallium arsenide (GaAs) diode depends for its lasing action on the production of excess carriers by means of a current passing through the p-n junction, and the subsequent emission of optical radiation as these carriers recombine radiatively in the junction. Optical regeneration is provided by a reflective coating on one end of the junction face and emission takes place over a rectangular region, on the other face, whose dimensions are typically 2 microns by 100 microns. The length of the junction (cavity) is less than 1 millimeter.

Diode lasers are efficient; for example, the newer type of close-confinement GaAlAs laser has a power efficiency of 10%. The room temperature laser is pulsed with high current pulses of about 150 nanosecond duration and the repetition rate can be as high as 5kc, limited primarily by the maximum average power dissipated. Recent values for threshold current densities are about 10,000 A/cm^2. Single diode peak powers can be as large as 50 watts.

The wavelength emitted depends on the composition of the junction and to some extent also on the temperature. Thus a GaAs laser emits at λ = 9050Å while with various compositions GaAlAs diodes emit from 9050Å down to 7200Å (at room temperature). Furthermore, during the pulse of excitation, as the diode heats up, the wavelength can shift by tens of angstroms. Thus temperature control is important when wavelength stability is needed.

Though single diodes have insufficient peak power to be of use in fog bank detection, large numbers of these lasers can be formed into a small array. One manufacturer advertises an array of 80 diodes, whose total peak power approaches 1 kilowatt.

The semi-conductor laser has a rectangular-shaped beam and diffraction at the confined junction dimension ($\sim 2\mu$) causes a divergence of about 25^{o} (half-angle) in the corresponding beam dimension. Along with the relatively large area of an array ($\sim .05 cm^2$) this makes it difficult to collimate the output beam to better than a degree or so. However, recent developments by several companies indicate that smaller source sizes are possible with the same high peak power. For example, RCA has developed the so-called "piggy-back" laser, in which three (or more) emitting junctions are formed in contiguous semiconductor material.

One version of this laser has an effective source size of 10 mils x 8 mils ($5 \times 10^{-4} cm^2$) and is said to be capable of peak powers of 200 watts, with pulse widths of less than 100 nsec and pulse repetition rate of ~100 pps. Apparently, by positioning four of these "piggy-back" lasers in a closely-spaced square, it should be possible to have almost 1 kwatt emitted from an area of about $3 \times 10^{-3} cm^2$.

Another approach to small source size is taken by Sperry-Rand (Gyroscope Division). Employing fiber light pipes, rectangular in cross-section and matching the area of the diode faces to which they are individually bonded, Sperry also claims

to be able to bring the entire light output from an array of 68 diodes into an area of $6 \times 10^{-3} cm^2$.

Several factors must be kept in mind when the GaAs (or GaAlAs) laser is considered for a system. First, the large beam angle emergent from the diode source requires very fast optics (~f/1.25) to collect as much as 80% of the energy. For a source of 1 mm, the beam spread of the output is given by $\theta \simeq \frac{0.1}{f(cm)}$ where f = focal length. If a beam spread of 10 mrad is desired, the focal length f→10 cm, and the f/1.25 lens would have a diameter of 8 cm (≃3").

Secondly, one must be aware of the shift in lasing wavelength as the diode warms up, even during a single 100-200 nsec pulse. There is a trade-off between pulse length and laser (optical) bandwidth. An associated problem is that the output wavelength of a diode is a function of the concentration of dopant. In an array, it is necessary to ensure that all the diodes have the *same* central λ, or to alter the receiver filter bandwidth accordingly.

There are several good detectors for wavelengths around 9000Å. These include silicon diodes and avalanche photodiodes (with quantum efficiencies of around 30-70%) and GaAs (selected) cathodes (Q.E. 8%) at 8600Å. These are discussed in more detail in Sec. 4.4.

By using GaAlAs diodes and "shifting" the output wavelength to 8100Å one can optimize the combination of laser efficiency and photomultiplier sensitivity. RCA has utilized this principal

in a range finder which employs the new GaAs photocathode material, with quantum efficiencies at 8100A of $\gtrsim$ 10%.

3.4.3 Ruby Laser

With an active medium consisting of Al_2O_3 doped with Cr^{+3} ions, ruby was the first material in which laser action was demonstrated. Q-switched ruby systems, containing cylindrical rods 1/4" x 3" long, can produce 30 nsec, megawatt pulses with ease. The emission, at 6943A is highly collimated (a few mrad).

The ruby rod is pumped by Xenon flash lamps in one of several configurations which enhances optical coupling. In order to attain population inversion (an excess of excited molecules over unexcited ones) and hence laser action, one must pump ruby relatively hard, since the lower laser level is the ground state. Typically 400 joules of electrical energy are required to produce a megawatt of optical power. As a result, this laser cannot be pulsed at high repetition rates and is not very efficient It will be seen that neodymium lasers are an order of magnitude more efficient and also somewhat safer than ruby with respect to eye damage (Section 4.2). Furthermore, the neodymium wavelength is invisible while ruby, in high intensities , is visible.

In general, there is little to recommend the ruby system for the present application.

3.4.4 Neodymium (glass)

Another solid-state laser material consists of neodymium (Nd^{+3}) ions in a glass host. The neodymium system differs from the ruby in several important features: 1) The wavelength is

in the near infrared at 1.06μ; 2) The neodymium energy-level scheme, known as a "four-level system", permits lasing action to occur between two levels, neither of which is the ground state. This reduces significantly the pumping energy required to reach laser threshold and makes the Nd-laser over an order of magnitude more efficient than the ruby laser (which is a three-level system). In addition, the two laser materials differ in the spectral width of their outputs, but we needn't be concerned with this difference since the neodymium linewidth, which is the broadest of the two, is not more than about 20A.

An air-cooled neodymium-glass laser, with peak pulse power of a few megawatts and pulse rates of a few per minute, can be obtained commercially. Unfortunately, as will be seen in Sec. 4.2, this peak power is far in excess of the eye-safety limits, even for large beam diameters. A more desirable system appears to be the Nd:YAG laser (see below) which allows a much higher repetition rate and emits at a power level more compatible with eye-safety requirements.

3.4.5 Nd:YAG

The Nd^{+3} ion can be substitutionally incorporated in yttrium aluminum garnet ("YAG") to produce high quality rods with good mechanical hardness and high thermal conductivity. The wavelength of emission is 1.06μ.

The YAG laser has become the most flexible of all solid-state lasers in that, because of its low threshold and good thermal conductivity, it is capable of being used in the CW

mode, with hundreds of watts of average power or in a variety of short-pulse modes. The highest performance in the pulse operation comes from using a *continuous* pumping lamp and repetitively Q-switching the cavity by an acousto-optic device. This mode is best suited for high repetition rates (a few kilohertz) since only then is efficient use made of the CW pumped energy.

For repetition rates of about 100 pps or less, *flash-lamp* pumping is used. In this case, since the average power dissipated is 10 times less than for CW pumping, air-cooling can be used instead of the expensive and power-consuming (~1 kwatt) refrigeration unit needed for CW systems. A second advantage of the flash-pumped system is that the effective lifetime of the lamp is increased considerably compared to CW operation. The two kinds of lamps used for Nd:YAG pumping are the tungsten-iodide and krypton arc. The latter has a shorter life (one manufacturer quotes 200 hours) but seems to be preferred for efficiency, power density and price. Since the lamp life is the "weakest link" in the whole system, replacement must be simple and inexpensive and is an important factor in choosing a final design.

One important parameter which will be needed below to determine safety limits is the pulse duration and peak power to be expected from each of the pumping modes. For the flash-pumped laser, at a prf of 100 pps., durations of 20 nsec can be obtained with peak powers of 100 kw. A c.w. pumped system yields a longer

pulse, typically 200 nsec for 500 pps. rep rates, and with peak powers of perhaps 10kw.

Beam divergence of the neodymium lasers is only a few mrad and the wavelength is invisible, an important consideration for the present purpose. Detectors available at 1.06μ include S-1 photo-multipliers and silicon diodes.

We include below a discussion of two laser systems, each of which has features worthy of mention in the present context. However, for reasons to be given, they are not considered suitable for use in a fog detector system, at the present time.

3.4.6 Pulsed Nitrogen Laser

Operating in the ultra-violet, at λ = 3371A, the pulsed nitrogen laser produces 10 nsec pulses with peak powers as high as 100 kwatts. The pulsed nature of the output follows from the excitation method, in which a discharge is produced in a channel (or tube) by a high voltage pulse generator. The optical gain is so high that two end mirrors are not required for oscillation.

A commercial version of this laser exists with pulse rates as high as 500 pps. The beam shape is rectangular (related to the optimum discharge geometry for the fast-risetime excitation pulse), with dimensions of 1/8" x 2" and corresponding beam divergence of about 30 mrad x 2 mrad.

At the rates mentioned above, a continuous flow of cooling water is required, although a closed-cycle system is available. The power requirement for the entire laser system is about 2500 watts. It appears that the components with shortest lifetime are

the energy storage capacitors (~1000 hours or 30 million shots) and the thyratron filaments (~2000 hours).

The potential advantages of such a system are the invisible radiation, the high repetition rate and high peak power available, as well as the availability of photomultipliers with high quantum efficiencies at 3371A. The fan-shaped beam, though a liability from the point of large field of view, may be used to advantage to spread the search area horizontally.

The question of eye-safety has not been resolved, and little or no data exists with respect to tolerable levels of eye exposure at 3371A. This radiation is attenuated strongly in the ocular media and therefore damage, if any, would be to the outer parts of the eye, e.g., the cornea. It is possible that the safety features of this laser are actually superior to the infrared lasers discussed above.

The nitrogen laser still must be proved in terms of field ranging applications. Such questions as environmental reliability, size of atmospheric backscatter signals and transmission properties in the atmosphere (including absorption) need more certain answers before this system could be recommended in favor of the more familiar ones. A significant disadvantage of this laser is the overall bulk of the system, including a mechanical forepump. It seems unlikely that this can be made much smaller.

3.4.7 Erbium in Glass

The erbium laser, which emits at 1.54μ, was developed mainly because its wavelength is strongly absorbed within the ocular

fluids[15]. As a result, it appears to be eye-safe even for energies as large as 1 joule entering the eye. As a laser material, erbium-doped glass is a 3-level system and as such, suffers from the same poor efficiency as ruby systems (~0.1%).

There are other disadvantages which may be severe enough to eliminate this laser as a fog detection device. For one thing, the wavelength is strongly absorbed by water vapor. Thus, one would expect the radiation to be absorbed by the fog bank target. Furthermore, it is likely that the meteorological conditions which lead to fog fronts also bring humid air into the region between the fog and the transmitter. The attenuation of the signal due to absorption over the round trip of several kilometers may be significant. (One report[16] suggests that the attenuation in 70% relative humidity is 70% per km).

It is felt that additional information, and some relevant experiments, are called for in these areas.

Another limitation to using this infrared wavelength lies in the detector selection. The best device presently available for detection, (which in fact was developed in parallel with the erbium laser) is the germanium avalanche photodiode. This device has an extremely small active area (~250 micron on a side) which puts impractical demands on the receiver optics.

4.0 DESIGN FACTORS FOR LIDAR SYSTEMS

4.1 OVERVIEW

Having narrowed the list of possible light sources, the next task is to examine the constraints imposed on the proposed laser backscatter system. We will see that factors such as eye-safe intensity, maximum "convenient" size of optics, and detector limitations combine to further limit the choice of lasers and, ultimately, the range over which the detector is sensitive.

As always in the design of a complex system, there are many parameters which must be chosen and which are often interrelated. In the present case, preliminary study has made it clear that to be of use, the system must be as sensitive as possible, since source intensity will be limited by safety requirements. Thus, whenever possible, we will choose parameters which offer the maximum sensitivity. For example, the receiver optics can be selected to be as large as conveniently possible. (We have chosen 20" as the maximum acceptable diameter.) In this manner we can arrive at an "optimum" system (or systems) with a minimum of trade-off considerations.

4.2 EYE SAFETY REQUIREMENTS

The potential hazard of a laser stems from its inherent brightness. Because of its high degree of collimation, the laser beam can be focused to a very small spot on the retina. Should the average power density (or, in the case of a pulse, the pulse

energy) falling on the retina be excessive, heating effects can cause tissue damage.

We will be concerned here with pulsed lasers, with durations varying from 10 to 200 nanoseconds. There exist several "official" reports, such as the Surgeon's-General Report[17], which consider safe levels of energy density at the cornea. For Q-switched pulses, the value given in the report mentioned is 10^{-7} Joules/cm^2. The same number appears in the appendix of the recently published regulations of the Massachusetts Department of Public Health[18]. A comprehensive treatment of laser eye hazards is presented in reference 19.

This value is considered by many to be overly conservative, particularly with regard to radiation in the near-infrared. In fact, though the Surgeon's General Report makes no distinction, the safety criterion for ruby (6943A) should be different than for neodymium (1.06μ) due to different transmission-absorption products of the lens and retina at these two wavelengths. Furthermore, the report assumes an almost diffraction-limited spot on the retina, corresponding to about 1 mrad, whereas in some cases (especially GaAs) the divergence is as much as ten or twenty times larger. Laboratory tests have indicated that spreading the retinal energy in a larger area increases the damage threshold.

The Air Force has issued a "Laser Health Hazard" report[20] which differentiates between ruby and Nd laser radiation. The

limits quoted therein for Q-switched pulse energy *into* the eye are $\sim 10^{-6}$J(6943A) and 45 x 10^{-6}(1.06μ). Taking a fully-opened iris of 8mm, the *corneal* energy density limits are then 2 x 10^{-6}J/cm^2(6943A) and 90 x 10^{-6}J/cm^2(1.06μ). These numbers are respectively one and two orders of magnitude larger than those of reference 17.

After some discussion with several workers who are experienced in the setting of laser safety standards, we conclude that a safe intensity (at 1.06μ) is 10^{-6}J/cm^2. We use this value below in computing Table 4.1.

Although data for GaAs safety levels are not yet widely available, the divergence of these lasers makes them inherently safer. The maximum energy into the eye (if diffraction-limited) would be 10^{-6}J/cm^2(9000A). With a beam spread more than 10 times the diffraction-limit of the eye, this energy can be increased. A conservative estimate yields 10^{-5}J/cm^2 and this conclusion is supported by experimental results reported in reference 21.

The two remaining sources (erbium and nitrogen) each have unique properties with respect to the eye. The ocular fluid and/or lens absorb both these wavelengths strongly. The erbium wavelength is relatively safe, especially with the beam geometry used in the present application, since ocular attenuation is more than 60 db greater than at 6943A. The Massachusetts Public Health document cited above considers the damage threshold for

wavelengths larger than 1.4 microns to be 10^4 times the threshold at 6943A. In this case, it is *corneal* damage which is involved.

Likewise the transmission of the eye to 3371Å is about 1% of the transmission at 6943Å. However, we know of no published safety values for the nitrogen laser. One would expect it to be somewhat safer than neodymium.

The numbers which we use in this report for safe energy densities at the cornea are summarized in Table 4-1.

TABLE 4-1. - SAFE INTENSITY LIMITS AT CORNEA (SEE TEXT)

	Energy/cm^2	Power/cm^2	Pulse Width
GaAs(9000Å)	10^{-5} J/cm^2	70w/cm^2	τ=150 nsec.
Nd(1.06μ)	10^{-6}	50	20
		5	200
Ruby(6943Å)	10^{-7}	2	50
Nitrogen(3371Å)	10^{-5}	500	20
Erbium(1.54μ)	10^{-3}	2×10^4	50

The energy densities given in Table 4-1 can be converted to *power* density by dividing by the pulse widths of the laser output. These values are given in the second column, for nominal pulse widths shown.

It will be convenient to represent, for each of these sources, the variation of *total* (safe) power with transmitter area. This is done in Figure 4-1.

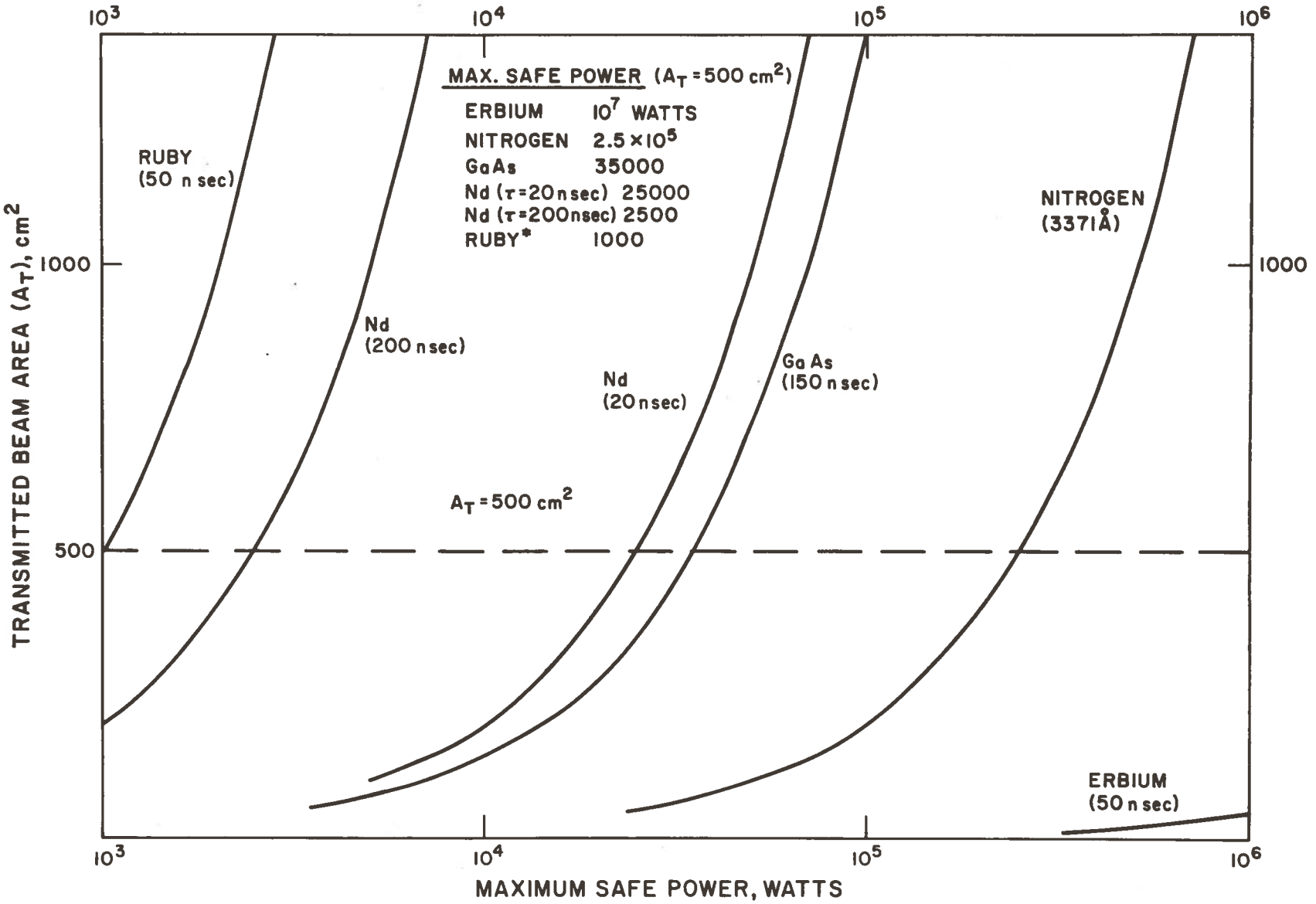

Figure 4-1.- Maximum "safe" power, P_o, versus transmitter area A_t. *The value for ruby is based on maximum energy density of 10^{-7}J/cm², as specified by Surgeon-General (Reference 17)

The larger the area of the transmitter, the greater the safe total power for a given system. We choose the *transmitter* optics to be 10", giving A_T = 500 cm^2. A larger diameter will make optical matching with the inherently small laser beam impractical. The horizontal dashed line in Figure 4-1 represents this choice of A_T. The intersection of this line with a curve corresponds to the safe limit of total power from the corresponding source.

Several comments are necessary here. The need to be eye-safe *at the transmitter* might seem to be too restrictive. If the device were mounted in the lighthouse, or at a reasonable height above the ground (and enclosed) then there is little chance that an eye will intercept the beam in the vicinity of the laser. However, a ship passing, say, 100 yards off shore could bring observers accidently into the line of sight. Because of the low divergence of the beam, the intensity at 100 yards would not be very different from that right at the transmitter. (For example, a 3 mrad beam expands by ~30 cm at 100 meters; if the beam were initially 10" (=25 cm) in diameter, its intensity is down by about a factor of 4 at 100 meters).

In the event that high pulse repetition rates are used, even the $10^{-6} J/cm^2$ value (for Nd:YAG) could be excessive. This depends on how rapidly the heat deposited on the retina can diffuse. There appears to be no conclusive published value for the critical P.R.F. but several informed sources have stated

that ten pulses per second act like 10 independent pulses on the retina, while 100 pps is in the realm of additive effects.

To push this question further, consider the following: According to the Mass. Department of Public Health chart[18], a safe *average* power for a c.w. laser is $10^{-5} w/cm^2$. The *average power* of a Nd:YAG laser with 10,000 watt (peak), 50 pps, τ = 20 nsec is 0.01^{W}. Over the area of A_T = 500 cm^2, the average power density is $2 \times 10^{-5} w/cm^2$. Therefore such a system can be considered "safe".

Finally, we have not discussed the question of beam cross-section uniformity. "Hot spots" in the beam can raise the local energy density, possibly as much as a factor of 10. One should therefore use a Gaussian output mode for the laser (i.e., TEM_{00}). (This is only necessary for low divergence lasers such as neodymium.)

4.3 ESTIMATE OF SIGNAL STRENGTH

We now estimate the size of the return signal as a function of distance to the fog bank, for several laser sources.

From Section 3.3, we obtain the expression for the relative return

$$G_R(r) \equiv \frac{P_R(r)}{P_o}$$

$$G_R(r) = 0.026\ T_o A_R \frac{e^{-2\gamma r}}{r^2} \qquad (4\text{-}1)$$

In order to be useful, this quantity should also represent the return *energy* ratio expected. Thus, the above expression holds only if the return pulse has the same *width* (and shape) as the transmitted pulse. This depends on the relative magnitudes of source pulse width and fog bank scattering length, as will be seen below.

Figure 4.2 shows the return ratio G_R as a function of r, for various values of the extinction coefficient γ. To make the calculation specific, we have chosen the maximum acceptable value for A_R (=1875 cm^2); T_o = .3 (=product of transmissions of narrow-band filter [$T_f \simeq .6$] and windows (and lenses) [$T_w = .5$]).

Thus, if P_o is the transmitter power (*after* the optics) and if the receiver field-of-view completely overlaps that of the transmitter, then the power received from a fog bank and entering the detector is $P_R = G_R P_o$. For the moment the *atmospheric backscatter is ignored.*

To estimate absolute returns for different laser systems, we must take account of the wide variation in pulse widths available. Due to the extended volume over which the fog backscatter is generated, a short pulse will be broadened out to a (spatial) length corresponding roughly to the optical depth of the fog bank.

We therefore define an *effective* peak power P_R' returned from the fog bank, where $P_R' = \left(\frac{\tau_o}{\tau_o'}\right) P_R$ and τ_o' is the width of broadened pulse. Thus P_R' is proportional to the <u>energy</u> received by an (optimum) gate of width τ_o'.

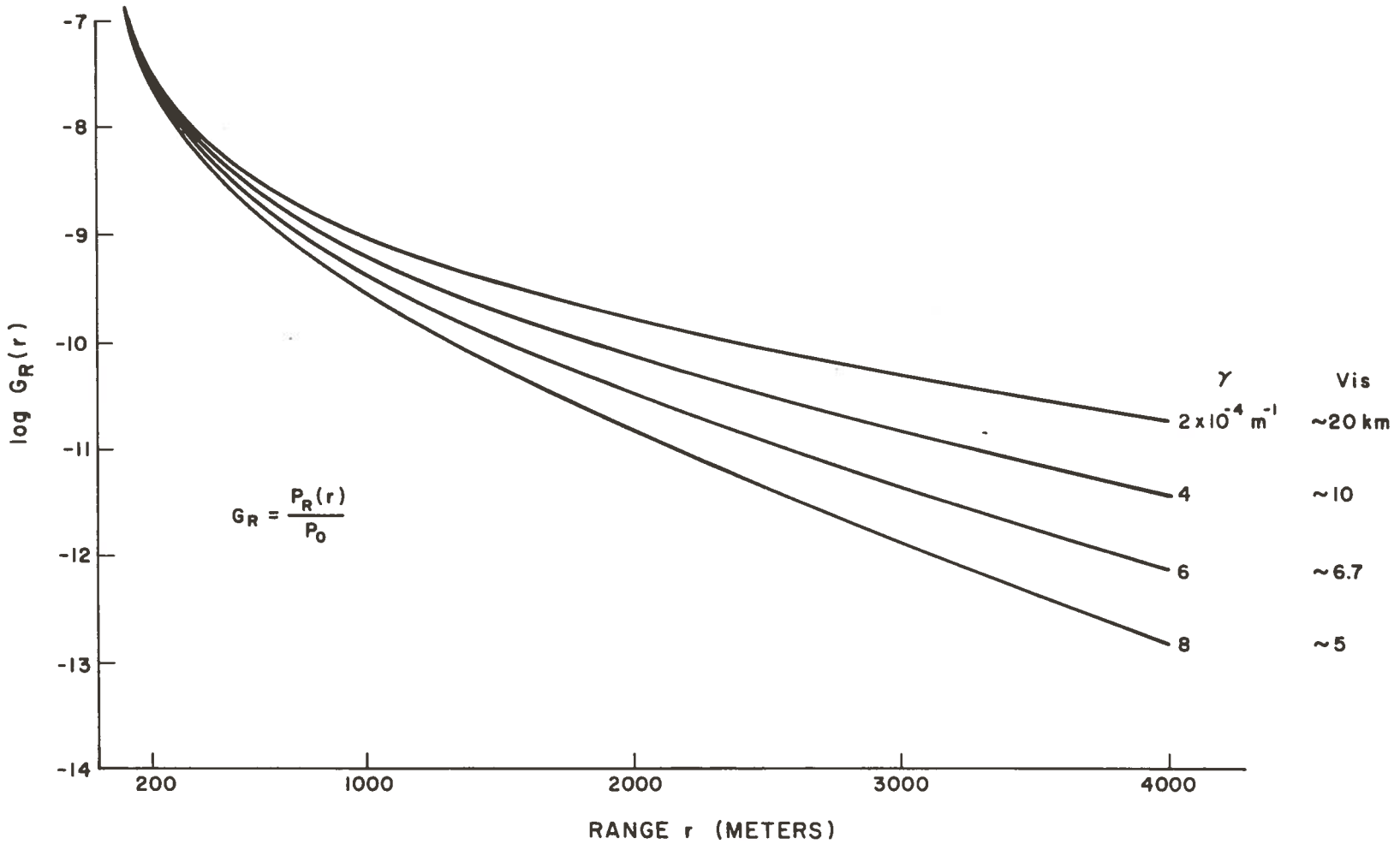

Figure 4-2.- Relative LIDAR return $G_R \equiv \frac{P_R(r)}{P_o}$ versus range (from Eq. (4-1)) $A_r = .18m^2$ (50 cm mirror); $T_o = 0.3$

Proceeding to get absolute values for P_R', we refer to the eye-safe values of P_o found in Figure 4-1. The results are shown in Figure 4-3. For all these curves, $\gamma = .00026\ m^{-1}$ (corresponding to a visibility of 15 km). In some cases, the maximum eye-safe power (determined with the 10" transmitter optics) exceeds the power which the laser can produce. For these cases, the *actual* output capability was used. Furthermore, all values were adjusted to account for transmitter optical system limitations (such as collection efficiency or reflection losses), and P_o represents the power *leaving* the transmitter.

Several comments: First, the values shown for P_R' are essentially maximum returns to be expected. If the receiver optics, or, in the case of safety-limited sources, the transmitter optics, are reduced in size, the value of P_R' must decrease. Furthermore, for poorer visibility, P_R' will be lower.

The return pulse width has been taken to be 200 nsec, corresponding to a fog extinction coefficient of $\gamma_f \approx .01\ m^{-1}$. While this is not a particularly dense fog, at this writing no better estimates exist on fog bank scattering properties. Also, effects of pulse *shape* changes have been ignored even though they will surely play a significant role in choice of an optimum gate width. If experiments show that $\gamma_f \approx .1\ m^{-1}$, for example, then $\tau_o' \simeq 20$ nsec and the curve for the 200 nsec YAG pulse would exchange with the 20 nsec YAG pulse curve. Therefore, the scattering depth characteristic of fog banks and its effect on

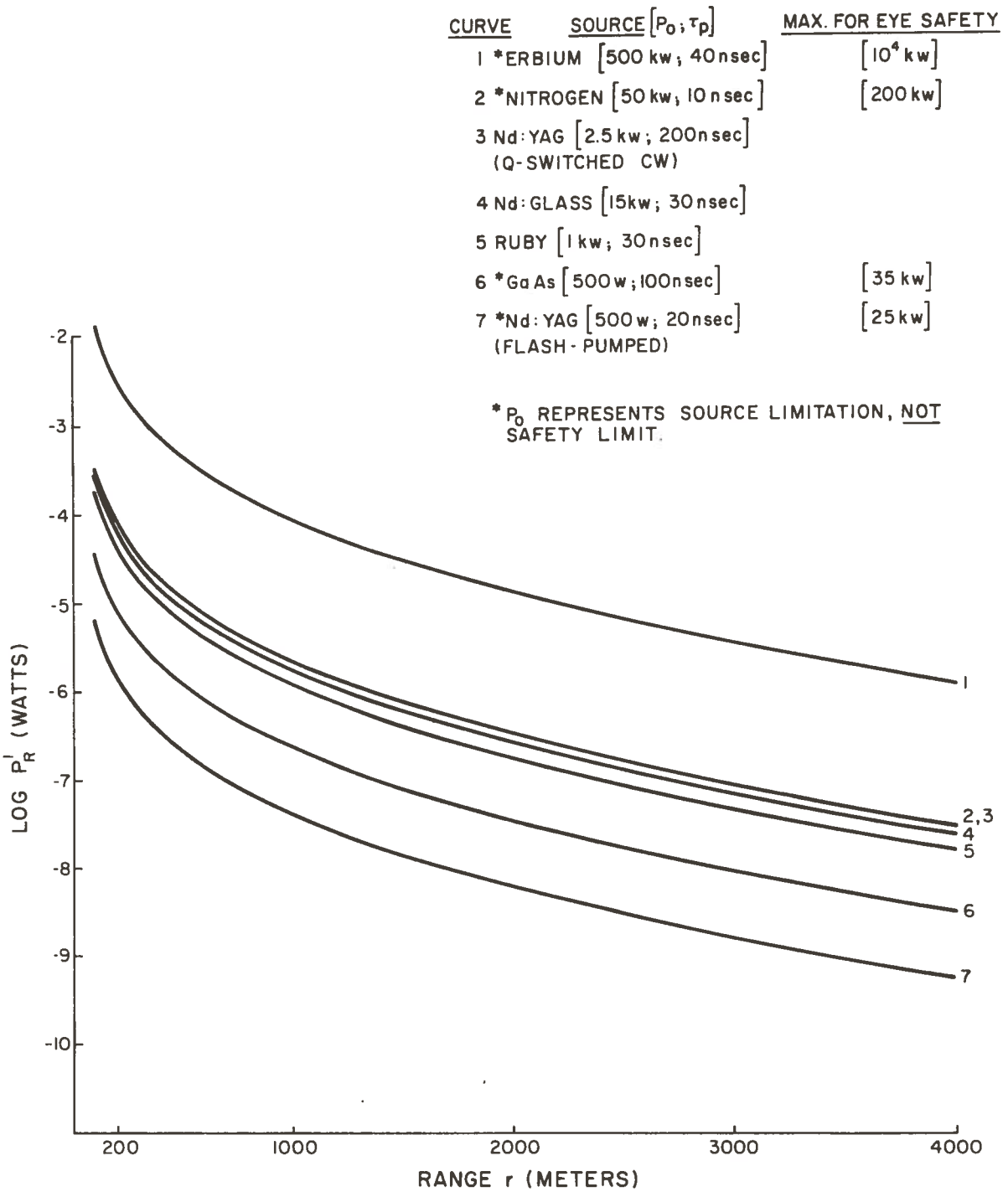

Figure 4-3.- Estimated fog bank returns for various laser sources: P'_R = peak return power at detector, assuming return pulse width ≃ 200 nsec., (T_o = 0.3; γ_a = .00026 m^{-1}; V_{is} ∿ 15 km; $\gamma\psi$ = 0.01 m^{-1}; A_R = 0.18 m^2; ρ_f = .1

pulse shape must be determined *before* system design can be completed with confidence.

Finally, should one of the "output-limited" lasers ("starred" in Figure 4-3) be chosen for the system, the transmitter optics can be reduced to the size at which eye-safe densities occur. (Thus, for example, an erbium laser putting out ~ 500 k watts will be eye-safe with a transmitter beam of diameter $D_T = 10" \times \left(\frac{500\ kw}{10^4\ kw}\right)^{1/2} \approx 2.5$ inches. Likewise the Nd:YAG (20 nsec. pulse) transmitter can be safe with 2" optics; the nitrogen laser, with 5" optics.

4.4 LIMITATIONS ON DETECTION

The presence or absence of a fog bank is indicated by the backscatter signal, as shown in Section 3.3. The certainty with which the fog status can be determined is limited by three main factors: noise in the detector associated with dark current or thermal effects; the solar background radiation incident on the receiver, and the relative size of the atmospheric backscatter.

4.4.1 Solar Background Radiation

During daylight hours, there is always some level of sunlight scattered into the field of view of the receiver. (We do not consider here the *direct* sunlight, since a working device must include a shutter which blocks the detector during the times of direct illumination.) The strongest indirect illumination incident on the receiver will probably be due to a sun-lit cloud

(or fog bank) in the field of view. The *steady* or average value of this background will not necessarily affect signal detection, since even for a simple threshold-sensing device, the D.C. background can in principle be "leveled out". (The steady background *could*, however, cause excessive photo-current in the detector and this will be considered below.)

It is the *fluctuations* about the average background that produce noise and hinder detection. To find the magnitude of this noise, we first must estimate the mean spectral radiance.

As a model for the worst background situation, consider the sun, near the zenith, on a clear day, and a cloud in the field of view of the receiver. (See Figure 4-4).

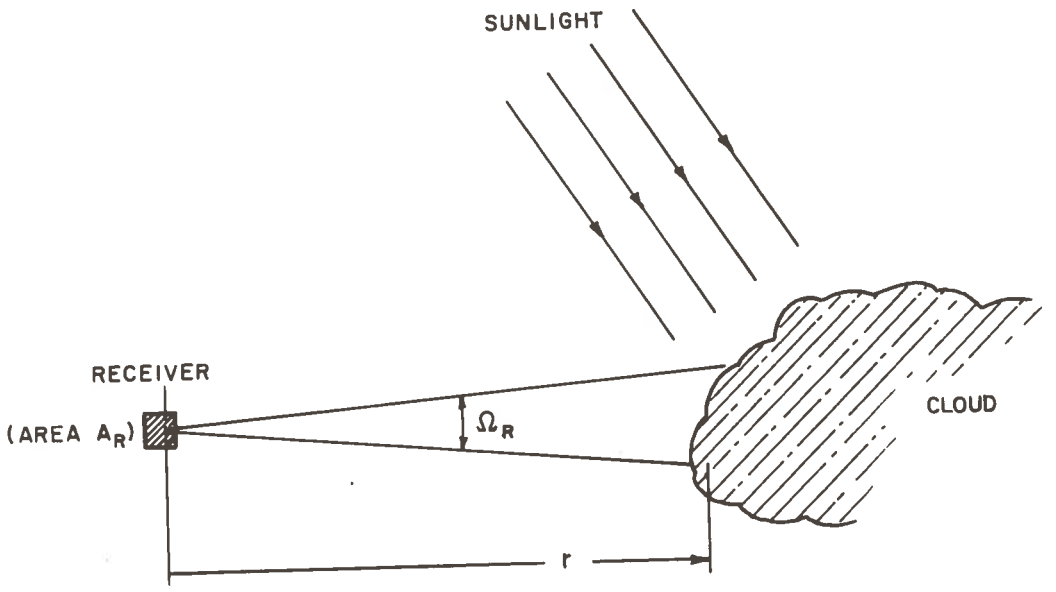

Figure 4-4.- Background radiation arising from sunlight scattered from cloud.

Let the illuminated area intercepted by the receiver f.o.v. be denoted A_s. If H_λ = solar spectral irradiance at the surface of the earth, and ρ = reflectivity of the cloud, then assuming Lambertian scattering, the spectral radiance from the cloud is $N_\lambda = H_\lambda \cdot A_s \cdot \frac{\rho}{2\pi}$. (We take the cloud surface to be approximately normal to the line of sight.) The total power reaching the receiver (of area A_R) is:

$$P_{Bd} = N_\lambda \Delta\lambda \cdot \frac{A_R}{r^2}$$

$$= H_\lambda \cdot \frac{\rho}{2\pi} \left(\Delta\lambda \cdot \Omega_R \cdot A_R \right)$$

where $\Delta\lambda$ = spectral bandpass, Ω_R = receiver f.o.v. and we have used the relation $r^2 \Omega_R = A_s$. From the above we can obtain a "specific" background power

$$\bar{P}_B = H_\lambda \frac{\rho}{2\pi} \quad \left(\text{watts/cm}^2\text{/str/Å} \right)$$

Using $H_\lambda \simeq 10^{-5}$ w/cm^2/A (see e.g., reference 22, Figure 16-1) and a reflectivity $\rho = .3$, we find

$$\bar{P}_B = 5 \times 10^{-7} \text{ w/cm}^2\text{/Å/str.}$$

Atmospheric attenuation of $\bar{P}_B$ over the distance r is ignored here; it is not significant compared with variations in $\bar{P}_B$ due to kinds of background targets.

If background radiation is the principle source of noise, the signal-to-noise voltage ratio on a pulse basis is given by[23]:

$$S/N = \frac{P_R' \sqrt{\eta}}{\sqrt{2\ P_{Bd}\ h\nu\ B}}$$

where η = quantum efficiency of detector

P_R' = peak power of return pulse

P_{Bd} = background power reaching detector

$= \bar{P}_B \cdot A_R \Omega_R \Delta\lambda T_o$ $\quad T_o = \left[\begin{matrix}\text{receiver \& filter} \\ \text{transmission}\end{matrix}\right]$

$h\nu$ = energy of photon at λ (joules)

B = bandwidth corresponding to pulse width

$= \frac{1}{2\tau}$.

4.4.2 Atmospheric Backscatter

As shown by Figure 3-8, the return received due to scattering by the atmosphere near the fog detector can swamp the fog bank signal, especially if atmospheric visibility is marginal. Some form of temporal resolution must be used to process the return. Thus, with a simple threshold detector and no time resolution, the *atmospheric return* would trigger the alarm even if no fog were present. The situation is improved considerably if "near-field blanking" is applied. In this case, detection is inhibited (gated "off") until a sufficient time elapses, after which only the weak atmospheric tail (and the fog, if present) can be seen.

An additional improvement is derived from the use of time-programmed gain (TPG). This technique, to be discussed further

in Section 4.5 below, reduces the near-field contribution, enhances the distant signals from fog banks and minimizes dynamic range problems in the amplifiers.

Electronic filtering should also serve to reduce the importance of the near-field return, since a high-pass filter will strongly attenuate the flat atmospheric tail (see Figure 3-8) while passing the signal pulse with little change.

An operating system would have visibility data available from the Videograph detector. The alarm threshold could then be empirically determined, as a function of visibility, such that the atmospheric return does not trigger the alarm.

As shown at the end of this section, *shot noise* from the atmospheric return will be significant when background noise is low (i.e., at night).

4.4.3 Detectors

A third limitation to the detection of a fog signal is the noise originating in the detector. For the optical detector we will be considering two basic types: the photomultiplier and the solid state photodiode. The latter includes the relatively new avalanche photodiode.

The detector parameters which can influence the detection problem include sensitivity, noise characteristics, speed of response and active area. In addition, we are concerned with the "gate-ability" of the device, or its convenient use with specialized signal processing circuits.

Photomultipliers Because of their internal and almost noiseless current amplification, photomultipliers are generally the most useful photo-detectors for low light levels. (The returns with which we are dealing may be as low as 10^{-7} to 10^{-8} watts.) In addition, these detectors have large areas, high reliability, a flat frequency response to 100 mc or more, and excellent linearity of output current with input light.

As stated earlier in this section, the signal-to-noise ratio in *background*-limited conditions is proportional to the square root of the quantum efficiency η. The quantum efficiency of photo-cathode surfaces ranges from 10-20% in the U.V. and visible, down to less than 0.1% at 1.06μ.

Very recent development efforts have led to photocathodes with improved quantum efficiencies at 9000Å and 1.06μ. These are included in Table 4.2, which summarizes relevant parameters for these tubes at the wavelengths of interest.

Photodiodes Photodiodes (silicon and germanium) have been widely used for laser detection, especially in the region of 0.7 to 1.5μ, where they have excellent quantum efficiency. They can be made to have very high frequency response. Furthermore they are inherently convenient to use in a system because of their small size, low voltage requirements and ruggedness. The linearity is good over 10 orders of magnitude in intensity.

TABLE 4.2.

WAVELENGTH	DETECTOR	Quantum Efficiency (%)	Radiant Sensitivity (at λ)	Dark Current	N.E.P.*	Area	Comments
1.063μ	S-1 photomult.	.05	0.4mA/w (cathode)	10^{-11}A (cathode)	-	∿10cm^2	e.g., RCA 7102
	InGaAs "	2.0	17mA/w (cathode)	10^{-13}A (cathode)	-	-	To be available in 1971(?)
	Silicon p-i-n diode	38	0.2A/w	5×10^{-7}A	4×10^{-8}	1cm^2	e.g., United Detector Technology: PIN-10
	Silicon avalanche photodiode	38	7.5×10^{4}V/w (overall)	5×10^{-8}A	2×10^{-10}w	10^{-1}cm^2	G.E. Model LE-103 $1500.00
9050Å	S-1 photomult.	0.3	2mA/w (cathode)	10^{-11}A	-	∿10cm^2	RCA 7102
	ERMA "	1	7mA/w	10^{-13}A	-	∿10 cm^2	RCA C31000E
	Silicon p-i-n diode	>70	.4A/w	5×10^{-7}A	2×10^{-8}w	1cm^2	UDT PIN-10
	Silicon avalanche photodiode	"	3.3×10^{5}V/w	5×10^{-8}A	10^{-10}w	10^{-1}cm^2	GE-LE-103
8600Å	Silicon avalanche photodiode	(same as at 9000Å					
	ERMA photomult.	3	21mA/w	10^{-13}A	-	∿10cm^2	RCA C31000E
	GaAs photomult.	8	57mA/w	10^{-14}A	-	∿1cm^2	RCA 31025C(Side-on)
6943Å	S-20 "	3.6	20mA/w	10^{-14}A	-	∿10cm^2	RCA 4465, e.g.
	ERMA "	7.1	40mA/w	10^{-13}A	-	∿10cm^2	RCA 31000E
	GaAs "	12.9	72mA/w	10^{-14}A	-	∿1cm^2	RCA 31025C(Side-on)
1.54μ	Germanium avalanche photodiode	25	6×10^{3}V/w (overall)	-	10^{-8}w	6×10^{-4}cm^2	Texas Instruments TI-XL76 ($1500.)(Area too small)

*see text for conditions of N.E.P.

With quantum efficiencies of order 0.5 and larger at near IR wavelengths, the photodiode (Si p-i-n, e.g.) is attractive in the background-limited case. Against this feature, however, one must balance its inherent noise limitation (shot current noise and/or load resistor thermal noise) which makes the photodiode less sensitive than the photo multiplier.

For load resistors R_L compatible with rise times of less than 100 nsec, i.e., $R_L = 100\Omega$ (typical diode capacitances ~300-1000 pf.), the dominant noise is thermal and the typical noise equivalent power (NEP) is $NEP \simeq R^{-1}\left(\frac{4kTB}{R_L}\right)^{1/2} \simeq 2 \times 10^{-8}$ watts. At this power, the signal-to-noise is unity. The value of R, the responsivity, was taken to be 0.5A/watt.

The use of silicon photodiodes above 8000Å involves an additional consideration. Because silicon is particularly reflective at these wavelengths, the detector requires an anti-reflection coating. Furthermore, since the absorption is less than at shorter λ, thicker silicon diodes are needed. This may affect the pulse-response characteristics. With these enhancements, quantum efficiencies at 1.06μ of 38% are claimed.[24]

Avalanche Photodiodes Recent developments in solid-state detectors have led to a device with internal multiplication analogous to photomultiplier gain. By operating the photodiode near the avalanche breakdown voltage, avalanche multiplication can occur and substantial improvement in N.E.P. is possible.

The increase in sensitivity of these devices over simple diodes can be as much as 100. The detector is more complex, requiring both a precise constant voltage source and constant temperature apparatus, though these additions have been module-produced in surprisingly small packages. One example is the Texas Instruments germanium avalanche photodiode,[25] which was developed to be used for detection of the erbium laser wavelength (1.54μ). It can be used also for detection at 1.06μ

Because of the constant voltage required for this device to operate optimally in the avalanche mode, time-programmed gain must be accomplished differently than with photomultiplier tubes. One satisfactory method appears to be the use of a high prf source and averaging over many pulses, the number of which increases as time (range) increases.

The major disadvantage of these detectors (especially the germanium avalanche diode) is the extremely small area ($<10^{-3}cm^2$) which causes severe design problems for an optical system.

Table 4-2 includes Si and Ge avalanche diode characteristics.

Signal-to-Noise An expression for the ratio of signal current i_s to the (rms) noise current $\overline{i}_N$ is (reference 23, page 105)

$$S/N \equiv \frac{i_s}{\overline{i}_N} = \sqrt{\frac{M^2 i'_s}{\frac{4kTB}{R_L} + 2qBM^2\left(i_d + i'_{sa} + i_b\right)}}$$

Here, M = internal current gain (assumed constant)

i'_s = photo-detected current due to fog signal

$= RP'_R$, where R = responsivity, P'_R = peak signal power on detector

B = bandwidth (cps)

k = Boltzmann constant = 1.38×10^{-23} joules/^oK

T = Absolute temperature (^oK)

R_L = load resistor (ohms)

i_d = dark current (amps)

i_b = background current = RP_{Bd}

i'_{sa} = photo-current due to atmospheric backscatter = $RP_{at.bs.}$

q = electric charge

The term in the denominator containing i'_s includes the photo current due to the *atmospheric* backscatter, even in the *absence* of signal power from a fog bank. The *shot noise* from this return can be significant when the background is not important (i.e., at night). See Table 4-3.

4.5 SIGNAL PROCESSING

Before proceeding to determine the range over which a laser backscatter fog bank detector can operate successfully, we first describe the detection and signal processing techniques as they are presently conceived. This will provide a framework in which the concept of "maximum detectable range" can be discussed.

There are several ways in which gating and other time-dependent behavior can be provided to the receiver. The detector gain can be maintained constant and the signal processed with time-programmed amplifiers. This is probably the simplest method,

TABLE 4.3

Source	Detector	Day (bright)*	Night	Comments
λ = 1.06μ	S-1 photomult.	$5\times10^{6}P'_R$	$4\times10^{7}P'_R$	Background (day) Atmospheric
(neodymium)	InGaAs "	$3\times10^{7}P'_R$	$3\times10^{8}P'_R$	Backscatter (night) (InGaAs not yet available)
	Silicon p-i-n	$10^{7}P'_R$	$10^{7}P'_R$	thermal noise (day & night)
$\theta\simeq$ 3 mrad (half angle) $P_{bd} = 10^{-5}$w	Silicon APD	$10^{8}P'_R$	$2.5\times10^{8}P'_R$	Background (day) Dark current (night)
	S-1 photomult.	$4\times10^{6}P'_R$	$10^{8}P'_R$	Background (D); atmos. bsc. (N)
λ-9050A	ERMA	$7\times10^{6}P'_R$	$2\times10^{8}P'_R$	Background (D); atmos. bsc. (N)
(GaAs)	Silicon p-i-n	$3\times10^{7}P'_R$	$3\times10^{7}P'_R$	Thermal noise (D, N)
θ_R= 10 mrad (half angle) $P_{bd} = 10^{-4}$w	Silicon APD	$10^{8}P'_R$	$10^{9}P'_R$	Background (D); dark current (night)
λ=8600A	Silicon APD	$10^{8}P'_R$	$10^{9}P'_R$	Background (D); dark current (N)
(GaAlAs)	ERMA, GaAs photomult.	$10^{7}P'_R$	$4\times10^{8}P'_R$	Background (D); atmos. bsc. (N)
$\theta_R\simeq$10 mrad $P_{bd} = 10^{-4}$w				
λ=6943A	GaAs "	$5\times10^{7}P'_R$	$7\times10^{8}P'_R$	Background (D); atmos. bsc. (N)
	ERMA			
θ_R= 3 mrad (half angle) $P_{bd}= 10^{-5}$w	S-20	$2.5\times10^{8}P'_R$	$3.5\times10^{8}P'_R$	
λ = 1.54w	Germanium	$10^{8}P'_R$	$10^{8}P'_R$	
θ_R= 3 mrad $P_{bd}= 10^{-5}$w				

*Based on P_{Bd} = 2μw/cm^2/A^o/str.

but it appears to be unsatisfactory in the present application (at least for photomultiplier detectors). The background power onto the detector can be as large as 10^{-6} or 10^{-5} watts, causing anode DC currents of perhaps 10mA or more. Such currents exceed the recommended average current through the tube and would rapidly lead to fatigue and deterioration.

We therefore recommend time-programming the gain of the photomultiplier, at least with respect to turning on and off.

Figure 4-5(a) shows the simplest alternative which reduces the average background-related current and also avoids the most

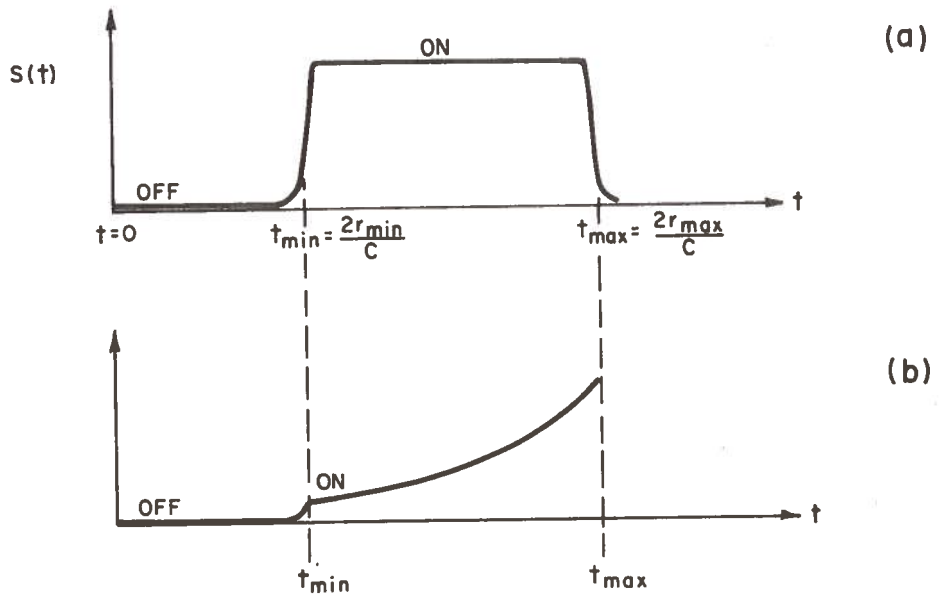

Figure 4-5.- Time-programmed gain
(a) Detector sensitivity S(t) = constant during "on" cycle
(b) $S(t) \propto t^2$

prominent effects of atmospheric backscatter. The detector is turned off until time $t_{min} = \frac{2r_{min}}{c}$ where $r_{min} \approx$ minimum range of detector and t = o is the time of laser firing. The detector sensitivity is then stepped to full value in a short time ($\lesssim$ 500 nsec) and left at this value until the time t_{max}.

Because returns from small r are more intense than distant signals (due to r^{-2} fall off of backscattered radiation), it is helpful to program the detector sensitivity to offset this difference. The dynamic range requirements on the receiver electronics are thereby reduced. Figure 4.5(b) shows how the sensitivity S(t) might be varied. (For this function it may prove more convenient to program the post-detection electronics.)

For $S(t) \propto t^2$, the $1/r^2$ falloff can be compensated. Further refinement is possible by using the instantaneous Videograph reading of visibility to alter the gain with respect to the exponential attenuation in the atmosphere.

To take full advantage of the pulse nature of the fog return signal, it would be desirable to have the receiver "open" only long enough to collect signal information (i.e., return pulse energy). This minimizes the background noise seen by the system and also reduces considerably the effects of atmospheric backscatter. However, since the "target" range can vary from 1/2 mile to over 2 miles, it is clear that a *fixed* delay signal-matching gate is not feasible.

We consider first the simplest form of signal processing, namely, threshold detection of single pulse returns. Here, the detector (or receiver electronics) is "turned on" a fixed delay time t_{min} after the pulse is transmitted. If, during the interval $t_{max} - t_{min}$, a return signal produces photocurrent sufficient to exceed a predetermined threshold, an "alarm" condition exists.

To prevent alarm alerts when spurious targets such as birds, planes or swarms of insects are involved, a hold-off method can be employed which requires successive signal confirmations for a period of, say, three minutes, before a fog signal is energized.

The threshold is determined by the average noise at the receiver output and the level of return power expected. It also depends on the signal-to-noise ratio required to give suitable probabilities of detection and false alarms.

If the output of the video amplifier (before the threshold sensing device) is integrated over n return pulses, the signal will increase as n but the noise only as $\sqrt{n}$. Thus, the signal-to-noise ratio of the system has been improved by $\sqrt{n}$ and the effective range capability is increased.

The most suitable source for integration techniques is one with moderate peak power and reasonably high p.r.f. The higher the *average* power the better, (within the bounds of eye-safety).

A Nd - glass laser pulsing at a rate of 4 per minute, with peak power = 10 kw in 30 nsec pulses, has average power of 2×10^{-5} watts; whereas a 500 watt (peak) GaAs transmitter, with 100 pps and 100 nsec pulse width, yields 5×10^{-3} watts.

The increased data rate from the high rep rate system can be used to advantage in other ways also. For example, it might be desirable to scan the transceiver beam in the horizontal plane, since it is not always possible to predict the position of the fog bank. A pulse system with high average power gives this capability.

Furthermore, the system with the GaAs source (e.g.) is readily adaptable to ranging, if this feature should be desired. By sweeping the range-gate, and using a gate matched to the return pulse width, the distance to the fog bank can be determined to perhaps 50 yards. Even without using the ranging capability, the moving gate is a convenient and relatively simple means of accomplishing integration over multiple pulses.

A requirement for any detection system is that the threshold must be automatically adjusted continuously, since the background radiation, the major daytime source of noise, will vary. The background must be sensed periodically, with the transmitter off.

4.6 MAXIMUM DETECTABLE RANGE

The maximum effective range of the fog bank detector will depend on the scattering parameters of the fog, transmission of the atmosphere, peak power of the transmitted pulse, receiver f.o.v. and aperture, background conditions (bright day, cloudy day, nighttime) and detector sensitivity. Briefly this can be reduced to: strength of signal, noise characteristics and detection criteria.

As a basis for the overall comparison of various systems, we now estimate the maximum effective ranges using several sources. To do so, we fix those parameters which are not system-related, and only vary those which are. The conditions under which these estimates will be carried out are as follows:

4.6.1 Visibility Conditions

We assume the same conditions as used for the computations represented in Figure 4.3.

$\gamma_a = .26\ km^{-1}$ (visibility = 15 km)

$\gamma_f = .01\ m^{-1}$

$\rho_f = .1$

4.6.2 Receiver

$A_R = 1875\ cm^2$ (20" diam. aperture)

$T_o = 0.3$ (attn. factor for receiver optics)

B = detection bandwidth = 5 MC

$\Delta\lambda$ = 100Å

4.6.3 Background Conditions

Daytime (reflected from clouds or fog bank within field-of-view): $\overline{P}_B = 2 \times 10^{-6}$ watts/cm^2/str/Å*

Nighttime (moonshine from clouds): $< 10^{-11}$ watts/cm^2/str/Å

The (effective) return power from a fog bank at the detector is

$$P'_R = \left(\frac{\rho}{2\pi}\right)\left(P_o T_o A_R\right)\frac{\rho}{r^2}^{-2\gamma_a r}$$

For the purpose of estimating the shot noise in *absence* of fog return, we take the atmospheric backscatter from a distance r = 500m, and a transmitter pulse energy of one milli joule. Then the power backscattered (energy in 200 nsec gate interval) is $P_{at.bs} \simeq 10^{-7}$w. (See Eq. 3.8).

4.6.4 Signal-to-Noise

From IV.D.3

$$S/N = \frac{i_s}{i_N} = \sqrt{\frac{M^2 i_s^2,}{\frac{kTB}{R_L} + 2qBM^2\left(i_d + i'_{sa} + i_b\right)}}$$

*This value is somewhat larger than estimated in 4.4.1.

4.6.5 General Comments:

For photomultipliers

i) Thermal (Johnson noise) term is negligible

S/N is independent of M.

ii) In daytime, $i_b >> i_d, i'_{sa}$; at night

limited by $i'_{sa} + i_d$.

iii) $R_L \simeq 1000\Omega$

For photodiodes (M=1)

i) $R_L \sim 100\Omega$

ii) thermal (Johnson noise) term can be comparable with background in daytime. At night thermal noise dominates.

Avalanche diodes: (M=20 (Germanium) M = 100 (Silicon)

i) $R_L \sim 50\Omega$

ii) Background-limited in daytime

thermal-noise limited at night

For background-limited systems, a useful form of the last equation is:

$$i_s/\bar{i}_N = \frac{\sqrt{\eta}\ P'_R}{\sqrt{2Bh\nu\ P_{Bd}}}$$

η=quantun efficiency

We will now choose reasonable detection criteria and estimate the signal-to-noise ratios needed to satisfy these criteria, for a threshold detector.

Without specifying values for the moment, we define the following parameters:

f = pulse repetition frequency

T_R = maximum round trip time for a pulse (receiver "on" time)

τ = pulse width

T_F = operating period during which no more than 1 false alarm is desired (e.g., 1 week or 1 month)

The total number of "receiver-on" periods (or pulses) in time T_F is $N = K\ f\ T_F$, where K is the fraction of time during which the fog bank detector is in use. Then the acceptable average false alarm rate $\overline{FAR}$ is $\overline{FAR} \leq \frac{1}{NT_R}$.

Assuming a "matched filter" ($B = \frac{1}{2\tau}$), the probability of false alarm is $P_{FA} = \overline{\tau \cdot FAR}$

Using this value of P_{FA}, and a probability of detection P_D, we can find the required signal-to-noise ratio by referring to published tabulations of detection statistics. (A convenient graph is found in reference 26, Figure 8.3.)

If pulse averaging is employed, with high repetition rates, and n pulses are integrated, then the S/N ratio required is less by approximately $\sqrt{n}$ (for low S/N ratios; see Reference 23, page 343). Figures 4.6 and 4.7 show the S/N level for a single pulse return and for 100-pulse averages. The choice of parameters is as follows:

T_F = 1 month = 3×10^6 seconds

K = .25

T_R = 30 μsec.

τ = 200 nsec.

P_D = .95

For the single pulse case, the value of f chosen was 4 pulses per *minute* ($P_{FA} \simeq 2 \times 10^{-7}$). The integration of 100 pulses is used for a system with f ∿ 100 pulses per second ($P_{FA} \sim 10^{-10}$). Table 4.4 gives the legend of transmitter-detector combinations represented in Figures 4.6 and 4.7.

TABLE 4.4.- TRANSMITTER-DETECTOR COMBINATIONS REPRESENTED IN FIGURES 4.6 AND 4.7

Symbol	Source	Detector	λ.
a	Nd:YAG(flash pumped)	S1 photomultiplier	1.06μ
b	Nd:YAG(Q-switched CW)	" "	"
c	Nd:glass	" "	"
d	Nd:YAG(flash pumped)	Silicon p-i-n diode	"
e	Nd:YAG(Q-switched CW)	" " "	"
f	Nd:glass	" " "	"
g	Nd:YAG(flash pumped)	Silicon APD	"
h	Nd:YAG(Q-switched CW)	" "	"
i	Nd:glass	" "	"
j	GaAs	ERMA photomultiplier	9050 Å
k	GaAs	Silicon APD	"
l	GaAlAs	ERMA or GaAs photomultiplier	8600 Å
m	GaAlAs	Silicon APD	"
n	ruby	ERMA photomultiplier	6943 Å
p	erbium	germanium APD	1.54μ

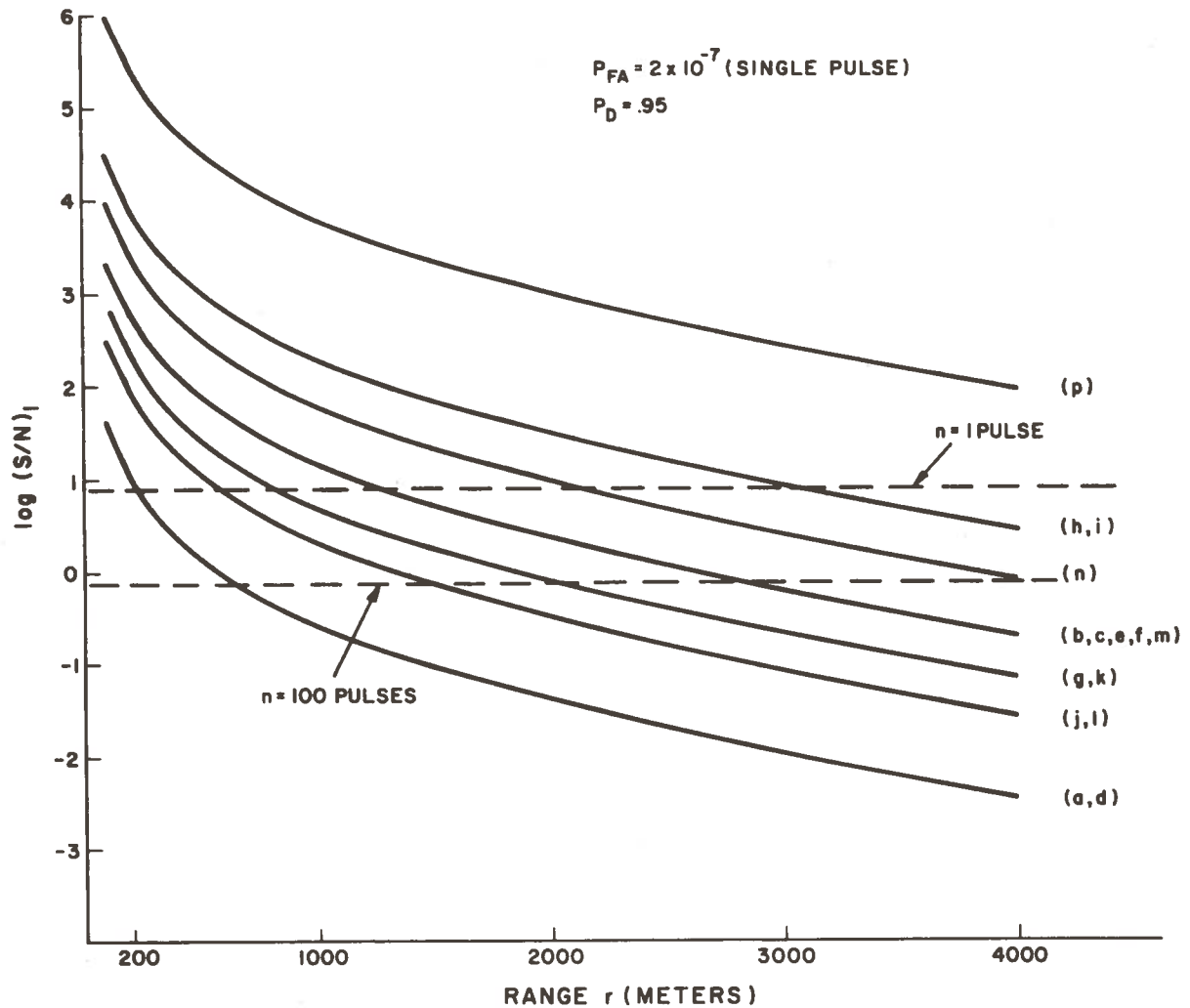

Figure 4.6.- Signal-to-noise (single pulse basis) vs fog bank range in *daytime*, for transmitter-detector combinations given in Table 4.4. Horizontal lines indicate levels required to satisfy criteria $P_{FA} = 2 \times 10^{-7}$ and $P_D = .95$, for single-pulse (n=1) and average of n = 100 pulses.

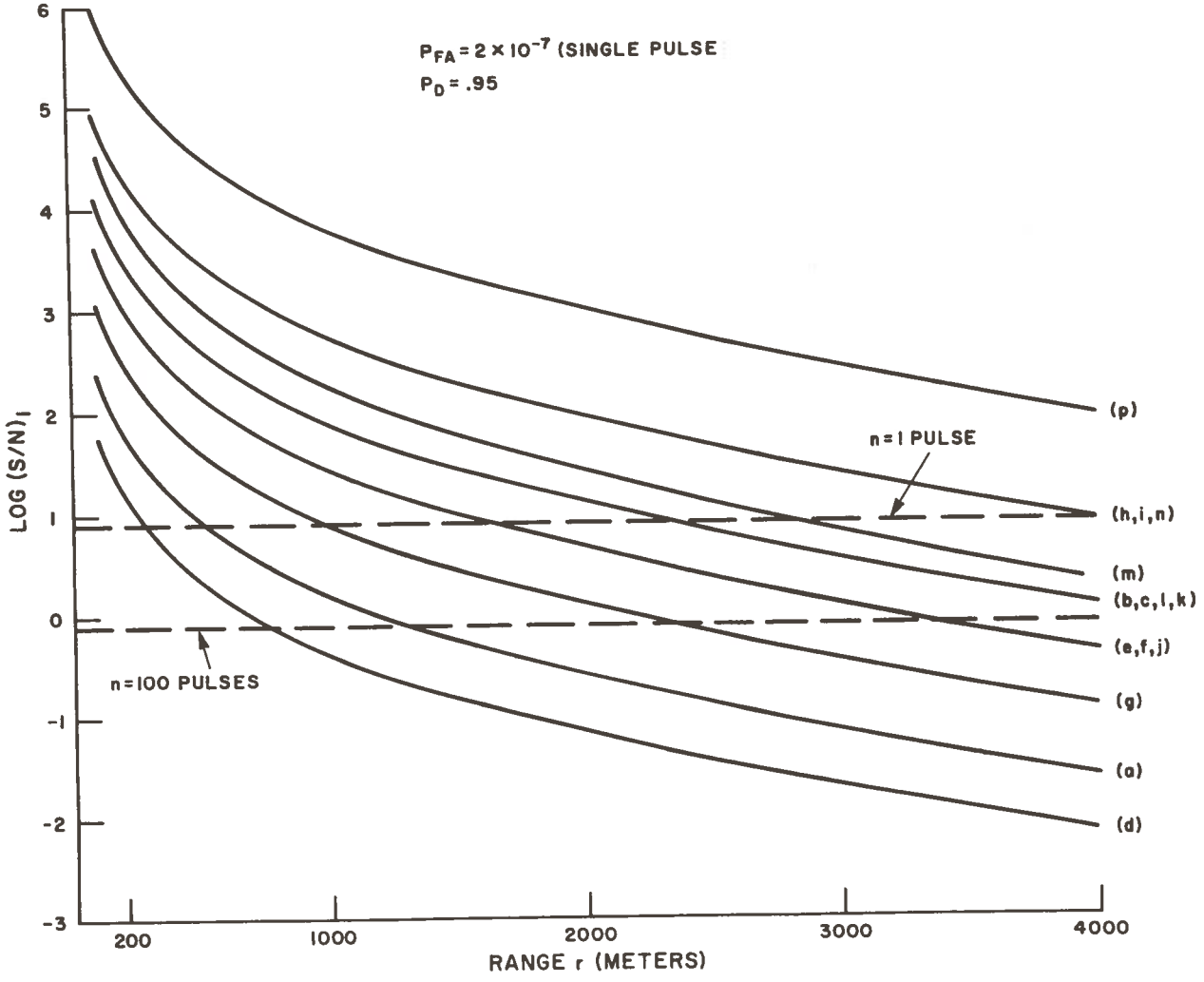

Figure 4.7.- Signal-to-noise (single pulse basis) vs fog bank range, *at night*, for transmitter-detector combinations given in Table 4.4. Horizontal lines indicate levels required to satisfy criteria $P_{FA} = 2 \times 10^{-7}$, $P_D = 0.95$, for single pulse (n=1) and average of n = 100 pulses.

4.7 SUMMARY

Figures 4.6 and 4.7 reveal a wide variety of performance for the laser-detector combinations examined. It must be remembered that the curves represented there do not of themselves lead to a practical fog bank detector solution. For example, the maximum range for given S/N is obtained with the erbium laser-germanium APD detector combination (curve p). As we have pointed out in Section 3.3.3, however, the erbium laser is still somewhat developmental and, more importantly, the germanium detector is inconvenient due to its extremely small size. Also, the nitrogen laser, though not included in the preceding analysis, would presumably rate well on the basis of S/N return. The bulk and complexity of this laser, however, and the lack of information on its scattering properties has led us to exclude it.

The combinations which follow the erbium system in order of *range effectiveness* are:

Group A: (h)Nd:YAG CW Q-switched/Si APD; (i) Nd:glass/APD; and (n) ruby/ERMA.

Group B: (m)GaAlAs (8600Å)/APD; (b)YAG CW Q-switched/S-1 photomultiplier; (C) Nd:glass/S-1 photomultiplier; (e) YAG CW Q-switched/p-i-n; (f) Nd:glass/p-i-n; (k) GaAs (9050Å)/APD.

Group C: (g)YAG flash pumped/APD; (j) GaAs (9050Å)/ERMA; (l) GaAlAs (8500Å)/ERMA.

Group D: (a) YAG flash pumped/S-1 photomultiplier; (d) YAG flash pumped/p-i-n.

The above groupings are used for the convenience of discussion, but it should be obvious that they are not strictly ordered. In particular, differences between day and night characteristics affect the order. Also, the repetition rate and/or number of integrated pulses will affect the order rather strongly.

The best candidate, based on *range capability*, is the Nd:YAG CW Q-switched laser with a silicon APD. Since the laser is capable of high repetition rates, the improvement in S/N with pulse averaging is significant. However, this system is considered *undesirable* for several reasons:

1) The CW Q-switched laser is at least 50% more expensive than the flash pumped laser.

2) The lamp life in the CW system is shorter.

3) Power consumption is an order of magnitude higher for CW than for flash pumped operation and the cooling requirements are greater.

4) Because of the complexity of the CW Q-switching, one expects it to be more susceptible to breakdown than the simpler flash-pumped system.

In addition to these points, the YAG laser presents a difficulty shared by all the solid state lasers (Nd and ruby) with small, highly collimated output beams. One of the assumptions underlying the preceding systems calculations was that the beam be large enough to be eye-safe. We chose as the output diameter 10", and to attain this size, magnification of approximately

50-100 times is required! This would necessitate optical systems which are cumbersome, lengthy and difficult to keep in alignment. If the diameter of the output beam is reduced, on the other hand, the safe output power is less by the *square* of the reduction factor (see Figure 4.1) and the range capability of the system is quickly compromised.

These are some of the reasons that we favor the *GaAs laser* system for fog bank detection. In addition, GaAs has other advantages in that:

1) A system employing a diode array can easily be adapted to state-of-the-art improvements. As more powerful arrays or smaller source sizes become available, these can be substituted for the older array with a minimum of difficulty.

2) The emission angle of GaAs diodes can be matched conveniently to reasonably-sized optics.

3) The presently attainable power from GaAs arrays ($\leq$500 watts out of optics) is below the safe limit and source improvements would lead directly to increased range capability.

4) The pulse width of the output is variable to some extent, allowing some flexibility in system parameters for optimizing the return signals.

The avalanche photodiode appears to be superior to photomultipliers in the 8600 - 9000Å region, especially for background-limited operation.

With the assumptions of Sec. 4-6, the maximum range of detectable fog banks is about 3000 meters for a kilowatt GaAs system

(integrating 100 pulses). The field of view was taken to be 10 mrad and the realization of smaller source sizes will facilitate angles down to about 3 mrad. This reduction in angle leads to a three-fold increase in S/N, for background-limited devices. On the other hand, the enhancement would reduce receiver optics (diameter) requirements by three, for the same S/N.

5.0 TWO CANDIDATE FOG BANK DETECTORS

5.1 INTRODUCTION

As has been discussed in Section 3.0, optical backscattering (LIDAR) and infrared radiometry are practical methods for sensing the presence of fog banks. Both methods, with different degrees of complexity and reliability in their implementation, could also be designed to measure the range of a fog bank.

We now describe in detail a complete LIDAR fog bank detector system and an infrared radiometric system. The LIDAR is to have a range capability of at least 3 km (day or night). It will operate only when energized by a signal (derived from the Videograph) indicating that general visibility is greater than a given value. Although this value is flexible and easily altered in the field, it should be recognized that operating the LIDAR under low visibility conditions will compromise the performance reliability. For the design given below we have taken the minimum operating visibility to be 8 miles.

5.2 LIDAR FOG BANK DETECTION SYSTEM

The LIDAR system proposed employs a GaAs laser diode array for the transmitter source. The array will emit at a repetition rate of 500 pps, with peak power of 1 kwatt and pulse widths of approximately 150 nsecs. The transmitter optics (reflective) provide a 10" diameter output beam which will be eye-safe. The receiver optics, also reflective, collect light backscattered from

fog banks and/or background radiation. This radiation is focused onto a photodetector, after passing through a narrow band optical filter.

A block diagram of the entire LIDAR fog bank detection system is shown in Figure 5.1.

The GaAs source array is driven by current pulses from the modulator. The modulator is gated by a timing signal (see letter (B) in Figure 5.1) derived from the transmitter clock (A). This clock also gates the photodetector "on" (C), after a delay of about 300 nsec which serves to reduce the atmospheric backscatter seen by the detector. The phototube remains on for the duration of the maximum round trip of a pulse ($\sim$40 μsec for a 3 mile range). This "on" gate occurs at twice the rate of the source modulator. Thus the receiver is looking half the time at "signal plus background" and the other half at only "background". The background is detected (H) and its average value (I) is compared to a fixed reference voltage V_1. The gain of the photodetector is thereby "leveled", ensuring that the background noise, by itself, will not exceed the threshold for fog signals, and preventing false alarms.

The video occuring during the 40 μsec "detector on" interval is fed to the range gate (G) where only the video signal within the 200 nsec gate width (F) is allowed to pass to the box car. The narrow range gate slowly sweeps through the 40 μsec detection interval, the entire sweep taking 15 seconds.

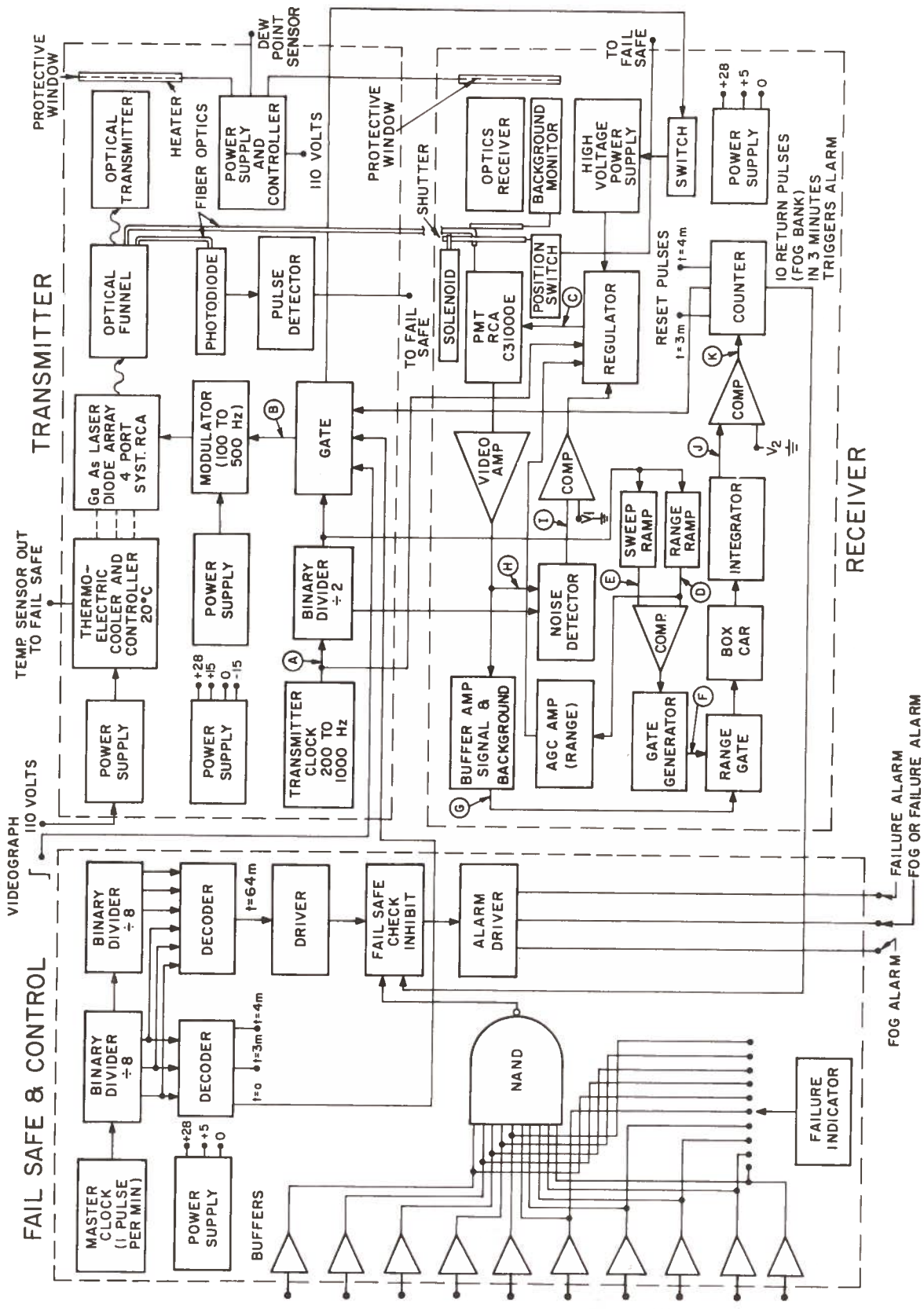

Figure 5.1.- LIDAR fog bank detector: system block diagram.

The box car output is integrated over approximately 100 "signal" pulses for a given range. A "fog detection event" occurs if the integrator output (J), averaged over these 100 pulse periods, exceeds a threshold, (ref. V_2). Each "detection event" produces a comparator output pulse (K) which is fed to the counter.

In the absence of a fog bank, the transmitter is normally "on" for 1 minute in every eight. If there are 3 "detection events" during this one minute interval, the transmitter is left on another two minutes. If, during the entire 3 minute interval, 10 "events" are recorded by the counter, the alarm is activated. The alarm will continue to operate for 12 minutes after the last "10 count" of events. The transmitter remains on during the alarm condition. The alarm is thus delayed from sounding for three minutes after the first "event", and delayed from being turned off until 12 minutes after the fog has disappeared.

The *fail-safe and control system* functions to ensure that a failure of essential components or critical voltages will result in a failure alarm condition. This system monitors certain conditions continuously and others at 64 minute intervals, as described below. The control system contains the master clock which provides timing sequences related to the fog bank alarm and self-check circuits.

The timing sequences which synchronize the fog bank detector logic are shown in Figures 5.2 and 5.3. The time channels are labeled to correspond to the symbols used in Figure 5.1.

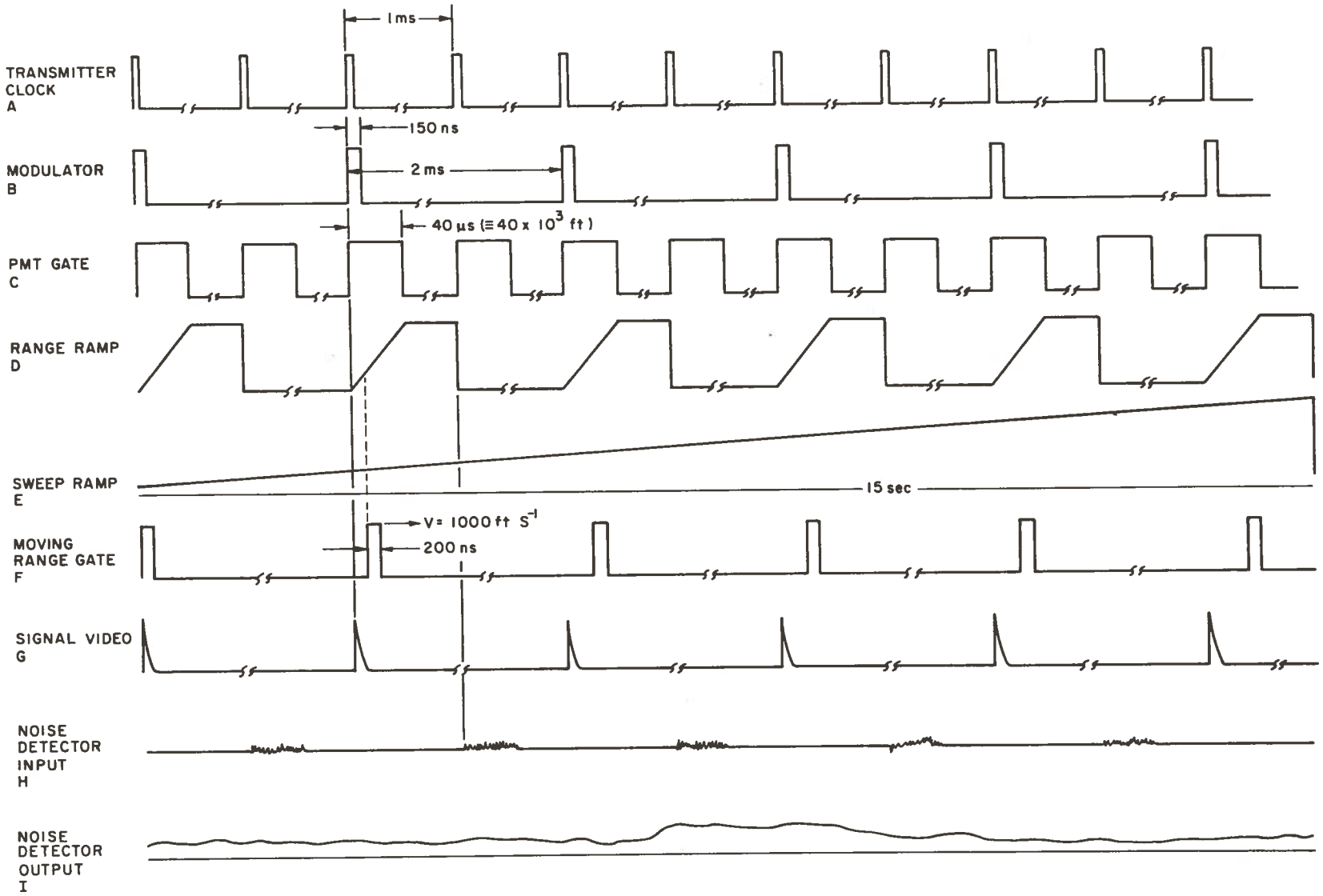

Figure 5.2.- LIDAR fog bank detector: timing sequence.

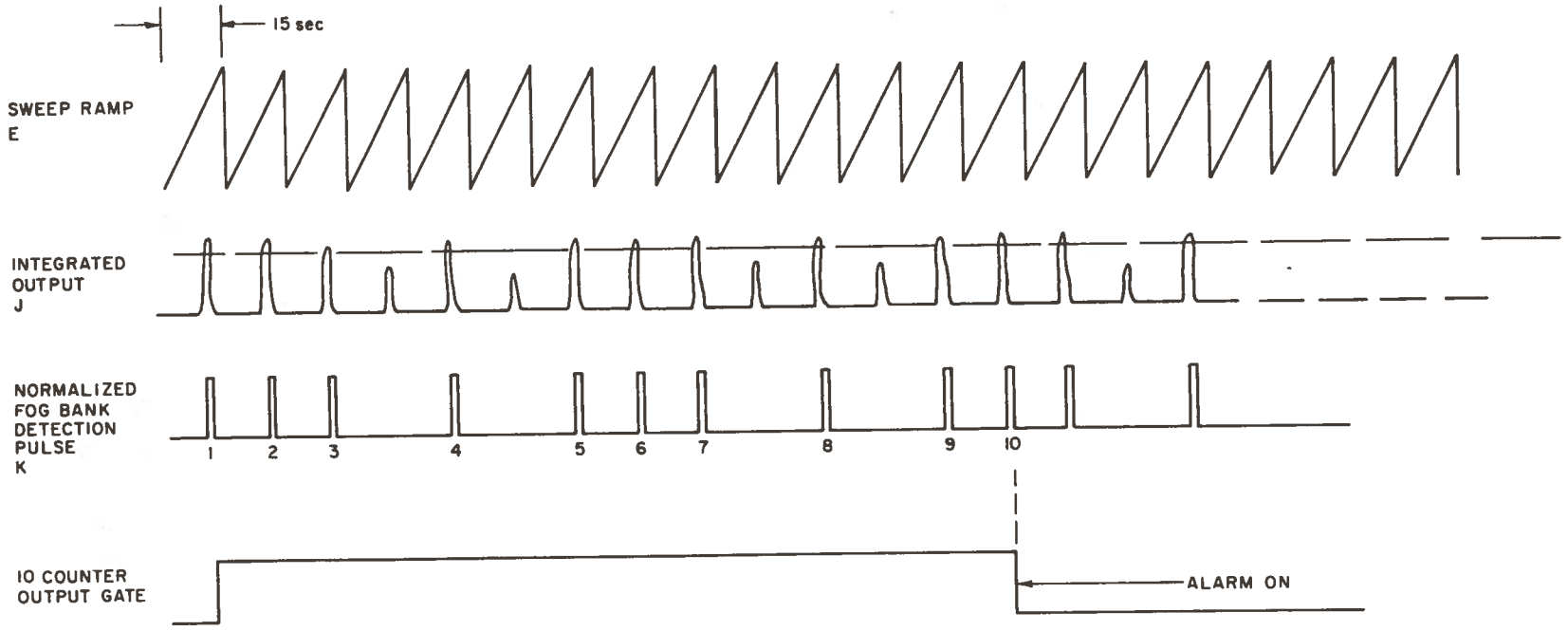

Figure 5.3.- LIDAR fog bank detector: timing sequence continued.

5.2.1 Fog Bank Sampling Program

The fog bank detector will operate only when the Videograph indicates visibility greater than 8 miles.

Case A: The transmitter operates for a period of one minute at intervals of eight minutes. If no fog bank is detected during the sampling period (1 minute) this sequence continues. (See Figure 5.4).

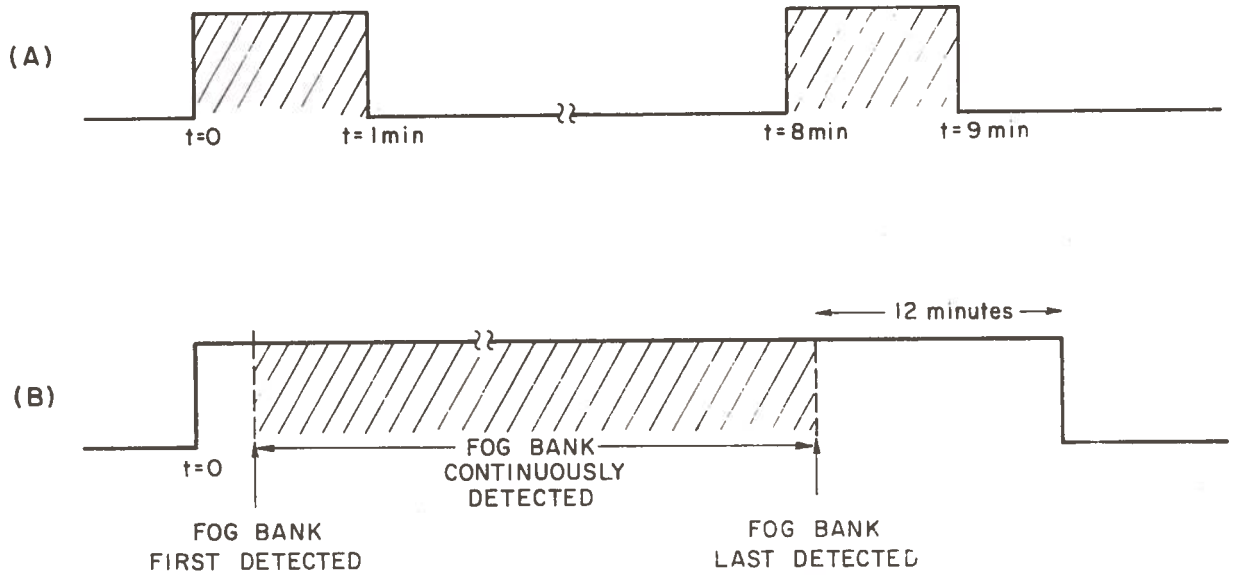

Figure 5.4.- Sampling program for the LIDAR fog bank detector: A) Visibility greater than 8 miles and no fog bank. B) Fog bank detected; in this case, the completion of the sequence is independent of the master clock.

Case B: In the course of the search sequence (Case A above), a fog bank is detected (i.e., 3 or more integrated returns exceed threshold in the one minute interval.) From that time the transmitter sequence is independent of the master clock and the

transmitter will continue sampling until 12 minutes after the last detection event, (Figure 5.4). If a total of 10 detection events occurs in 3 minutes the fog alarm is initiated, as shown in detail in Figure 5.5.

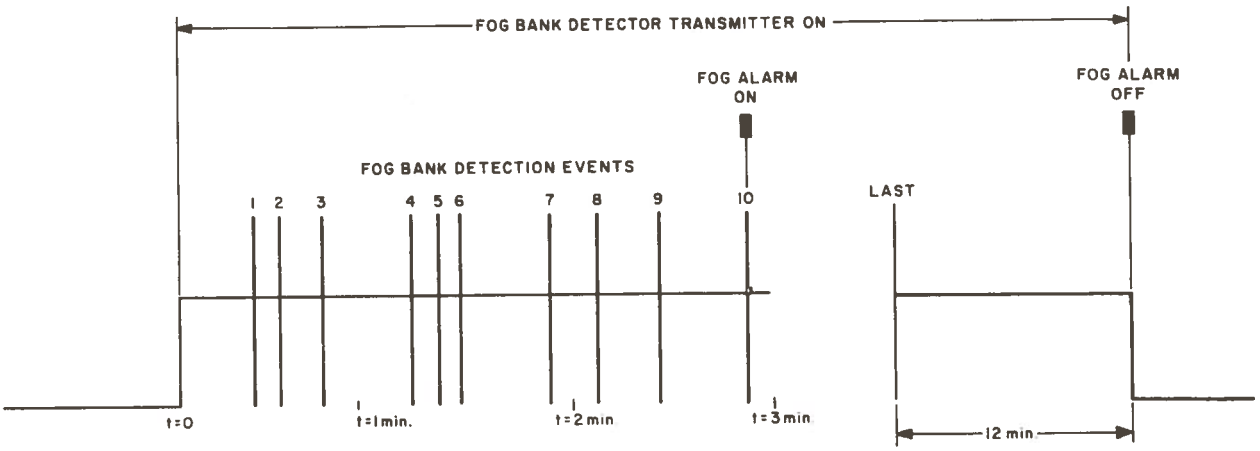

Figure 5.5- Initiation of fog alarm by LIDAR detection events: When three or more fog bank detection events occur during any one minute of the transmitter sampling cycle (Case B, Fig. 5.4) the transmitter continues operation. If 10 events are recorded within 3 minutes, the fog alarm is initiated and remains "on" as long as the rate of detections remains at or above this value. The alarm will be turned off 12 minutes after the detection rate falls below the prescribed value.

Timing Cycle: The master clock consists of a 1 ppm oscillator and two ÷ 8 circuits. The first ÷ 8 circuit is decoded and signals from the decoder occur for one minute intervals every 8 minutes. These signals are: t = 0 which exists from "0" time to

of the ÷ 2 goes to the laser modulator through the gate. The gate is opened for one minute every 8 minutes during the search operation.

Video Section of the Receiver: The incoming light is detected by the photomultiplier and amplified in the video amplifier. The video amplifier feeds two buffer amplifiers: one, a fast response channel for video; the other, a slow response for background noise. The video channel feeds the signal processor circuits and the noise channel feeds the automatic gain control amplifier.

The AGC amplifier receives information from the noise channel of the video amplifier and from the transmitter pulse. The gain of the photomultiplier is adjusted by varying the high voltage depending on the noise level. This is referred to as Noise AGC.

A different form of AGC is obtained from the range ramp. The receiver gain is increased with increasing position of the range gate. This improves the dynamic range characteristics.

Video Signal Processor: The moving range gate is generated by comparing two analog ramps, one of which is synchronized with the modulator and the other being a slow (15 second) free running ramp, (Figures 5.1 and 5.2, (D) and (E), respectively.) When the level of the fast ramp equals that of the slow ramp the comparator output triggers the range gate with a "one-shot" pulse, approximately 200 nsec wide.

Since the slow ramp is constantly changing, the trigger point of the comparator is changing, thereby moving the range

gate with respect to the start of the range ramp, i.e., the occurence of the laser pulse.

The video which passes the range gate is sampled by the box-car (a peak detector pulse stretcher) and then passed to the integrator. If the integrator output reaches a prescribed threshold, the comparator triggers and this causes a count to be recorded in the counter.

Counter Circuits: The counter circuits serve to minimize false alarms, and to delay the turning on and off of the fog alarm.

The return signal from the integrator feeds a 4 bit binary counter, which is reset at the 3 minute interval.

If the counter receives 3 pulses during the one minute "transmitter-on" interval, it sets a flip-flop whose output goes to the transmitter gate, keeping the transmitter on for a total of 3 minutes. If during the 3 minute interval the counter receives 10 pulses, the signal is entered into the shift register. The shift register serves as a further turn-on delay and turn-off delay. These delays are adjustable in 3 minute intervals to 12 minutes.

5.2.2 Optical System

Transmitter and Receiver Optics: The optics for both the transmitter and the receiver will be of the two-mirror type. The mirrors will be manufactured from Tenzalloy, an alloy of aluminum and magnesium, which has excellent structural stability and can take day and night temperature changes without distortion.

The ground and polished Tenzalloy is then coated with a 2 mil (.002") layer of Kanogen. This material is hard and chemically very stable. It can be well polished, and the polished surface gives low scattering due to the amorphous structure of the Kanogen.

The reflective coating will be a thin layer of gold. In order to aid in the adhesion of the gold, a thin layer of inconel is evaporated onto the polished Kanogen surface. Finally, an overcoating of SiO is applied to the gold to prevent weathering and scratches.

Optical "Packaging": The criteria which guided the choice of optical configuration are two-fold:

1) It seems likely that the technology of GaAs lasers will develop in the next few years. By designing the transmitter to accept the GaAs array as a plug-in unit, later versions can be substituted for more power, smaller source size or lower cost. Furthermore the transmitter and receiver will be in two separate blocks with a minimum of interconnections, increasing the system flexibility.

2) The optics will be separated from the electronics, providing more reliability and ease of servicing. The front half of the receiver will contain the optics in a sealed compartment and the back part will hold the electronics as a plug-in unit.

Windows: Protective windows will be provided for both transmitter and receiver to keep moisture, dirt and salt spray out of the optics. The optical chambers will have dessicants for

eliminating moisture and can be filled with an atmosphere of dry nitrogen if necessary.

The windows will be heated to keep their surface temperature above the dew point. Two heating options are available:

1) The window surface can be made electrically conductive by depositing a thin metal film uniformly and circulating a current through it.

2) A grid of vacuum deposited metal can be used to conduct the heating current.

Either of these methods require much less electrical power than surrounding the window circumference with a heating element and relying on thermal conductivity to warm the window. Optical distortion is also much less.

5.2.3 Specifications: LIDAR Fog Bank Detector

Transmitter

Wavelength	9050 A	8500 A
Source	GaAs	GaAIAs
Configuration	square array	
Average power	7.5×10^{-2} w	
Peak power	1 kw	
Pulse width	150 nsec	
Pulse repetition rate	100 to 500 pps	
Beam aperture	10 inches	
Beam divergence (full angle)	1^{o} ($\sim$15 mrad)	
Equivalent focal length*		
Optical configuration	two mirrors	
Optical material	Tenzalloy + Kanogen	
Optical coating	inconel + gold	
Optics protective coating	SiO	

*To be specified in final design

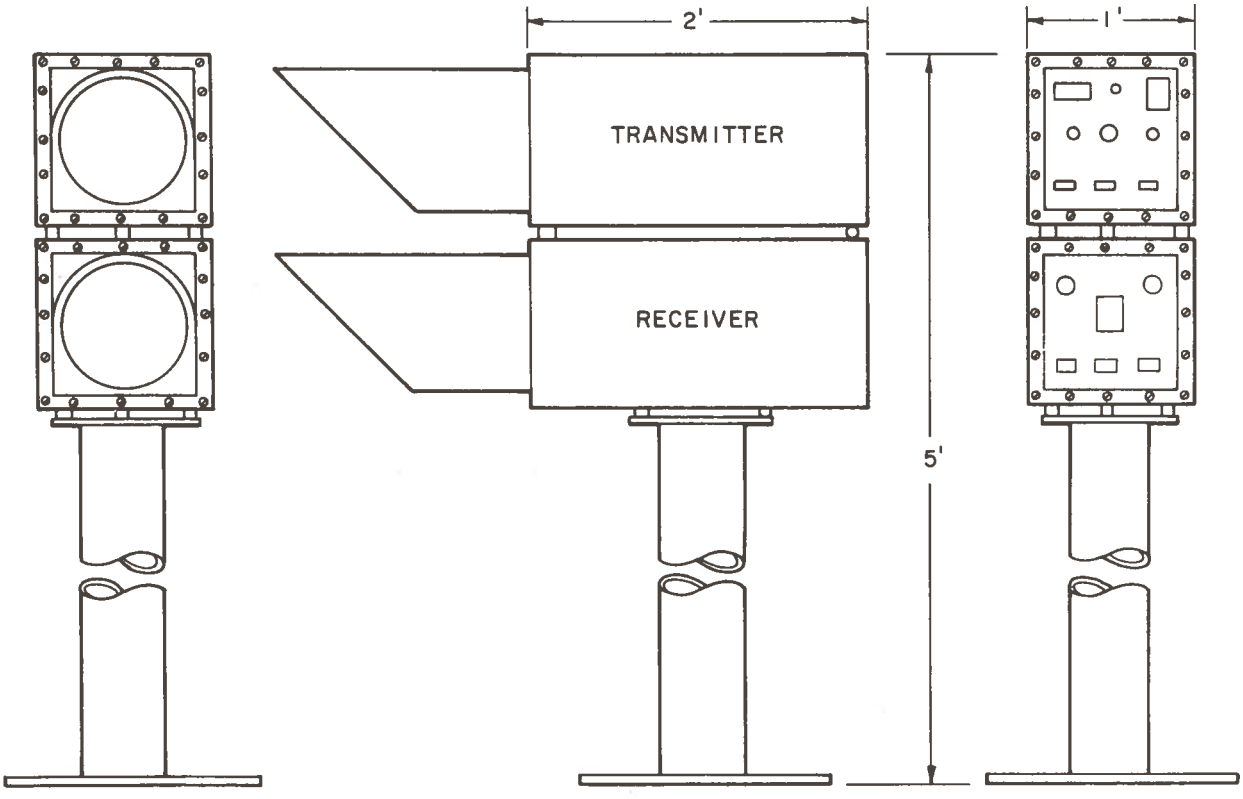

Figure 5.6.- Housing and pedestal for proposed LIDAR fog bank detector

Optical finish	λ
Optical compartment	sealed; dessicants added
Equivalent f/number	1
Protective window*	
Baffle*	
Temperature controller (laser diode array)	
Temperature setting	30°C
Temperature regulation	±2°C
Power	105-120 V, 60 Hz, 30 w

Power to heat protective windows*	
Maximum size*	
Weight*	

Receiver:

Wavelength	8500 A (if GaAlAs source) 9050 A (if GaAs source)	
Interference filter		
Bandpass	100 A	
Transmittance	70%	
Color filter	Schott RG 10; 3 mm.	
Beam aperture	10 inches	
Beam divergence (full field of view)	adjustable	
Equivalent focal length		
Optical configuration	two mirrors	
Optical material	Tenzalloy + Kanogen	
Optical coating	inconel + gold	
Optics protective coating	SiO	
Optical finish*		
Equivalent f/number*		
Protective window*		
Detector		
Type	Avalanche photo-diode silicon (G.E.)	RCA PMT C31000E
Spectral response	---	ERMA
Sensitive area (diameter)	3 mm	45 mm
Responsivity	3.3×10^{5} VW^{-1} @ 9000 A	20×10^{-3} AW^{-1} @ 8500 A 7×10^{-3} AW^{-1} @ 9050 A
NEP	5.5×10^{-14} WHz$^{-1/2}$ @ 9000 A	
Dark current (anode)		10 nA @ 30 A/lumen

Maximum voltage for above characteristics	2500 V
Power	105-120 V, 60 Hz, 30 w
Maximum size*	
Weight*	

Fail Safe and Control:

Fail Safe 100% of the time:

Line voltage, 110 v

Temperature of GaAs array

Power supply, +28 v

" " , +15 v

" " , -5 v

" " , -15 v

Fail safe sequentially (1 minute every 64 minutes):

Laser output

Receiver (using laser light coupled via fiber optics).

Position of photomultiplier shutter

Control:

Transmitter operates only at specified temperature.

Transmitter operates only with a signal from Videograph.

Photomultiplier shutter closes only when background is high.

Fog alarm: Relay, DPDT contacts, 3 A max, 110 V.

Failure alarm: Relay, DPDT contacts, 3 A, 110 V

Failure indicator:

Read out edgewise panel meter	Bad--Marginal--Good
Rotary switch selector to locate failure	12 positions

Enclosure

Material: Aluminum 6061-T6
Aluminum 356-T77 (casting)

Finish: Iridite MIL C 5541 for all parts that require electrical conductivity.
1 coat zinc chromate MIL 8585
Outside: 2 coats vinyl medium texture finish, Federal color # 26373; baked.
Inside: Parts enclosing optical path, 1 coat air-dried 3M Velvet black #101.

Hardware: All stainless steel.

Finish: Chromic acid anodize, type 1 MIL 8625 for all parts that do not require electrical conductivity. Painting same as for other parts.

Environmental Performance

Operating conditions:

Temperature	$0^{o}C$ to $50^{o}C$
Humidity	Up to 95% at $40^{o}C$

Vibration	Normal handling
Degree of enclosure	Drip proof, corrosion resistant
Non-Operating conditions	(packaged for shipment)
Temperature	-40°C to +75°C
Humidity	Up to 100% at 75°C
Shock and vibration	special handling

5.3 INFRARED RADIOMETER FOG BANK DETECTION SYSTEM

The use of infrared radiometry to detect fog banks depends on the existence of a difference in radiance between the sea and the fog bank, as described in Section 3.0. The radiometer must be mounted at a sufficient height above sea-level to avoid observing the sea at a grazing angle. (The system proposed assumes a height of approximately 20-30 meters.)

Figure 5-7 shows a block diagram of the proposed radiometric fog bank detector. The system will have reflective optics and the energy collected will be fed to an infrared detector of the thermal type (thermistor, thermocouple, etc.) This detector will be enclosed in a reference black body cavity. In addition to the detector, the reference cavity will contain a bandpass filter with a 1 micron bandwidth, centered at 9.5 microns, and a tuning fork. A mirror mounted on the tuning fork switches the radiation seen by the detector such that 50% of the time the detector sees the field of view subtended by the optics and 50% of the time

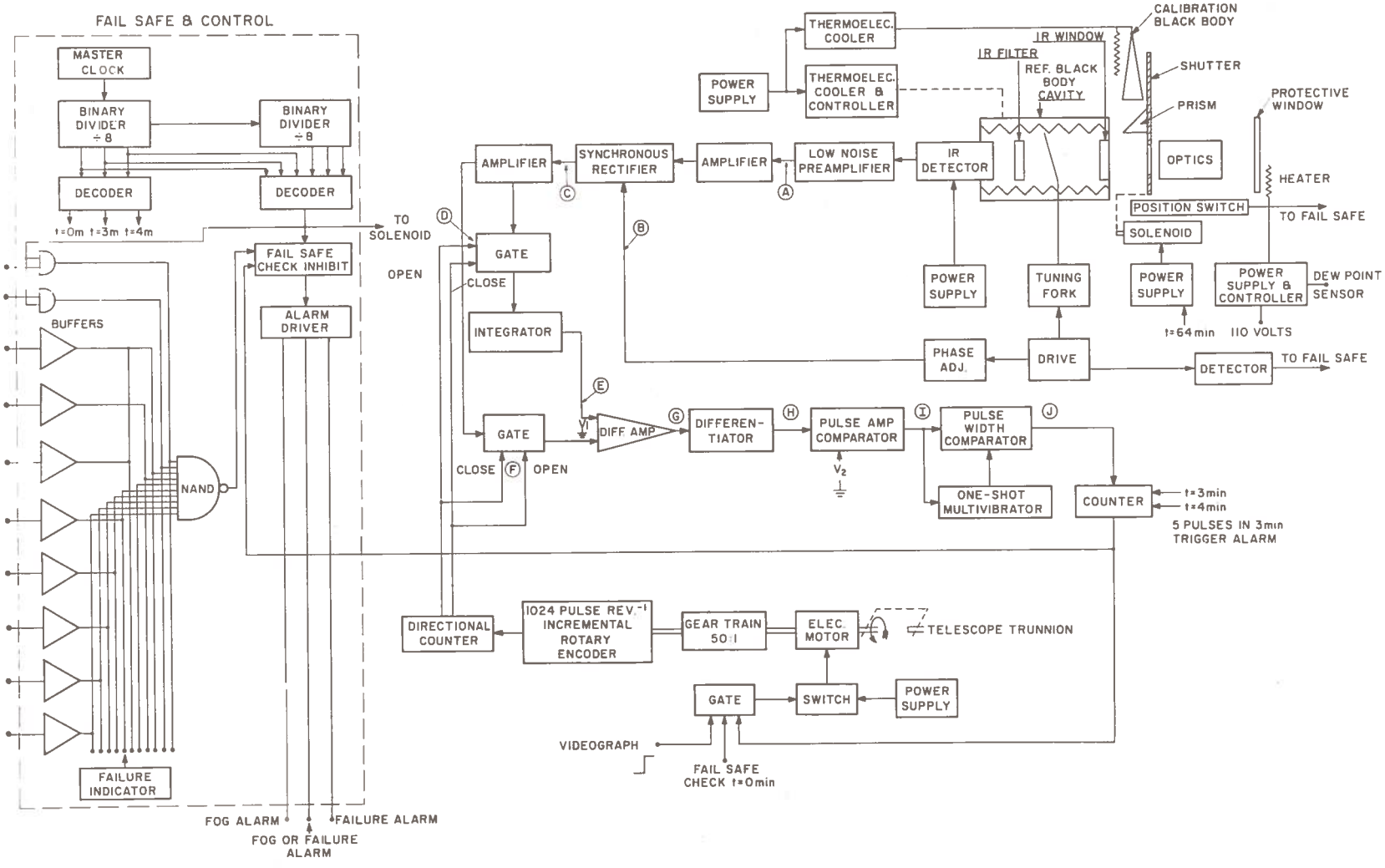

Figure 5-7.- Infrared radiometer fog bank detector: system block diagram.

it looks at part of the reference black body. The black body will be sealed with an infrared-transmitting window.

The tuning fork will operate at a frequency between 10 and 20 Hz. The detector output will be amplified by a low noise preamplifier and then be fed to an amplifier which in turn feeds a phase-sensitive rectifier. The rectified output will be a signal proportional to the difference in radiance between the optical field of view and the reference black body. Since the temperature of the reference black body cavity will be kept constant using a thermoelectric cooler and controller, the signal will be proportional to the irradiance of the area of the optics.

The instrument will scan in a fixed vertical plane, starting at an angle a few degrees below the horizon (looking at the water) and continuing through the horizon and above it by 2 or 3 degrees. During the first 300 yards (approx.) of scanning on the water, the instrument establishes a reference level. Beyond this point the instrument continues to measure the radiance subtended by the field of view of the optics. If the radiance is constant, the output of the system is zero. If at a certain point along the scan the signal increases, the electronic circuitry processes the difference between the reference and the increasing signal. See Figure 5.8.

If the increasing signal satisfied certain criteria, with regard to its rate of increase with scan angle, etc., the instrument will indicate that detection of a fog bank has occurred.

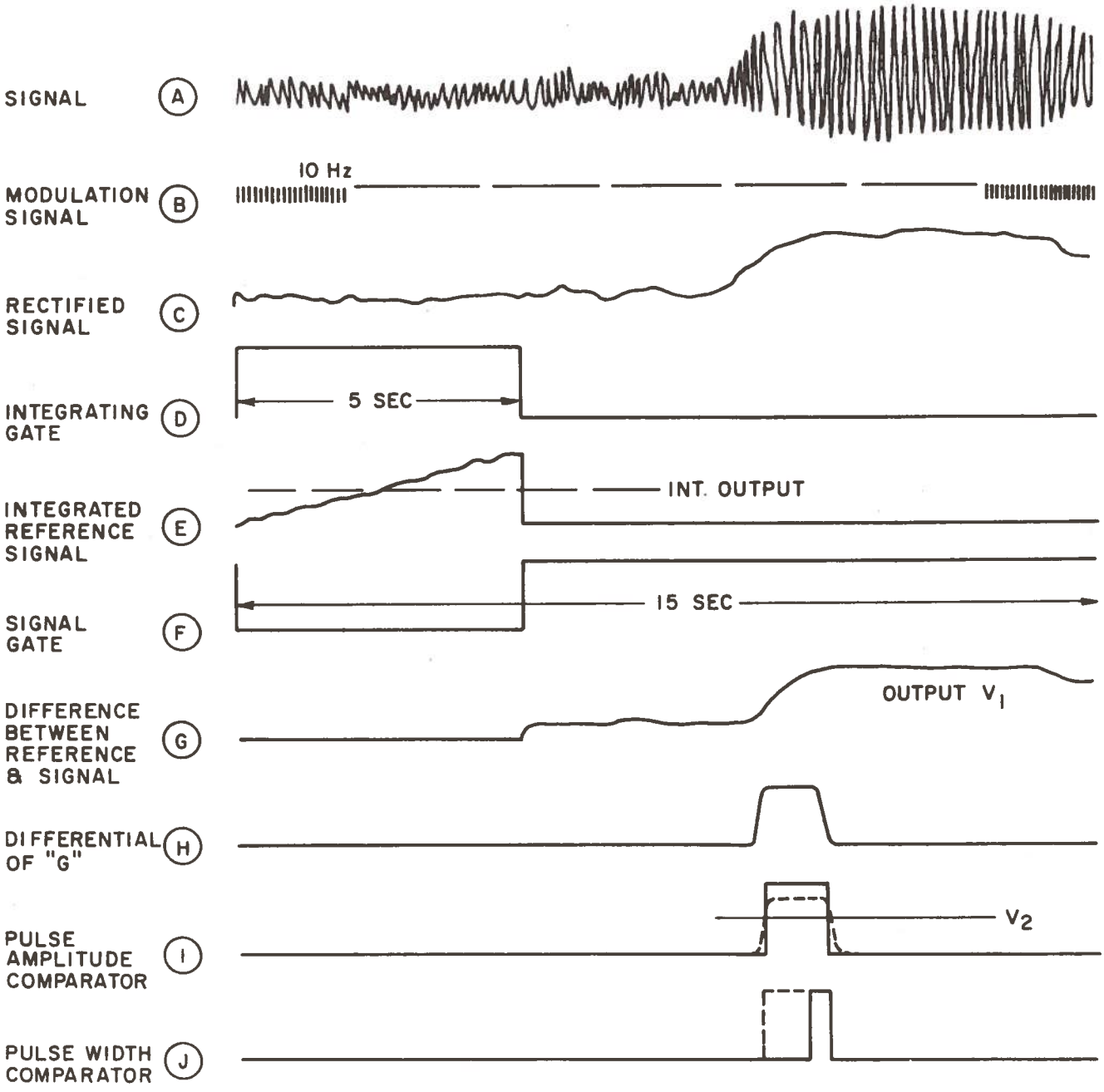

Figure 5.8.- Infrared radiometer fog bank detector: timing sequence.

The criterion for a positive fog bank identification (and initiation of an alarm) will be that at least 4 or 5 of these signals occur within a time of 3 minutes. The search mode and sampling sequence (Figure 5.9) as well as the "turn-on" criterion for the fog alarm (Figure 5.10) are similar to those proposed for the LIDAR Fog Bank System.

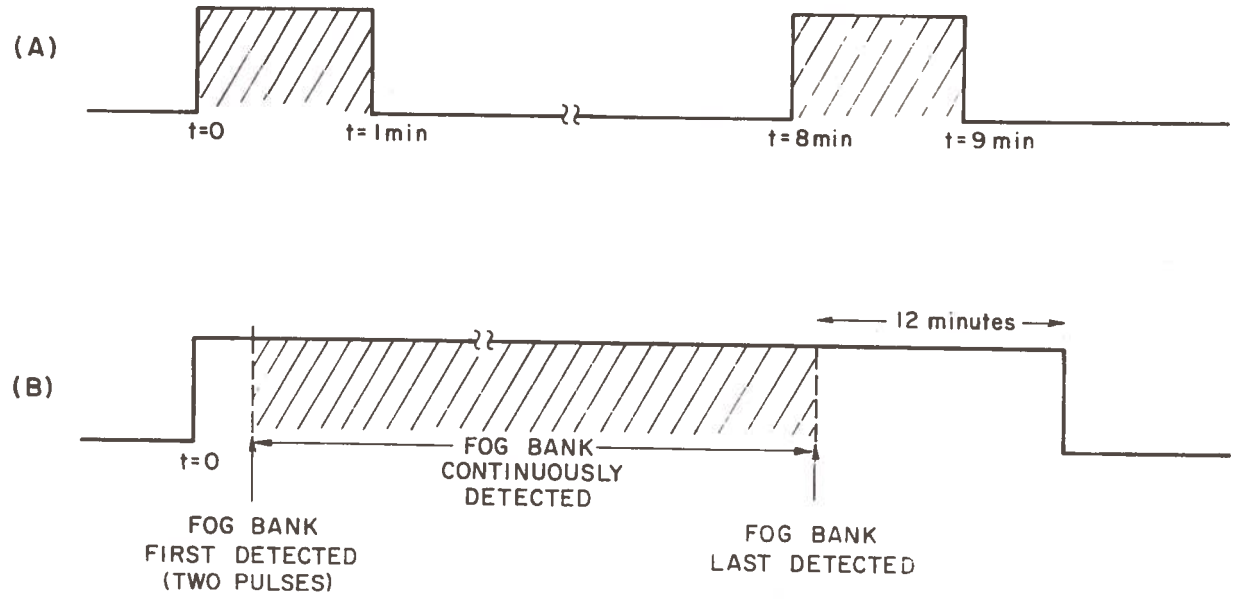

Figure 5.9.- Sampling program for the infrared radiometer fog bank detector: A) Search mode (Videograph indicates "good" visibility). No fog bank. B) Fog bank detected: Sampling sequence becomes independent of master clock.

The system will be self-calibrating and will be provided with fail safe circuitry similar to that proposed for the LIDAR detection system.

For calibration purposes, a calibration black body cavity (15^{o} cone) is periodically introduced in the field of view of the

radiometer. Since this cavity and the reference black body are temperature controlled the radiometer will "see" a constant IR signal independent of changes of environmental temperature.

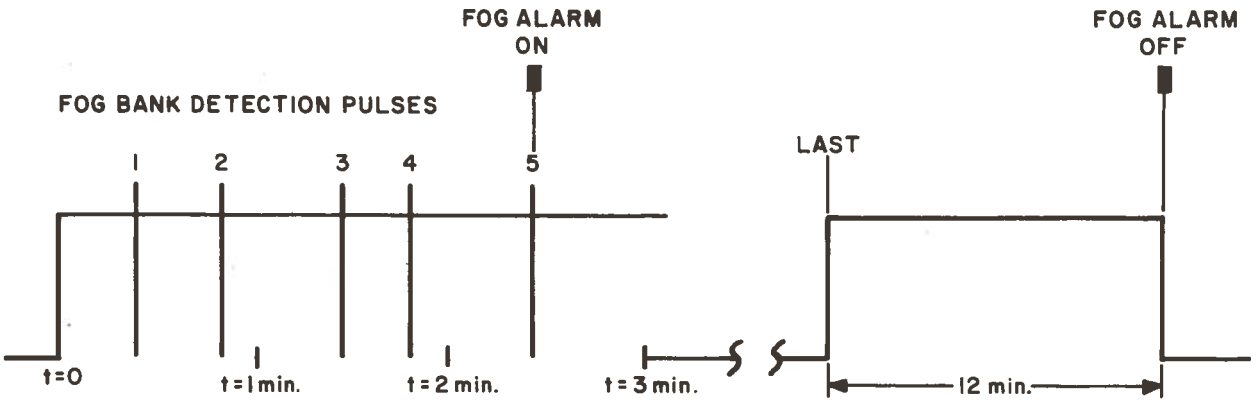

Figure 5.10.- Initiation of fog alarm by the infrared radiometer detection events: When two detection events or pulses occur during a one minute search interval (i.e., during two successive angular scans) the instrument continues to scan (see Fig. 5-9, case B). If 5 pulses are counted within 3 minutes, the fog alarm is turned on and remains "on" as long as the rate of detections remains at this value. The alarm will be turned off 12 minutes after the detection rate falls below the prescribed value.

The instrumental embodiment of the infrared radiometric fog bank detection concept has been described in considerable detail above. However, the design of this system has been based on assumptions which need verification. One such assumption, for example, relates to the magnitude and profile of the temperature gradient between the sea and the fog bank; another, to the relatively constant emissivity of the sea surface. The ability of the proposed system to sense fog banks by "slope" detection depends strongly on these assumptions.

Furthermore, the timing sequences and intervals are tentative for similar reasons. The field tests suggested in Section 6.0 are designed to provide information in these areas.

5.3.1 SPECIFICATIONS: Infrared Radiometer Fog Bank Detector

Wavelength	9.5 microns
Bandpass (50% points)	1 micron
Beam aperture	6 inches
Beam divergence (full angle)	2 mrad
Equivalent focal length*	
Optical configuration	2 mirrors
Optical material	Tenzalloy and Kanogen
Optical coating	gold
Reference black body	15° grooves
Reference temperature	adj. 20 to 25°C ±0.5°C
Calibration black body	15° cone
Calibration temperature	adj. 20 to 50°C ±1°C
Infrared detector	thermal detector
Modulator	tuning fork
Modulation frequency	10 to 20 Hz.
Protective window*	
Power*	
Power to heat protective window*	
Complete scanning cycle	15 seconds
Maximum size*	
Maximum weight*	

Fail Safe and Control

Fail safe 100% of the time:

- Line voltage
- Temperature sensor (reference cavity)
- temperature sensor (calibration black body)
- power supply, +28 v
- " " , +15 v

*To be specified in final design

Power supply, -5 v

power supply, -15 v

Fail safe sequentially (1 minute every 64 minutes):

Reference signal

Others

Control:

Sampling sequence begins only with appropriate signal from Videograph

Instrument operates only if both black body cavities within specified operating temperatures.

Enclosure and Environmental Performance:

Similar to those of the LIDAR system

6.0 SUMMARY AND RECOMMENDATIONS

After a careful analysis, the number of suitable techniques for fog bank detection has been reduced to two: the laser "radar", using a GaAs transmitter, and an infrared radiometer.

GaAs LIDAR was chosen as the best combination of safety, efficiency, range effectiveness, reliability, convenience and cost. Its likelihood of success is good, based on results obtained from optical radar work on *clouds*.

The IR radiometric detection scheme is at this point still experimental. Preliminary results included in Sec. 3.2.2 indicate that the radiometric scan has a strong potential for detecting the temperature differences between large masses of fog and water. If, in fact, fog bank temperatures are consistently different from the neighboring water surface, and if the interfaces are sufficiently well-defined, infra-red passive sensing may provide a more effective, and considerably simpler and cheaper, method of fog bank detection than optical radar.

It is our recommendation that specification of a final fog bank detector design be delayed pending the outcome of an *in situ* test program. This test program is to be performed on the West Coast during the season of frequent fog bank occurrences. According to Coast Guard personnel, this would be late summer and early fall, for example, at Point Bonita, California. Thus experiments could be analyzed and final decisions made by the end of the calendar year 1971.

The *in situ* tests will be performed with a Nd:glass or ruby laser and the IR radiometer discussed previously. Thus we will be able to compare the effectiveness of the two techniques side-by-side. The information we hope to obtain includes:

1) The *optical depth* and *boundary profile* of real fog banks. This will allow us to determine return pulse width and shape and to design appropriate transmitter pulse widths and receiver gates.

2) The magnitude of the typical *background radiation* on days when visibility is good. In particular, we wish to find if the optical detector will be background-limited, as has been assumed in our earlier calculations, and how the background varies from day to day. The results will indicate whether a photomultiplier or Si APD is the best detector to use.

3) The characteristics of "near-field" backscatter from the atmosphere, on good visibility days. This will aid in specifying the laser transmitter-receiver relative beam geometry and/or the optimum "inhibit" time for the receiver electronics.

4) The general properties of fog banks which determine how precisely one must search for them. These include the width and height of the "front"; the distance, if any, between the sea surface and the "bottom" of the fog bank; and the rate of motion of the fog mass.

5) The range of effective temperature *differences* between fog and sea surface or between sea surface and sky, e.g. This is relevant to the infra-red method.

6) Meteorological conditions accompanying fog bank occurrence. Are there characteristics of "fog bank weather" which have been overlooked but which might have a bearing on detection methods? For example, the humidity may be locally high in a layer near the sea, influencing the infrared emission characteristics and perhaps also causing scattering of optical signals in excess of that predicted from the value of general visibility.

7) Depending on the definition with which signals can be seen, the degree of signal processing required can be determined. This is particularly important for the IR radiometer, where the degree of complexity of interpretive electronics can significantly affect the price.

The experiments are planned tentatively for the months of August and September, with actual tests taking approximately 3-4 weeks (depending on weather) and perhaps 2-3 weeks taken up in the packing, moving, unpacking and set-up time. At the conclusion of the experiments, the data will be assessed and the results summarized. A technical summary with final system recommendations will be prepared and presented soon thereafter to the Coast Guard.

APPENDIX A - INFRARED RADIOMETER: EXPERIMENTAL DETAILS

Some details of the IR radiometer, discussed in Ch. 3, are given in this appendix.

The instrument consists of an infrared spectrometer (Perkin-Elmer Model 99), and a telescope which forms the image of a distant scene on the slits of the spectrometer. The telescope is mechanically scanned at a rate corresponding to 3^{o}/min. by a motor drive. The optical system is shown in Fig. A.1. A NaCl window is used to isolate the spectrometer from thermal gradients and air currents.

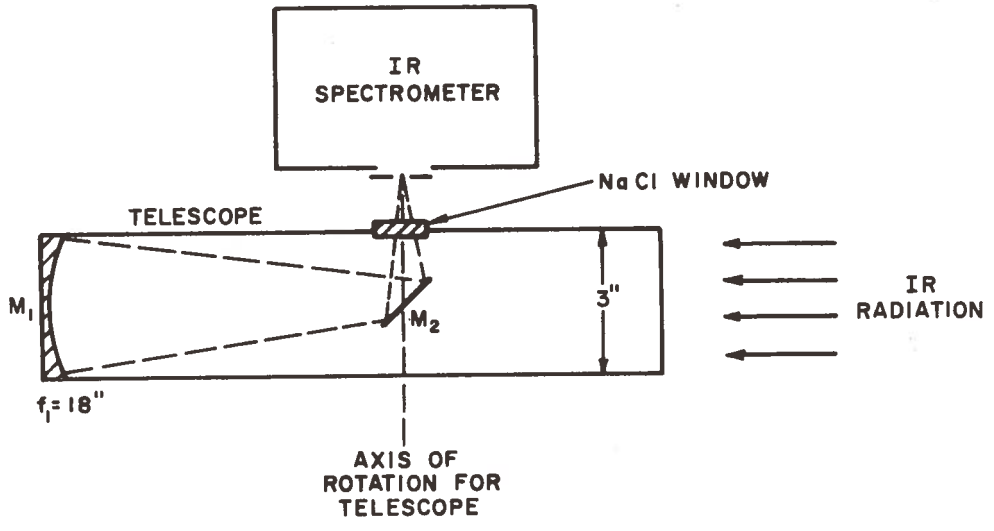

Figure A.1.- Scanning telescope and spectrometer. (Layout is in horizontal plane.)

We can calculate the irradiance at the spectrometer slits from a body at temperature T which fills the entire field of view of the telescope. Let the aperture of the telescope be D and the field of view be θ. If $N_\lambda(T)$ is the spectral radiance of the body in question, then the flux through the slits (assuming the spectrometer is matched to the telescope f.o.v.) is:

$$\Phi_\lambda = N_\lambda(T) \frac{\pi D^2}{4} \cdot \Pi\theta^2 \cdot \Delta\lambda$$

For our case, $N_\lambda(T) \simeq 600\text{-}800 \mu w/cm^2/str./micron$ [see reference 13; $\lambda \sim 10\mu$ and T $\sim 0^oC$ to 20^oC.] Also D = 5 cm^2, $\theta \simeq 2$ mrad. and $\Delta\lambda \simeq 0.2\mu$. The small f.o.v. is needed to resolve distances near the horizon. (See Figure A.7 below.) The bandpass of our instrument is determined largely by the 2mm slit width and was deduced from broadening of polystyrene absorption lines. With radiance *differences* expected to be less than 200 $\mu w/cm^2/str./micron$, the changes in flux we are looking for will not exceed $\Delta\Phi \sim 10^{-9} - 10^{-8}$ watts.

The sensitivity of the spectrometer was determined by placing a commercial black-body source within a few centimeters of the entrance slits. By comparing the instrument deflection (for the calculable black-body energy received) with the noise level in the absence of signal, the minimum detectable power was found to be 5×10^{-10} watts. The time constant was 3 seconds.

A photograph of the receiving telescope and the spectrometer are shown in Figure A.2.

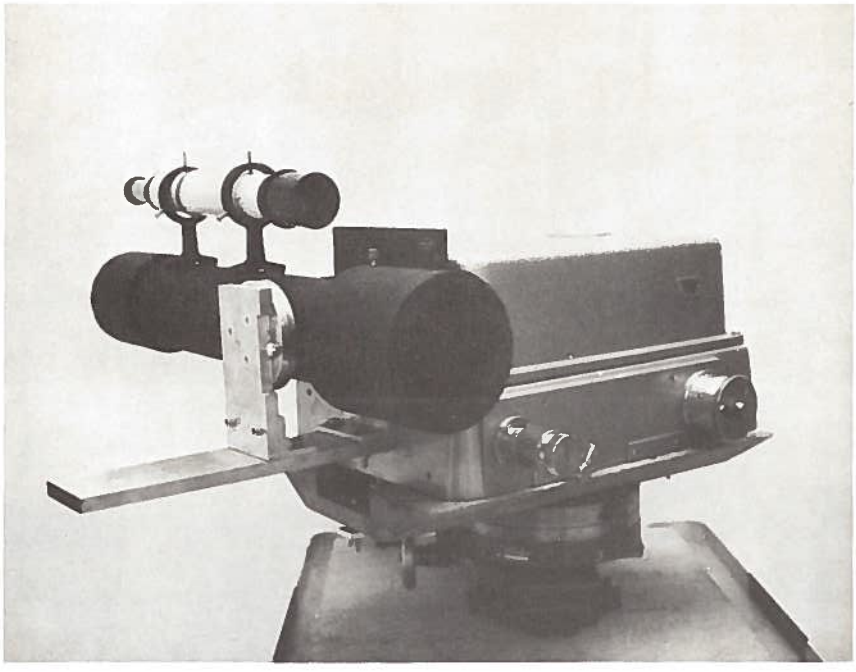

Figure A.2.- Scanning telescope (drive not shown) and infrared spectrometer. Also shown is the viewing scope.

The geometry shown in Figure 3.4 can be used to derive several important relations. First, the distance to the horizon, $\overline{OB}$, can be found as a function of the height h of the instrument. This is shown in Figure A.3.

The relationship between the scan angle α_x (Figure 3.4) and the distance $\overline{ox}$ at which the instrument is looking is given by

$$\Delta\alpha \equiv \alpha_x - \alpha_\beta \simeq \frac{h}{x} - \left(\frac{2h}{R}\right)^{1/2}$$

where α_β is the direction of the horizon and is a constant for a given installation height. The approximation is valid for $\frac{h}{x} >> \frac{x}{2R}$.

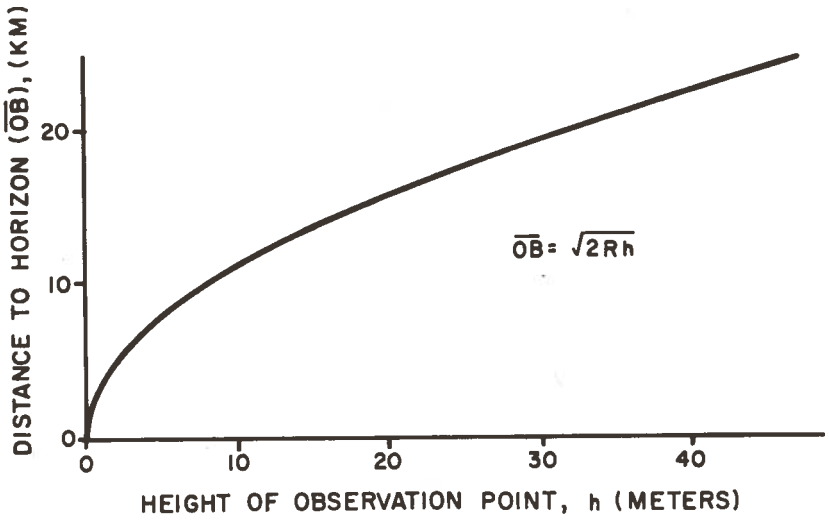

Figure A.3.- Distance to horizon, $\overline{OB}$ as a function of height of observation point (See Figure 3.4). R = radius of earth = 6.4×10^6 meters.

It is clear from this last expression that the distance x is a non-linear function of the scan angle. This has two related effects. First, the instrument's recorder output, which runs linearly with time, corresponds to an angle scan and must be recalibrated in terms of distance. Secondly, in order to resolve a fog front (i.e. a water-fog interface) at 3 miles from the water-sky interface at the 11 mile horizon, the field-of-view must be kept quite small. Figure A.4 shows the non-linear relationship between $\Delta\alpha$ and x.

The experiment was carried out from a height of 30 meters above sea-level. Figure A.5 shows the geometry.

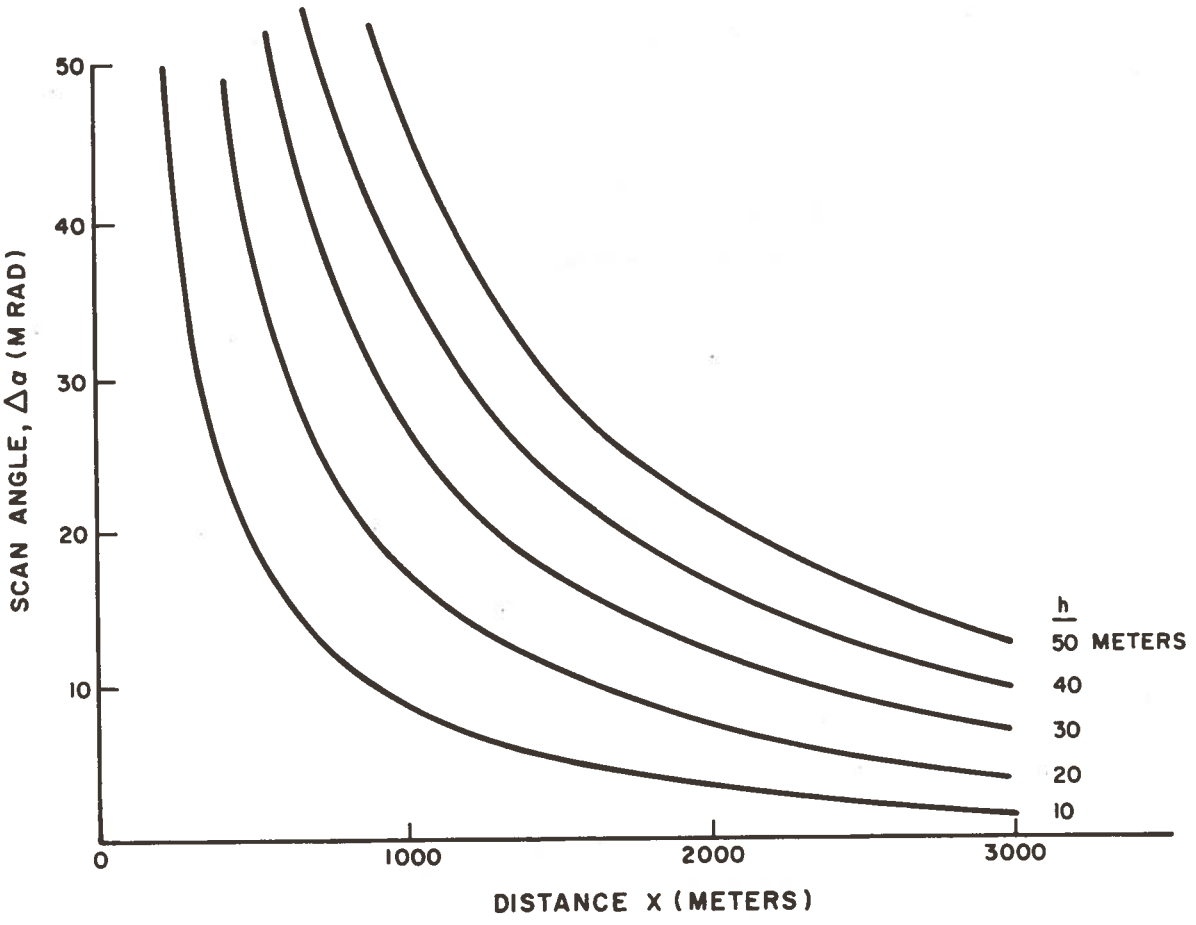

Figure A.4.- Scan angle $\Delta\alpha=\alpha_x-\alpha_\beta$ vs distance x to the "scene" point.

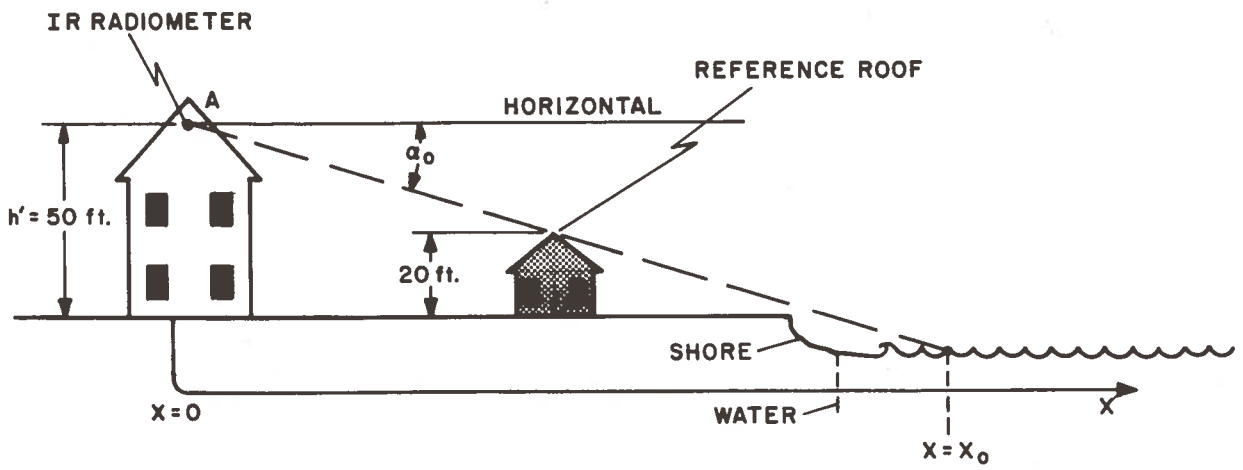

Figure A.5.- Diagram of experimental geometry.

The roof shown is used as a reference point for the scan start. The position $x = x_o$ represents the first view of water seen as α_x passes through α_o. The distance x_o in our case is 300 meters. A photograph of the area seen from the radiometer platform is presented in Figure A.6. The vertical dotted line represents the plane in which the instrument scans.

Figure A.6.- Photograph of "scene" for radiometer measurements

By using Figure A.5, the geometry of the angular field of view in the above photograph can be converted to a distance scale, as shown in Figure A.7.

Thus the non-linearity between $\Delta\alpha$ and x causes the region between 3 km and 19 km (or between 2 miles and the horizon at 11 miles) to be compressed into about 5% of the entire scan. This

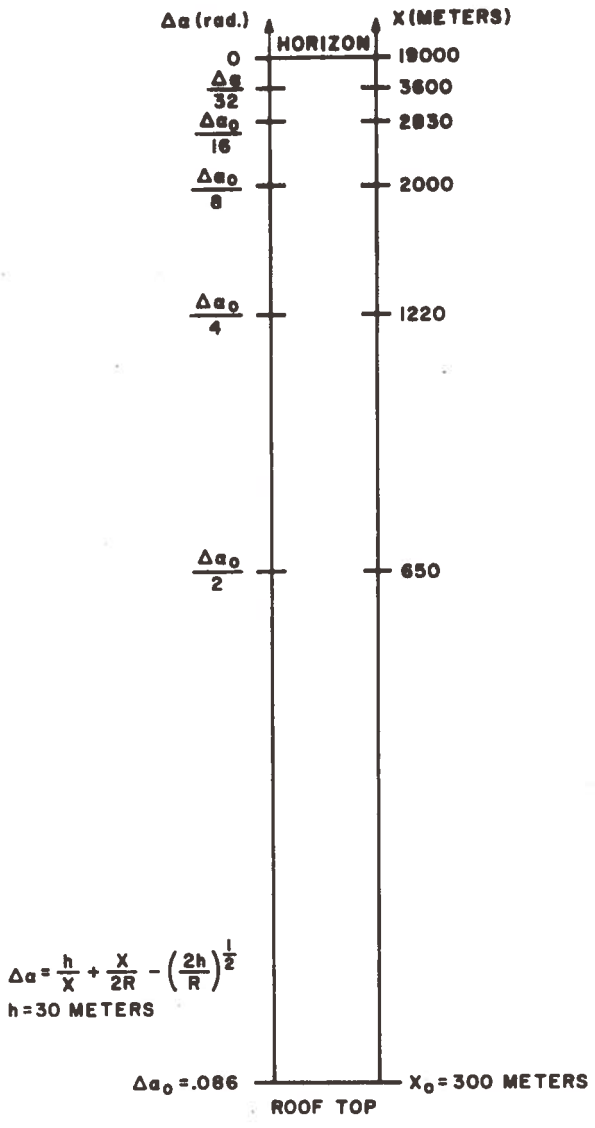

Figure A.7.- Calibration of angular scan in terms of distance.

corresponds to a field of view of only 2.5 mrad. (=8.5 minutes of arc) To discern a fog-water interface at 2-3 miles from the water-sky interface at the horizon, by *angular position alone*, may be difficult. However, it is likely that fog banks will give a *qualitatively different* appearance to the IR scan.

APPENDIX B - LIDAR: EXPERIMENTAL DETAILS

Details of the ruby LIDAR preliminary experiments (see Section 3.2.1) are given below. The experiments were carried out with a Holobeam 3" ruby system (3" x 1/4" rod), Q-switched by a pthalocyanine (in nitrobenzene) saturable absorber. The output pulse had a width of approximately 50 nsec and energy of 10 mJ.

The receiver consisted of an f/5 (50 cm focal length) objective lens and a variable field stop in the focal plane which allowed the field of view to be altered. The detector, either a photomultiplier or a PIN diode, was mounted after a narrow-band filter which passed the 6943 A return light but blocked the background radiation scattered from the cloud. The output of the detector was then displayed on a Tektronix 556 oscilloscope whose time base allowed the pulse round trip time to be measured.

The features of this system are shown in Figure B.1. The laser output was made *coaxial* with the receiver optical axis by the adjustable pair of right angle prisms mounted in the front of the unit. The entire system was mounted on a heavy-duty rolling tripod with adjustable elevation angle. The optics were boresighted by means of the eyepiece-beam splitter combination shown at the top of the figure. A photograph of the complete LIDAR system appears in Figure 3.1.

To make use of the experimental results from clouds, the backscatter results (such as shown in Figure 3.2(d)) were

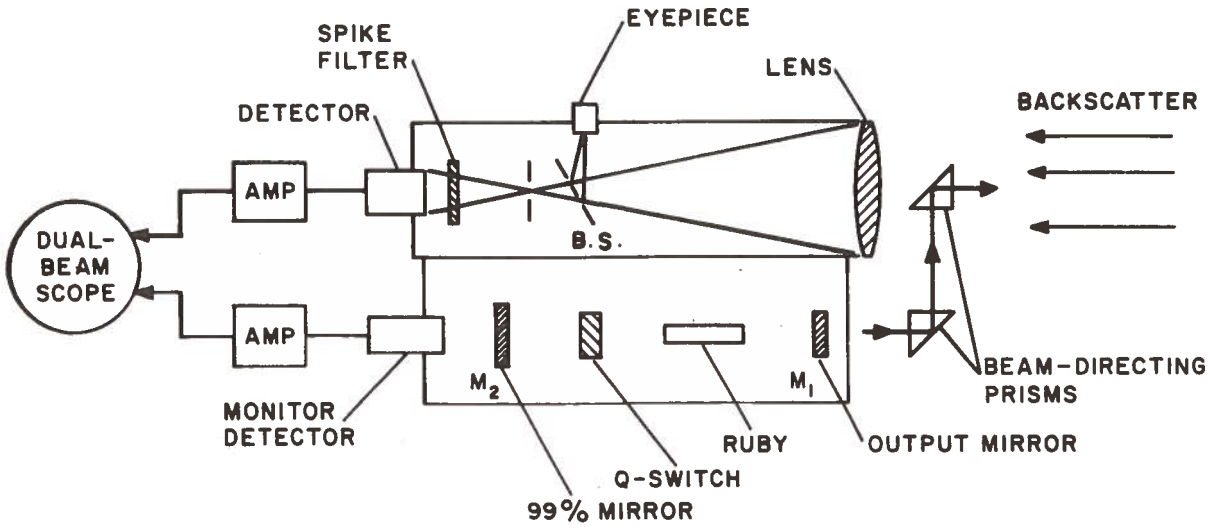

Figure B.1.

compared with a predicted signal-to-noise estimate based on the theory presented in Section 3.3 and 4.3. In particular, the returns were compared with the equations

$$P_R' = \frac{\rho}{2\pi} (P_o T_o A_r) \frac{e}{r^2} e^{-2\gamma_a r}$$

$$i_s/i_N = \frac{\sqrt{\eta} P_R'}{\sqrt{2B\ h\nu\ P_{Bd}}} \quad . \qquad \text{(Background - limited case).}$$

The experimental parameters are:

Receiver: $A_R = 100\ cm^2$

θ_R = f.o.v. = 3 mrad $\rightarrow$ $\Omega_R = \pi\theta^2 = 2.7 \times 10^{-5}$ str.

$\Delta\lambda$ (filter) $\simeq$ 10 A

T_o = (total) effective transmission of optics = .2

Assuming background radiance = 2×10^{-6} w/cm^2/str./A, then

$$P_{Bd} = (2 \times 10^{-6}) \cdot (A_R) \cdot (\Omega_R) \cdot (\Delta\lambda) \cdot T_o = 10^{-8} \text{ w.}$$

Detector: EMI 9558 (S-20) : η = .02 (6943 A)

$h\nu = 3 \times 10^{-19}$ J

B = 10^6 cps (R_L = 10K)

Pulse propagation and reflection:

P_o = 2 MW (in 50 nsec pulse)

ρ = 0.1

r = 7 miles $\simeq$ 11 km.

$\gamma_a = \frac{3.9}{V} = .00026 \text{ m}^{-1}$ (V = 16 km)

$P_R' = 10^{-9}$ w.

$\frac{S}{N} = 2$

This result appears at first surprisingly close to the experimental results of Figure 3.2(d). However, this close agreement is considered fortuitous, for two reasons. First, the value for P_R' is calculated as if the return pulse were equal in width to the transmitted pulse. This is not expected to be true (see discussion of 4.3 and the effect of pusle broadening would be

to reduce the estimated S/N. The bandwidth of our detection system was limited to 1 mc by the large load resistor required to give signal voltages above the amplifier noise level. As a result, pulse widths less than 500 nsec. could not be resolved. If, in fact, the return pulse was 500 nsec. wide, the estimated S/N would be reduced by 10, and the above agreement is compromised.

Furthermore, the estimate of the background is somewhat uncertain. The value of the radiance of the cloud is based on the observed noise and a rather rough estimate of the photomultiplier gain. This radiance could be off by a factor of 10 or more, leading to an uncertainty in the S/N estimate of perhaps 30 to 50%.

In spite of these limitations in comparing the predicted and observed signal-to-noise ratios, the experiments provided early confidence in our understanding of the phenomena involved.

REFERENCES

1. Lomer, L.R., "Fog Detectors for Unmanned Aids to Navigation", U.S. Coast Guard Field Testing and Development Center, Report No. 512, 1970.

2. Middleton, W.E.K., Vision Through the Atmosphere, University of Toronto Press, Toronto, Canada (Reprinted 1963).

3. Van de Hulst, H.C., Light Scattering by Small Particles, John Wiley and Sons, New York, 1957.

4. Twomey, S. and Howell, H.B., "The Relative Merit of White and Monochromatic Light for the Determination of Visibility by Backscattering Measurements", Appl. Opt. 4, 501 (1965).

5. Fenn, R.W., "Correlation Between Atmospheric Backscattering and Meteorological Visual Range", Appl. Opt. 5, 293 (1966).

6. Curcio, J.A. and Knestrick, G.L., "Correlation of Atmospheric Transmission with Backscattering," J. Opt. Soc. Am. 48, 686 (1958).

7. Vogt, H., "Visibility Measurement Using Backscattered Light", Journal of the Atmospheric Sciences, Sept., 1968.

8. Hochreiter, F.C., "Analysis of Visibility Observation Methods", U.S. Department of Commerce, ESSA Technical Memorandum WBTM T&EL 9, 1969.

9. Brown, R.T., Jr., "Backscatter Signature Studies for Horizontal and Slant Range Visibility," Final Report No. RD-67-24, Project No. 450-402-01E, FAA, Washington, D.C., 1967.

10. Collis, R.T.H., Viezee, W., Uthe, E.E., and Oblanas, J., "Visibility Measurement for Aircraft Landing Operations", Final Report No. AFCRL-70-0598, Stanford Research Institute, Menlo Park, Calif., 1970.

11. Frungel, F., Bull. de l'A.I.S.M. n.^{o} 40, April 1969 (p.9-16).

12. Oetjen, R.A., Bell, E.E., Young, J., and Eisner, L. "Spectral Radiance of Sky and Terrain at Wavelengths between 1 and 20 Microns", Part I, J. Opt. Soc. Am. 50, 1308 (1960).

13. Eisner, L., Bell, E.E., Young, J. and Oetjen, R.A., (id, Part III), J. Opt. Soc. Am. 52, 201 (1962).

14. Carrier, L.W., Cato, G.A. and von Essen, K.J., "The Back-scattering and Extinction of Visible and Infrared Radiation by Selected Major Cloud Models", Appl. Optics 6, 1209 (1967).

15. Thornton, J.R., Rushworth, P.M., Harper, L.L., Kelly, E.A., and McMillan, R.W., "Erbium Laser Transmitter Module", ECOM-0336-F, Martin Marietta Corporation, Orlando, Florida, 1970.

16. White, K.O., Holt, E.H. and Woodcock, R.F., "The Positive Potential of Erbium", Laser Focus, July, 1970, p. 41.

17. TB MED 279 (NAVMED P-5052-35), "Control of Hazards to Health from Laser Radiation", Departments of the Army and the Navy, Washington, D.C., 1969.

18. "Rules and Regulations Relative to the Use of Laser Systems", Department of Public Health, The Commonwealth of Massachusetts, 1970.

19. Clarke, A.M., "Ocular Hazards from Lasers and Other Optical Sources", CRC Critical Reviews in Environmental Control, November, 1970, p. 307.

20. Department of the Air Force, AFM 161-8, Laser Health Hazards Control, Washington, D.C., April 1, 1969.

21. Lund, D.J., Carver, C.T. and Powell, J.O., "Gallium Arsenide Laser Damage Threshold Study", Frankford Arsenal, Philadelphia, Pa., July, 1970 (AD 876-981).

22. Gast, P.R., "Solar Irradiance", Handbook of Geophysics and Space Environments, S.L. Valley, Ed., Cambridge, Mass. (AFCRL), 1965.

23. Ross, M., Laser Receivers, John Wiley and Sons, Inc., New York, 1966, (p. 70).

24. "Silicon Photodetector Design Manual", United Detector Technology, Santa Monica, Calif.

25. See e.g., Schaunfield, W.N., Boone, D.W. and Deppe, D.G., "Getting the Most Out of the APD", Electro-Optical Systems Design, March, 1971; p. 15.

26. Electro-Optics Handbook, RCA Commercial Engineering, Harrison, N.J., 1968.